# ABSTRACT

Title of Dissertation: SEDIMENT CONNECTIVITY BETWEEN THE LOWER SUSQUEHANNA RIVER AND UPPER CHESAPEAKE BAY

Emily Rebecca Russ, Doctor of Philosophy, 2019

Dissertation directed by: Associate Professor Cindy Palinkas, Marine, Estuarine and Environmental Science

Excess fine sediment is one of the main pollutants contributing to water quality degradation in the upper Chesapeake Bay. Recent management efforts have focused on reducing sediment inputs within the Bay watershed to achieve water quality standards set in the Chesapeake Bay Total Maximum Daily Load (TMDL). However, the models used to develop the TMDL did not account for the evolving sediment loads to and storage in the Bay, which include reduced sediment capacity in the Conowingo Reservoir, the last reservoir on the Susquehanna River, increased shoreline protection measures, and resurgence of SAV in the upper Bay in a region known as the Susquehanna Flats. The overall goal of this dissertation is to assess the current sediment dynamics of the upper Bay and specifically evaluate the connectivity of sediment transport from the Susquehanna River through the Flats into the upper Bay.

First, I evaluated sedimentation on the Susquehanna Flats over seasonal to decadal time scales using radioisotopes within the context of submersed aquatic vegetation (SAV) biomass and geomorphology. Seasonal-scale sedimentation variability was related to river discharge, sediment supply, and geometry over the SAV bed, while decadal-scale sedimentation was influenced by flood events and changes in SAV biomass abundance. Next, I analyzed sediment geochemical patterns in the upper Bay using statistical analyses. Elements associated with aluminosilicate minerals, rare earth elements, and heavy metals explained the most variability in the dataset due to changes in grain size, salinity, and anthropogenic input, respectively. A sediment-provenance analysis was performed using the sediment-geochemistry data and indicated that the Susquehanna is the dominant source of fine-grained material throughout the upper Bay. Finally, I developed an updated sediment budget through quantitative analysis of sediment sources (Susquehanna River and shoreline erosion) and sinks (Susquehanna Flats and mainstem sediment-accumulation rates). Conservation-management practices have reduced Susquehanna River sediment loads at low flows, but sediment loads at high flows have increased, consistent with a decreasing scour threshold for bottom sediments in Conowingo Reservoir as it has filled. Increases in shoreline stabilization have reduced shoreline erosion inputs.

# SEDIMENT CONNECTIVITY BETWEEN THE LOWER SUSQUEHANNA RIVER AND UPPER CHESAPEAKE BAY

by

Emily Rebecca Russ

Dissertation submitted to the Faculty of the Graduate School of the
University of Maryland, College Park, in partial fulfillment
of the requirements for the degree of
Doctor of Philosophy
2019

Advisory Committee:
Associate Professor Cindy Palinkas, Chair
Jeffery Cornwell
Ming Li
Karen Prestegaard
Lawrence Sanford

# Dedication

To my family, for always giving me the push I needed.

# Acknowledgements

I would like to thank the many people who contributed their time and effort to help me complete this dissertation. First and foremost, I want to first thank my advisor and mentor, Cindy Palinkas, for her continuous support and guidance. When I arrived at Horn Point, I was unfunded and did not really know how to do independent research, but Cindy helped me discover my potential. She let me take ownership of my research project and encouraged me to explore my own questions, which helped me grow into an independent and confident researcher. It has truly been an honor to be her student.

I also would like to thank Jeff Cornwell for letting me tag along on multiple field excursions to collect mud from the Conowingo Reservoir, as well as his guidance in interpreting the sediment geochemical patterns from Chapter 3. Additionally, I would like to thank my committee members Ming Li, Karen Prestegaard, and Larry Sanford for each offering a fresh perspective to my research and always providing thoughtful feedback, which greatly improved my dissertation.

This research would not have been possible without those who assisted me in the field and lab, particularly Debbie Hinkle, who worked tirelessly and always made herself available to help me. Thank you to Mike Owens, Cassie Gurbisz, Connor Reyer, Isabel Sanchez, Stella Castro, Ted Suman, and Kristi Moore, who all provided essential field and lab support.

I would like to thank my funding sources: Maryland Sea Grant, the Doughty Fellowship, and Horn Point Laboratory. I particularly want to thank Bob and Cris Doughty for the honor of being the first recipient of the Doughty Fellowship. Their financial support helped me cover analytical costs, which greatly improved the quality of my research, and afforded me the opportunity to attend national conferences.

I want to thank Maryland Sea Grant Extension Agents, Jen Dindinger and Krisztian Varsa, for serving as my outreach mentors and for introducing me to the field of extension. I want to particularly thank Jen for being an incredible mentor to me and always being available and willing to offer outreach, career, or life advice. She played an instrumental role in helping me apply for (and ultimately receive) the Knauss Fellowship.

Thank you to all of the friends I have made at Horn Point for helping me find balance during graduate school.

I want to thank my parents and Erik for their constant love and support and for always being excited to learn about my work. They helped me find the motivation to push through the finish line.

Lastly, I would like to thank Andy McCarthy. You are the most important thing in the whole world to me, and have been the steadiest thing in my life over the past 9 years. Thank you for always challenging me to be the best version of myself.

# Table of Contents

# List of Tables

# List of Figures

# Chapter 1 : Introduction

Estuaries are highly dynamic and productive coastal environments, often forming the transition zone between rivers and oceans. Estuaries are ephemeral geologic features, and modern estuaries are relatively young, forming ~6,000 years ago as sea level began to stabilize following a period of rapid marine transgression (Dalrymple et al. 1992). Since their formation, these estuaries have been filling in with sediment from external (rivers and oceans), internal (*in situ* production), and marginal (shoreline) sources. The rate of accretion within estuaries is a function of sediment supply and accommodation space, both of which vary with changing geography and geology (Dalrymple et al. 1992). Fluvial sediment supply is largely controlled by basin area, geology, elevation, temperature and precipitation (Syvitski and Kettner 2011), while marine sources are transported landward by waves and tides through estuary mouths (Meade 1969; Dalrymple et al. 1992). Accommodation space is determined by antecedent topography, tectonics, subsidence, and sea-level rise (Syvitski et al. 2005). Once completely filled in with sediment, estuaries transform into prograding deltas (ex. Mekong River Delta; Ta et al. 2002).

In addition to these natural processes, humans have significantly modified sedimentation within estuaries, particularly through alterations to sediment delivery (Syvitski et al. 2005; Walling 2006). Estuaries have long been ideal locations for human settlement due to access to abundant resources and navigation (Day et al. 2011). Although evidence of human influence on sediment supply is present in the sediment record as early as 4000 years ago (i.e. Anthony et al. 2014), dramatic

changes began ~300 years ago as a result of increased population and industrialization. Major changes in land use, including deforestation, mining, increased agriculture, and urbanization resulted in higher rates of soil erosion and subsequent increases in global river sediment loads (Syvitski et al. 2005; Syvitski and Kettner 2011). However, the relatively recent (~1940s-1950s to the present) increase in dam construction has resulted in trapping of much of these loads behind large dams, thus decreasing total sediment delivery to estuaries and coasts (Syvitski et al. 2005; Walling 2006). Humans have also altered sediment input from shoreline erosion through increased development, which increased sediment loads, and subsequent shoreline stabilization, which decreased sediment loads (Gittman et al. 2015). Lastly, humans have directly affected accommodation space through periodic dredging to maintain navigation channels (i.e. USACE 2017). Dredging modifies channel hydrodynamics and sediment transport, leading to increased channel sedimentation and thus more frequent maintenance dredging (i.e. van Maren et al. 2015).

These alterations in the sedimentary environment have led to many sediment-related issues in coastal and estuarine environments. Some areas have too little sediment like coastal Louisiana, where sediment deficits have led to rapid land loss and the inability of coastal marshes to accrete sediments on pace with sea-level rise (Templet and Meyer-Arendt 1988). Similarly, many deltas around the world are submerging due to sediment-load reductions from retention behind large reservoirs, such as the Yangtze River (Yang et al. 2006) and Mississippi River Deltas (Blum and Roberts 2009). These deficits are compounded by those induced by shoreline-

protection structures that disconnect natural exchange at the land-water interface (Dugan et al. 2011). In contrast, some areas receive too much sediment, such as the coasts of tropical countries (e.g. Papua New Guinea, Indonesia) due to increased deforestation and mining (Wolanski and Spagnol 2000; Syvitski et al. 2005). Excess sediments decrease light availability to submersed plant communities (Dennison et al. 1993), increase nutrient loads fueling hypoxia/anoxia and harmful algal blooms (Diaz and Rosenberg 2008), impede navigation (Gottschalk 1945), and smother benthic ecosystems (Restrepo et al. 2006).

Evolving coastal and estuarine sediment dynamics can also be attributed to climate change. For example, East and Southeast Asian river sediment loads to the Pacific Ocean have shown high correlation with precipitation patterns, where loads during years with major floods are much greater than during droughts (Wang et al. 2011). Therefore, changing climate dynamics, such as increases in winter-to-spring precipitation and storm intensity in the northeastern United States will likely result in increased streamflow and sediment loads (Najjar et al. 2010; Boesch 2008). Conversely, increased incidences of droughts in summer and fall, will likely decrease sediment loads (Boesch 2008). In addition to anthropogenic-induced sediment deficits, wetland loss in the Mississippi-Atchafalaya River System (Bianchi and Allison 2009; Anderson et al. 2013) results from increased rates of relative sea-level rise (combined sea-level rise and subsidence) and wave attack, suggesting that continued increases in sea level will result in increased coastal erosion.

The upper Chesapeake Bay serves as an excellent example of these trends. In the Chesapeake Bay, sediment can act as both a pollutant and a resource; i.e. excess

fine sediment supply degrades water quality but is also necessary for marsh survival (Kirwan et al. 2011). Excess fine sediment has contributed to degraded water quality (US EPA 2010; USACE 2015) and benthic habitats, such as oyster reef mortality due to burial (Rothschild et al. 1994; Colden and Lipcius 2016), and loss of submersed aquatic vegetation (SAV) from both burial and reduced light availability (Bayley et al. 1978; Dennison et al. 1993). Excess sediments transport particulate nutrients, which enhance eutrophication by fueling algal blooms that reduce water clarity and lead to oxygen depletion in the water column and/or harmful algal blooms (Kemp et al. 2005). Approximately $4x10^6$ $m^3$ of sediment is dredged from the Bay each year to maintain navigation channels, which is costly and disruptive to benthic ecosystems (USACE 2017). Therefore, improving water quality by reducing sediment inputs has been a major management focus within the Bay watershed and one of the main goals of the Chesapeake Bay Total Maximum Daily Load (TMDL) developed by the U.S. Environmental Protection Agency (EPA) to achieve water quality standards by 2025 (USEPA 2010). However, sediment is an important resource to Chesapeake Bay marshes, which have become increasingly vulnerable to coastal erosion due to decreases in sediment delivery and acceleration of relative sea-level rise (Kearney and Stevenson 1991; Kirwan et al. 2011). Marsh survival depends on the availability of both mineral and organic sediment to build elevation at approximately the same rate as sea-level rise. Many marshes along the lower Eastern Shore of the Chesapeake Bay do not receive adequate sediment supply to keep up with current sea-level rise and are submerging (Kearney et al. 2002; Ganju et al. 2015; Beckett et al. 2016). Although marshes of the upper Bay are currently keeping pace with current sea-level

rise rates, accelerating rates of relative sea-level rise will likely outpace future sediment delivery (Boesch 2008).

Humans have altered the main sources of sediment to the upper Chesapeake Bay for >300 years, although the greatest impacts occurred after industrialization (Brush 2009). Sediment loading from the Bay's main tributary, the Susquehanna River, has a complex history. Susquehanna River watershed sediment loads increased in the mid-19$^{th}$ and early 20$^{th}$ centuries as humans cleared forests to support intensive agriculture and mining activities, but loads declined following farm abandonment and the implementation of conservation-management practices (Brush 1984). Susquehanna sediment loads bound for the upper Bay were further altered in the early 20$^{th}$ century by construction of three sequential hydroelectric dams in its lower reaches (~50 km; the lower Susquehanna River Reservoir System) and subsequent sediment trapping in associated reservoirs, Lake Clarke, Lake Aldred, and Conowingo Reservoir (Langland 2009; Langland 2015). These reservoirs historically captured ~75% of the annual Susquehanna River sediment load, but the sediment-trapping efficiency of these reservoirs has decreased over time due to sediment infilling. In fact, Lakes Clarke and Aldred reached dynamic equilibrium (i.e. sediment inputs and outputs are approximately equal over long time scales; Langland 2009) in the 1950s-1960s. Recent work suggests that Conowingo Reservoir has also reached this state, resulting in increased sediment loads to the Bay (Hirsch 2012; Zhang et al. 2013; Langland 2015).

The Susquehanna currently delivers 85% of the total freshwater and 67% of the sediment load to the upper Bay (Schubel and Pritchard 1986; Langland 2015).

The other ~1/3 of the sediment load comes from shoreline erosion, which becomes the dominant sediment source south of the Chesapeake Bay Bridge (Schubel 1968; Biggs 1970). Shoreline erosion varies spatially depending on factors such as shoreline orientation, fetch, bathymetry, sediment composition, and land use (Langland and Cronin 2003). Shoreline development increased after World War II, exacerbating erosion rates (Hardaway and Byrne 1999). Furthermore, extensive shoreline loss has been linked to increasing rates of relative sea-level rise (Kearney and Stevenson 1991; Boesch 2008) and intense storms (Hennessee and Halka 2005). In response, more than 300 miles of stabilization structures, such as seawalls and bulkheads, have been installed between 1978 and 1997 (Titus 1998; Hardaway and Byrne 1999; Halka et al. 2005). These structures can reduce fastland erosion (above mean low water (MLW); used interchangeably with "shoreline erosion" in this dissertation) and turbidity caused by fine-grained particles. But, structures can increase nearshore erosion (below MLW) by decreasing sand supply to adjacent habitats and/or reflecting, rather than dampening, wave energy (Hardaway and Byrne 1999; Halka et al. 2005).

Previous studies have quantified upper Bay sedimentation rates (e.g. ~$3x10^6$ t $y^{-1}$; Officer et al. 1984a); however, the impact of evolving sediment supplies is unclear. Importantly, the connection between the Bay and its major tributary is missing from previous studies, especially sediment processing through the transition zone formed by the Susquehanna Flats. Thus, the overall goal of this dissertation is to evaluate the connectivity of sediment transport from the Susquehanna River through the Flats into the upper Bay. The Susquehanna Flats is the subaqueous delta of the

Susquehanna River and is colonized by dense submersed aquatic vegetation (SAV) beds. These beds were historically dense, but they disappeared following Tropical Storm Agnes (1972). There was little change in plant abundance between 1972 and 2000, and then a rapid resurgence of both SAV bed area and density began in ~2001 (Gurbisz and Kemp 2014). SAV enhance sediment deposition by attenuating wave energy and flow velocity (Ward et al. 1984; Fonseca and Fisher 1986), but it is not clear how the Susquehanna Flats SAV bed modulates sediment delivery to the upper Bay. This is the focus of Chapter 2, which evaluates vegetation influences on sediment burial over seasonal and decadal time scales.

Susquehanna sediment arriving in the upper Bay joins with that supplied from shoreline sources. Susquehanna and shoreline sediments have different impacts to Bay ecosystem dynamics. Relative to shoreline sediments, Susquehanna sediments are typically finer and more nutrient-rich, thus more likely to increase turbidity and fuel algal blooms (Marcus and Kearney 1991). Determining the relative contributions of these sources to upper Bay sediments is important for management but requires sophisticated analytical techniques that have only recently become available. These techniques and their potential application to sediment-provenance analyses are presented in Chapter 3, which focuses on sediment geochemistry. In particular this chapter examines how geochemical patterns in surficial and down-core sediments vary spatially and the underlying processes driving this variability. These results are then used to perform a sediment-provenance analysis to evaluate source contribution to bottom sediments in the upper Bay.

Another approach to quantifying the relative role of fluvial versus shoreline sediments is through constructing sediment budgets. The most recent sediment budget for the upper Bay was developed in 1992 (Hobbs et al. 1992) and thus does not reflect the current sedimentary environment. Importantly, it does not include two recent changes along the river-estuary continuum: 1) recent infill of the Conowingo Reservoir (Langland 2015); and 2) the resurgence of SAV beds on the Susquehanna Flats (Gurbisz and Kemp 2014). In chapter 4, the impacts of these recent changes are evaluated through quantitative analysis of sediment sources (Susquehanna River and shoreline erosion) and sinks (mainstem sediment-accumulation rates) and synthesized into an updated sediment budget of the upper Bay.

# Chapter 2 : Seasonal-scale and decadal-scale sediment-vegetation interactions on the subaqueous Susquehanna River delta, upper Chesapeake Bay

**Abstract**

Submersed aquatic vegetation (SAV) have been a prominent feature on the Susquehanna Flats, the shallow, subaqueous delta of the Susquehanna River, Maryland. SAV were absent from the Flats between 1972 and 2000, but have since recovered. While it is well established that SAV can improve water quality by promoting sediment and nutrient retention, it is not well understood how SAV on the Flats modulate sediment input from the Susquehanna River into the Upper Chesapeake Bay over different time scales. This study evaluates sedimentation on the Flats over seasonal to decadal time scales, using naturally occurring radioisotopes ($^{7}$Be, $^{210}$Pb) within the context SAV biomass and Flats geomorphology. Results indicate sedimentation on the Flats is both spatially and temporally variable. Although this variability cannot be explained by relationships with grain size and SAV biomass, river discharge, sediment supply, and geometry over the SAV bed likely control sedimentation in this system. Decadal-scale sedimentation is influenced by both flood events and changes in SAV biomass abundance. Average annual sediment accumulation was higher when SAV was present than when SAV was absent. SAV bed area was strongly correlated with average annual accumulation rate. These results suggest that a positive feedback between SAV abundance and

accumulation rate exists; however, sediment supply and transport pathways are also important factors.

## Introduction

Submersed aquatic vegetation (SAV) are known ecosystem engineers that modify their environment through interactions with both water flow and sediment dynamics (Jones et al. 1994; Koch 2001). SAV canopy friction increases flow resistance, attenuating wave energy and current velocities inside the plant bed (Fonseca et al. 1982; Fonseca and Fisher 1986; Gambi et al. 1990; Fonseca and Cahalan 1992). These zones of reduced flow promote sediment deposition and suppress resuspension (Ward et al. 1984; Gacia and Duarte 2001), providing a positive impact on water quality by retaining sediment and attached nutrients.

SAV historically were abundant in the shallow coastal zones of the Chesapeake Bay (Stevenson and Confer 1978; Orth and Moore 1984). However, SAV populations began to decline following European colonization, due to poor water quality and the advent of intensive agriculture (Davis 1985), and vanished from most Chesapeake habitats following tropical storm (TS) Agnes in 1972 (Orth and Moore 1984; Brush and Hilgarten 2000). SAV beds in the freshwater reaches of the upper Bay were especially sensitive to TS Agnes flooding, where abundances declined by more than 60% (Kerwin et al. 1976). In particular, the dense SAV beds that occupied the Susquehanna River subaqueous delta, known as the Susquehanna Flats (hereinafter referred to as "the Flats"), disappeared following TS Agnes (Bayley et al. 1978). However, the SAV beds on the Flats made a remarkable recovery in the early 2000s in response to improved water quality from a combination of

conservation management actions and several years with relatively little precipitation (Gurbisz and Kemp 2014). Additionally, the bed was able to withstand a relatively large storm event in 2011 (Tropical Storm Lee) (Gurbisz et al. 2016).

While it is well established that SAV promote sediment and nutrient retention, it is not well understood how SAV on the Flats affect sediment input into the Upper Chesapeake Bay over different time scales. Because of its location at the interface between the Chesapeake Bay and its major tributary (Susquehanna River), the Flats plays an important role in modulating sediment input into Chesapeake Bay and thus also sediment supply to downstream ecosystems (e.g., marshes, oysters). More broadly, sediment-vegetation interactions at the fluvial-estuarine interface are not yet well understood, and seasonal and decadal shifts in SAV abundance on the Flats offer a unique opportunity to examine how SAV modulate sediment input from rivers into adjacent estuaries.

The objectives of this study are to 1) determine seasonal-scale sedimentation patterns within the context of SAV biomass and Flats geomorphology; and 2) assess whether historical changes in SAV abundances are reflected in decadal-scale sedimentation rates.

## Methods

### *Study Site*

The Flats are located on the shallow, seasonally vegetated (growing season June-October; Bayley et al. 1978; Gurbisz and Kemp 2014), subaqueous sandy deposit at the confluence of the mouth of the Susquehanna River and the upper

Chesapeake Bay (Fig. 2.1a). The Flats are in the tidal freshwater region of the Bay, where salinity ranges between 0 and 3. The average depth across the Flats at mean lower low water (MLLW) is 1 m, with a mean tidal range of 0.6 m (Bayley et al. 1978). The main stem Bay channel (ranging from 3-7 m in depth) is located west of the Flats; however, discontinuous channels are located to the north (Fig. 2.1b). Waves in the upper Bay are fetch-limited and primarily wind-generated (Sanford 1994); significant wave heights are typically <1 m with a mean period of <2.5 s (https://buoybay.noaa.gov/). Current velocities rarely exceed 0.2 m $s^{-1}$, even when SAV are absent (LSRWA 2015).

The Susquehanna River largely controls circulation on the Flats, directing freshwater and sediment seaward (Schubel and Pritchard 1986). The Susquehanna River is the largest source of freshwater and sediment to the upper Bay, with an average river discharge of 1100 $m^3$ $s^{-1}$ (Schubel and Pritchard 1986) and annual sediment load of $2x10^6$ tons (Langland 2015). The Susquehanna River exhibits strong seasonality in river discharge, with annual maximum flows coinciding with the spring freshet, and minimum flows occurring in late summer (Schubel and Pritchard 1986). Sediment load is tightly coupled with river discharge, and in a typical year (i.e. one without major flood events) 50-60% of the annual Susquehanna River sediment load is associated with the spring freshet (Gross et al. 1978). Discharge has twice exceeded 20,000 $m^3$ $s^{-1}$ (at the USGS Conowingo Dam gauging station, ~15 km upstream of the Flats; http://www.water.usgs.gov) – during TS Agnes (1972) and in association with the remnants of TS Lee (2011). Tropical Storm Agnes produced the highest river discharge (~32,000 $m^3$ $s^{-1}$) ever measured on the Susquehanna River and delivered the

largest sediment loads (30 x $10^6$ tons) to the Chesapeake Bay (Gross et al. 1978). The second highest recorded discharge was associated with TS Lee (~22,000 $m^3$ $s^{-1}$) and delivered an estimated 6.7 to 19x$10^6$ tons of sediment to the Chesapeake Bay (Cheng et al. 2013; Hirsch 2012).

The Flats historically supported dense SAV beds during the growing season; however, SAV populations began to decline in the 1960s due to poor water quality, and largely disappeared following TS Agnes. There was little change in the SAV abundance between 1972 and 2000; a rapid resurgence began ~2001, with an increase in both bed area and plant density, lasting through 2008, when the bed reached a stable area of ~55 $km^2$ (Gurbisz and Kemp 2014). SAV area decreased to ~25 $km^2$ following TS Lee (Gurbisz et al. 2016), and although the bed area remained below 35 $km^2$, it gradually increased in size between 2012 and 2016 (Orth et al. 2016). Co-dominant SAV species on the Flats include wild celery (*Vallisneria Americana*), water stargrass (*Heteranthera dubia*), Eurasian watermilfoil (*M. spicatum*), and *Hydrilla verticillata* (Bayley et al. 1978; Gurbisz et al. 2016).

*Field methods*

Patterns of sedimentation were assessed at five primary sites inside the Flats SAV bed (Fig. 2.1b). Three replicate push cores (30 cm long, 5 cm diameter) were collected at each site during three sampling trips (4 August 2014, 29 May 2015, and 26 August 2015) to evaluate seasonal-scale sedimentation. These periods generally corresponded to SAV presence (August) and absence (May). One push core was collected at an additional eight sites within the SAV bed (secondary sites; Fig. 2.1b)

in August 2014 and May 2015 to increase spatial resolution. After collection, push cores were taken to the laboratory and sectioned into 1-cm intervals for analysis of grain size, bulk density, organic content, and the naturally occurring radioisotope $^{7}Be$ (half-life 53.3 days). SAV above-ground biomass data, collected for a companion study during the same three sampling trips, are reported in this study (C. Gurbisz unpublished data).

One vibracore (3 m long, 8 cm diameter) was collected at each of the five primary study sites in August 2014 to evaluate decadal-scale sedimentation. Vibracoring is a commonly used coring method in coastal sedimentary environments, with 80-100% core recovery in homogeneous sands and sandy muds (Lanesky et al. 1979), similar to those found on the Susquehanna Flats. Vibracores were frozen upon arrival to the laboratory. Cores were thawed and subsampled into 1-cm (top 20 cm), 2-cm (20 cm-80 cm), and 4-cm (80 cm-end of core) increments prior to performing grain size, bulk density, organic content, $^{210}Pb$, and $^{137}Cs$ analyses. Increment lengths varied down the core to reflect expectations of sediment age; i.e., highest resolution near the top of cores (youngest sediment), decreasing toward the base of cores (oldest sediment). Note that vibracores disturb the upper few centimeters of the sample, and so the upper sediment layers of the core were treated as a surface mixed layer to account for potential mixing during sediment collection.

*Laboratory methods*

Grain size was analyzed by wet-sieving samples at 64 μm to separate the mud (silts+clays; <64 μm) and sand (>64 μm) fractions. The mud fraction was

disaggregated with 0.05% sodium metaphospate in an ultrasonic bath and then analyzed using a Sedigraph 5120. The sand fraction was dry-sieved through a standard set of 13 sieves, from 500 μm to 64 μm (at ¼-phi size intervals; phi=-$\log_2$(particle diameter, mm)). The mud and sand data were joined to calculate median diameters. Bulk density was assumed to be a function of porosity, calculated from water loss after drying at 60°C until constant sediment weight was reached, assuming sediment density of 2.65 g $cm^{-3}$. Organic content was determined using a modified version of the methods of Johnson and Bustin (2006); sediment was digested in 30% $H_2O_2$ on hotplates set to 90°C. $H_2O_2$ was added to the sediment, at 10 mL increments, until it no longer effervesced. After the sediment was completely dry, it was rinsed with deionized (DI) water and placed in drying ovens set at 60°C. This method was chosen over loss on ignition due to the presence of coal in the sediment (Hainly et al. 1995).

Push-core samples were prepared and analyzed for $^{7}$Be activities following the methods of Palinkas et al. (2005). $^{7}$Be is a naturally occurring radioisotope produced through cosmic-ray spallation of nitrogen and oxygen in the atmosphere. It is deposited onto the Earth's surface through precipitation and dry deposition, where it is adsorbed onto sediment particles that are subsequently eroded and transported into adjacent waters, settling on the bottom sediment surface (Olsen et al. 1986). $^{7}$Be is well suited to measure seasonal deposition, and it has been used previously in dynamic estuarine environments (Olsen et al. 1986; Dibb and Rice 1989) and in seasonally vegetated tidal freshwater marshes (Neubauer et al. 2002; Palinkas et al. 2013).

To prepare samples for $^{7}$Be analysis, bulk sediment from the 1-cm increments of the push cores, starting with the topmost 1 cm (0-1 cm), was ground and placed into 60-mL plastic jars, which were filled to the same height to ensure consistent counting geometry. $^{7}$Be activities (dpm g$^{-1}$; disintegrations per minute per gram) were measured through gamma spectroscopy of the 477.7 keV photopeak, using germanium detectors, calibrated following Larsen and Cutshall (1981); gamma emissions were counted for 24 hours. For each core, analysis proceeded with every 1-cm section down the core until $^{7}$Be activity was not detected; one additional section below this horizon was counted. Measured $^{7}$Be activities were decay-corrected to the time of core collection and used to calculate depth-integrated $^{7}$Be inventories ($I_{total}$; dpm cm$^{-2}$) (ex. Fig. 2.2)

$$I_{total} = \sum_{i}^{n} A_i \cdot \rho_i \cdot h_i \quad (1)$$

where $A_i$ is the activity (dpm g$^{-1}$) in interval i, $\rho_i$ is the bulk density (g cm$^{-3}$) in interval i, and $h_i$ is the thickness (cm) of interval i. Errors in $^{7}$Be inventories were calculated by propagating the counting error associated with measuring $^{7}$Be activities. Total inventories were assumed to represent "new" sediment deposition between each sampling period, since >77 days (mean lifetime of $^{7}$Be) passed between each period.

Total $^{210}$Pb (half-life 22.3 y) activities were analyzed using alpha spectroscopy and following the procedures of Palinkas and Engelhardt (2016). $^{210}$Pb is produced naturally through $^{238}$U decay, and thus all sediment has "supported" $^{210}$Pb from the decay of its effective parent, $^{226}$Ra. Particles eroded from land and transported into adjacent waters can scavenge "excess" $^{210}$Pb from the water column, supplied from the atmosphere (gaseous $^{222}$Rn escapes to the atmosphere, decays to $^{210}$Pb, and is

scavenged by precipitation) and direct runoff (Koide et al. 1972; Nittrouer et al. 1979). $^{210}$Pb geochronology has previously been applied to vegetated habitats (Arnold et al. 2000; Palinkas and Koch 2012; Palinkas et al. 2016). In the present study, $^{226}$Ra-supported $^{210}$Pb activity was assumed to be equal to the activity at the bottom of each core and was calculated via gamma spectroscopy from a weighted average of the $^{214}$Pb energies (295 and 352 keV) and $^{214}$Bi photopeak (609 keV) (Palinkas and Engelhardt 2016). Excess $^{210}$Pb activities were obtained by subtracting supported $^{210}$Pb activity from the measured total $^{210}$Pb activities. All activities were decay-corrected to the time of collection; excess activities were normalized to the corresponding measured mud fraction, because $^{210}$Pb preferentially adsorbs to fine particles (Nittrouer et al. 1979; Goodbred and Kuehl 1998).

*Calculating sediment accumulation rates*

Two age-depth models were considered for calculation of sediment accumulation rates: the constant flux/constant sedimentation (CFCS) and constant rate of supply (CRS) models (Appleby and Oldfield 1978). The CFCS model assumes a constant supply of unsupported $^{210}$Pb to the sediment and steady-state sedimentation. Sedimentation rates (S; cm y$^{-1}$) are calculated by

$$S = -\lambda_{210Pb} * m \quad (2)$$

where $\lambda_{210Pb}$ is the $^{210}$Pb decay constant (0.031 yr$^{-1}$) and $m$ is the slope of the line fit between the log of excess $^{210}$Pb activity and depth. The constant rate of supply (CRS) model also assumes constant supply of unsupported $^{210}$Pb but allows for time-variable sedimentation rates. In this model, sediment age at depth $z$ ($t_z$) is calculated by

$$t_z = 1/\lambda_{210Pb} * \ln(A_0/A(z)) \quad (3)$$

where $\lambda_{210Pb}$ is the $^{210}$Pb decay constant (0.031 yr$^{-1}$), $A_0$ is the cumulative inventory of excess $^{210}$Pb activity in the sediment column, and $A(z)$ is the cumulative inventory of excess $^{210}$Pb activity below depth $z$. $^{210}$Pb inventory for each interval is calculated by multiplying excess $^{210}$Pb activity by the bulk density and thickness of that interval. The sedimentation rate is calculated by dividing sediment depth by its calculated age.

Sedimentation rates were calculated with both the CFCS and CRS models and verified with $^{137}$Cs, an independent chronometer. $^{137}$Cs activities were measured through gamma spectroscopy of the 661.6-keV photopeak, following the methods described above for $^{7}$Be (Palinkas and Nittrouer 2007). $^{137}$Cs is an anthropogenically derived radioisotope that was introduced to the atmosphere through nuclear weapons testing, first appearing in the sedimentary record in 1954. The maximum fallout of $^{137}$Cs occurred in 1963 prior to the Partial Nuclear Test Ban Treaty ratification (Walling and He 1997). The depths of the 1954 and 1963 horizons identified from $^{137}$Cs for each core were compared to the depth range predicted by the CRS model for these years.

*Comparing SAV distribution to sedimentation*

Submersed aquatic vegetation (SAV) density data on the Flats (1984-1987; 1988-2014) were obtained from the Virginia Institute of Marine Sciences (VIMS) SAV in Chesapeake Bay and Coastal Bays GIS data server, which reports data from annual aerial surveys (http://web.vims.edu/bio/sav/gis_data.html; Orth et al. 2016). The density class (0%, <10%, 10-40%, 40-70%, and 70-100%) was extracted at each

primary site and reported as the median percentage in each range (i.e. 0%, 5%, 25%, 55%, and 85%).

To assess the relationship of sediment accumulation rates with historical SAV presence/absence on the Flats, annual accumulation rates at each primary site were calculated by interpolating between the sediment ages from the CRS model. The annual sedimentation data then was directly compared to SAV density maps. Because SAV density data were not collected prior to 1984, sediment accumulation rates and SAV density were compared qualitatively within 3 time periods: 1) abundant SAV prior to TS Agnes in 1972 (<1972; Bayley et al., 1978); 2) no SAV between TS Agnes and a resurgence in the early 2000s (1972-2000; Gurbisz and Kemp 2014); 3) abundant SAV following the resurgence (2001-2014).

*Supporting data*

Daily Susquehanna River discharge ($m^3$ $s^{-1}$) data at Conowingo, MD (the last downstream gauge on the Susquehanna River) were obtained between 1 March 2014 and 1 September 2015 from the USGS National Water Information System (http://www.water.usgs.gov; station 01578310). Suspended-sediment concentrations (SSC; mg $L^{-1}$) at the Conowingo Dam outlet were obtained over the same time period from the Chesapeake Bay Program water-quality database (http://www.chesapeakebay.net/data). Suspended-sediment concentrations data were collected ~1-2 times a month, depending on flow conditions, while Susquehanna River discharge data were averaged for each day. Assuming that the instantaneous SSC measurements represent daily conditions, daily SSC values were calculated by

establishing an empirical relationship with daily Susquehanna River discharge. First, additional SSC and discharge data were obtained from 4 October 2011 to 1 September 2015 to establish a longer record. 4 October 2011 was chosen to exclude discharge from TS Lee in September 2011 (Palinkas et al. 2014) and instead include only similar discharges as occurred during the study period. Then, an exponential model was fit to Susquehanna River discharge data on days with available SSC measurements to predict daily SSC values over the entire study period ($R^2$=0.72, $p<0.001$). Daily Susquehanna River discharge and calculated SSC were multiplied to obtain a daily sediment load. The daily sediment loads were summed over the 77 days (mean lifetime of $^7$Be) prior to sampling in order to estimate sediment loads associated with seasonal-scale coring observations.

*Statistical Analyses*

All statistical analyses were performed in R version 3.3.2. I used the package "lme4" (Bates et al. 2015) to perform a linear mixed-effects analysis to determine the effect season (fixed effect) had on surficial sediment grain size, $^7$Be inventory, and above-ground biomass among the core locations (random effect). Analysis of variance (ANOVA) tests, comparing models with and without fixed effects, were used to obtain p-values. Pairwise linear regressions were performed to determine correlations between sediment grain size, $^7$Be inventory, and above-ground biomass over the three sampling periods. An intervention analysis using the package "struccchange" (Zeileis et al. 2003) was performed to identify breakpoints, or structural changes, in the sedimentation time series. These breakpoints were then used

to examine differences in decadal-scale accumulation rates among the three periods with different SAV abundances (<1972, 1972-2000, 2001-2014). Additionally, linear regression models were developed to determine the CFCS fit for the vibracores and the relationship between SAV bed area and annual accumulation rates. For all statistical tests, p-value <0.05 was considered significant. A Bonferroni correction was made to adjust the p-value to account for errors due to multiple comparisons.

## Results

*Susquehanna River discharge and sediment supply*

Average river discharges preceding the August sampling in 2014 and 2015 were similar: 980±92 $m^3 s^{-1}$ and 940±74 $m^3 s^{-1}$, respectively (Fig. 2.3a). Prior to the May 2015 sampling, average river discharge was 1670±110 $m^3 s^{-1}$, ~1.5-2 times larger than the August discharges. Maximum river discharges during the study period were associated with the 2015 spring freshet (4560 $m^3 s^{-1}$ on 12 April) and periods of prolonged precipitation during late spring 2014 (4900 $m^3 s^{-1}$ on 19 May) and early summer 2015 (2600 $m^3 s^{-1}$ on 2 July). All of these discharges exceeded the $90^{th}$ percentile of Susquehanna River flows at Conowingo since monitoring began in 1968 (>2400 $m^3 s^{-1}$).

Because SSC was calculated directly from river discharge, higher SSC tended to occur in the spring, when river discharge was highest, and lower SSC occurred in the summer, when river discharge was lowest (Fig. 2.3b). Average SSC values preceding the August 2014, May 2015, and August 2015 samplings were 9.0±1.2 mg $L^{-1}$, 14.0±1.3 mg $L^{-1}$, and 7.8±0.4 mg $L^{-1}$, respectively. Maximum calculated SSC

values during each study period occurred on the same dates as maximum discharge and were 85.8 mg $L^{-1}$, 69.3 mg $L^{-1}$, and 20.1 mg $L^{-1}$ on 19 May 2014, 12 April 2015, and 2 July 2015, respectively.

The total sediment loads (calculated as the product of river discharge and SSC) delivered by the Susquehanna River prior to the August 2014, May 2015, and August 2015 samplings were $1.1x10^5$ tons, $2.3x10^5$ tons, and $6.6x10^4$ tons, respectively.

*Seasonal variability of sedimentation and vegetation biomass*

Although the general character of surficial sediment on the Flats was sandy (>64 um), median grain size of the upper 1 cm of push cores varied both spatially and temporally, ranging from 113.1 to 405.3 μm over the study period (see Table A.1 in the supplementary material). The average median grain size across all sites (n=13) was statistically similarly (p-value=0.68) at 290.5±22.6 μm and 281.1±16.4 μm in August 2014 and May 2015, respectively (Table 2.1). Over the primary sites (n=5), the average median grain size in August 2015 was 215.0±31.7 μm, but was not significantly different from May 2015 after applying a Bonferroni correction (p=0.05). Grain size typically decreased with distance from the river mouth. Larger grain sizes were also observed at sites near the main channel (west of the bed) and the discontinuous channel (north of the bed; see Fig. 2.1b). During both Augusts, the smallest median grain size was observed in the middle of the SAV bed at SF3. Organic content was negatively correlated with grain size and ranged from 0.50 to 5.78% over the three periods (Table A.1).

Total $^{7}$Be inventories also varied spatially and temporally (Table 2.1 and Table A.1). Over the study period, $^{7}$Be inventories ranged from below detection (minimum detection activity for this study 0.5 dpm $g^{-1}$) to 3.53 dpm $cm^{-2}$. Sites where $^{7}$Be activity was not detected were assigned an inventory of 0 dpm $cm^{-2}$, which assumes no deposition. Average $^{7}$Be inventory was 0.71±0.21 dpm $cm^{-2}$ in August 2014, where six of the thirteen sites contained detectable $^{7}$Be, and 0.67±0.23 dpm $cm^{-2}$ in May 2015, where four of the thirteen sites contained detectable $^{7}$Be (Table 1). Although the average $^{7}$Be inventories in August 2014 and May 2015 were statistically similarly ($p=0.92$), the locations with detectable $^{7}$Be activity were different between the two seasons. In general, the sites with detectable $^{7}$Be activity in August 2014 were adjacent to a narrow, unvegetated channel that ran northwest to southeast along the center of the SAV bed, while in May 2015, the sites with detectable $^{7}$Be were near the southwestern and southern boundaries of the bed. In August 2015, $^{7}$Be was present at all five sites sampled, with an average $^{7}$Be inventory of 2.23±0.52 dpm $cm^{-2}$. When only the five primary (SF1-5) were included in the statistical tests, mean $^{7}$Be inventories were significantly higher in August 2014 ($p=0.01$) and August 2015 ($p<0.001$) than in May 2015.

SAV was collected along with push cores at all sites, except sites SF1 and SF5 that were outside the 2014 and 2015 SAV bed boundaries (http://web.vims.edu/bio/sav/maps.html). Average above-ground biomass was 301.1±458.0 g $m^{-2}$ in August 2014 (n=11), 40.9±230.4 g $m^{-2}$ in May 2015 (n=11), and 271.8±113.9 g $m^{-2}$ in August 2015 (n=3) (C. Gurbisz unpublished data; Table 2.1). Spatial heterogeneity of biomass is indicated by the relatively high standard

deviations, as well as aerial imagery from August 7, 2014 (Landsat-8 USGS 2017; see Fig. 2.1b). This photo highlights areas inside the SAV bed boundary with sparse or absent vegetation, as well as a channel near the transect of primary sites.

There were no statistically significant linear relationships between grain size, $^{7}$Be inventory, or above-ground biomass over the three sampling periods after applying a Bonferroni correction factor (Table S2).

*Decadal patterns of sedimentation*

Vibracores from all sites (n=5) had relatively coarse material (median grain size >196 μm) in the upper 10 cm; however, grain-size trends below this depth varied for each site. For example, SF1 had the largest range in median grain size and a distinct coarsening upward trend, in which median grain size ranged from 6.3 μm at the bottom of the core (120-124 cm) to 359.0 μm towards the top of the core (13-14 cm), with an average of 231.5±29.96 μm. Grain size at SF5 varied from 5.9 μm (at 50-52 cm depth) to 205.7 μm (at 2-3 cm depth), with an average of 123.8±19.6 μm. Sediments in the upper 20 cm of the core contained fine and medium sand (median diameter 196 to 390 μm), underlain by a layer of finer material (82.5 to 150 μm) between ~20 and 40 cm. Median grain size was finer for the remainder of the core (50-76 cm), ranging from 5.9 to 96.5 μm. Median grain size varied the least at SF4, ranging from 102.0 to 234.1 μm, with an average of 185.6±11.6 μm. Similar to the patterns at SF5, cores from SF2 (average median grain size of 210.1±43.3 μm) and SF3 (average median grain size of 189.7±25.8 μm) did not have any consistent trends

with depth but rather had interlayering of medium and fine sand (125-390 μm) with very fine sand and silt (9-125 μm).

Organic matter in the vibracores ranged from 0 to 4.6% with an average of 1.4±0.42% at SF1, from 0.44 to 6.85% with an average of 2.37±0.41% at SF2, from 0 to 6.55% with an average of 2.56±0.38 at SF3, from 0.39 to 16.75% with an average of 2.77±0.87% at SF4, and from 0 to 3.77% with an average of 1.69±0.25% at SF5.

Trends in excess $^{210}$Pb activities (normalized to mud content) also varied among cores, reflecting differences in the nature of sedimentation. As noted in the Methods, steady-state accumulation is usually indicated by a relatively steady log-linear decrease of $^{210}$Pb activities with depth, whereas more variable down-core $^{210}$Pb activities indicate non-steady-state accumulation. The former is present in SF1 (underneath a ~20 cm thick surface layer) and SF5 (Fig. 2.4a). In contrast at SF2 and SF4, excess $^{210}$Pb activities decreased log-linearly to ~30 cm, then varied with depth, indicating non-steady-state accumulation (Fig. 2.4b). SF3 also showed non-steady state behavior, with excess $^{210}$Pb activities initially increasing from 8 to 23 dpm $g^{-1}$ in the surface layer (0-15cm), then decreasing (Fig. 2.5b). Intervals with low $^{210}$Pb activities and high mud content were present in all cores, such as those at 29 and 65 cm at SF3 (Fig. 2.5a and 2.5b).

Figure 2.5 shows an example $^{210}$Pb profile, CFCS model fit, and CRS-determined accumulation rates for SF3. SF1, SF4, and SF5 had relatively robust CFCS model fits, with $R^2$ values of 0.71, 0.60, and 0.75 and p-values 0.0001, 0.006, and, 0.0004, respectively. The average accumulation rates calculated by the model were 0.68 cm $y^{-1}$ at SF1, 0.52 cm $y^{-1}$ at SF4 and 0.41 cm $y^{-1}$ at SF5. The model fits at

SF2 and SF3 were relatively weak ($R^2$=0.24 and 0.27, respectively) and not statistically significant (p=0.2 and 0.06, respectively). The CRS core-averaged accumulation rates decreased with increased distance from the Susquehanna River mouth, ranging from 0.91±0.05 cm $y^{-1}$ (1.25±0.12 g $cm^{-2}$ $y^{-1}$) at SF1 to 0.46±0.03 cm $y^{-1}$ (0.63±0.04 g $cm^{-2}$ $y^{-1}$) at SF5. The average accumulation rates calculated with the CFCS model were within 15% of those from the CRS model at SF4 and SF5, but were 25% lower at SF1 (Table 2.2).

Average sedimentation rates were also calculated from the 1954 and 1963 $^{137}$Cs horizons. Note that the 1954 and 1963 horizons were identifiable in all cores except at SF2, where only one horizon was present and assumed to be 1963, since its activity was comparable to the 1963 horizon in other cores. Average sedimentation rates calculated from the $^{137}$Cs horizons (1954 and 1963) are listed in Table 2.2. The average accumulation rates at SF4 and SF5 calculated from the CFCS model were within 10% of the rates calculated from the $^{137}$Cs horizons, while SF1 was within 30%. The 1954 and 1963 horizons indicated by the $^{137}$Cs data were within the depth range predicted by the CRS model (see Table 2.2; Fig. 2.5d) for all intervals except the 1963 horizons in cores SF2 and SF4, which were within 2 cm.

Sediment ages could only be calculated up to 1990 in core SF1 due to the large surface mixed layer. Therefore, results obtained from SF1 were omitted from the following average annual SAV density and accumulation calculations. Average SAV was <4% between 1984 and 2000 (Fig. 2.6a). SAV density generally increased between 2001 and 2007, except for declines in 2003, 2004, and 2006. SAV density remained high and stable from 2008 through 2010, and then decreased in 2011 and

2012. SAV density remained constant between 2012 and 2014. SAV bed area showed similar patterns to changes in SAV density over time, with total bed area <25 $km^2$ between 1984 and 1999, and rapidly increasing to 55 $km^2$ between 2000 and 2010 (Gurbisz and Kemp 2014). SAV bed area then decreased to 25 $km^2$ in 2012, and remained <30 $km^2$ through 2014 (Orth et al. 2016).

Average annual accumulation rates ranged from 0.95±0.16 to 1.06±0.16 g $cm^{-2}$ $y^{-1}$ 1950-1972, from 0.76±0.12 and 0.93±0.16 g $cm^{-2}$ $y^{-1}$ between 1972 and 2000, and from 0.95±0.16 to 1.09±0.19 g $cm^{-2}$ $y^{-1}$ between 2001 and 2008 (Fig 2.6b). Statistical structural breaks (see Methods) occurred at 1971, 1979, 1992, and 2000 in the time series. Average annual accumulation rates prior to 1950 are not reported because this was the earliest date that was calculated for SF2 using the CRS model. Calculating average annual accumulation rates beyond 2008 were limited by surface mixed layers. Average accumulation rates when SAV were present (i.e. 1950-1972 and 2001-2008) were significantly greater ($p<0.001$, for both periods) than when SAV were absent (1972-2000). SAV bed area explained 75% of the variability in average annual accumulation rates ($p<0.001$; Fig 2.7).

## Discussion

### *Seasonal-scale dynamics*

The spatial patterns of grain size on the Flats are consistent with other river-dominated deltaic environments, where grain size generally decreases with distance from the river mouth. These changes are typically driven by increases in basin width and decreases in fluvial influence (Fisk et al. 1954; Wright 1977), which decrease

energy (current velocities) and fine-sediment supply with distance from the river mouth. Thus, larger grain sizes near the main channel reflect higher current velocities that produce stronger shear stresses capable of winnowing away finer particles and/or preventing them from settling (Kuehl et al. 1986). Grain-size differences in the middle of the SAV bed between spring (no SAV) and summer (SAV) likely also reflect changes in energy, since high plant densities decrease current velocities and allow finer particles to settle (van Katwijk et al. 2010; Sand-Jensen 1998).

However, sediment deposition on the Flats is highly variable in time and space, as shown by the variability in $^{7}$Be inventories. Because this variability could not be explained through relationships with grain size and SAV biomass, differences in pathways of sediment supply to individual sites likely influence sediment deposition. Sediment-transport pathways over marshes are functions of discharge, topography, vegetation, proximity to channels/marsh edges, and hydrodynamic gradients (Temmerman et al. 2005; D'Alpaos et al. 2007; Marani et al. 2003). Furthermore, interactions between hydrodynamics and vegetation are important controls on the geomorphic evolution of tidal landscapes (Temmerman et al. 2007; van Wesenbeeck et al. 2008; Vandenbruwaene et al. 2011). On the Flats, differences between spring and summer $^{7}$Be inventory patterns likely arise from differences in flow patterns between seasons, due to differences in river discharge, sediment supply, and vegetation coverage. Although sediment supply is significantly greater during the spring, the statistically similar average $^{7}$Be inventories measured during spring and summer on the Flats along with the presence $^{7}$Be at sites on the southwestern and southern edges of the SAV bed in the spring suggest that downstream sediment

transport, and thus bypassing of the Flats, is facilitated by higher river discharges and the absence of vegetation to increase bottom friction.

Spatial patterns in $^{7}$Be inventories in August and May are not simple functions of distance from sediment source (i.e. Susquehanna River), but rather appear to be driven by geomorphic differences. The geomorphology of the Flats is spatially complex, as shown in Fig 2.1b by the unvegetated patches and shallow channels through the SAV bed. Water flow can be diverted around and between vegetation patches, increasing current velocities and associated near-bottom shear stresses (Cotton et al. 2006; Bouma et al. 2007) and thus promoting non-deposition and/or erosion (van Wesenbeeck et al. 2008; Vandenbruwaene et al. 2011). These faster velocities are not conducive for plant growth or seed germination, creating a feedback loop that prevents lateral expansion of the vegetation patch (van Wesenbeeck et al. 2008) and maintaining channel morphology. I propose that these channels influence the sedimentation patterns by directing sediment-rich fluvial waters into the interior of the bed without much interaction with upstream vegetation. These waters can then "spill over" onto shallower areas on the sides of the channel, so that sites closest to the channel receive relatively large suspended-sediment inputs. This is consistent with observations of higher $^{7}$Be inventories at sites adjacent to channels. Sediment supply decreases with distance from the channel due to increased sediment settling facilitated by vegetation that intercepts sediment and slows currents (French and Spencer 1993; Leonard and Luther 1995; Christiansen et al. 2000; Neubauer et al. 2002; Palinkas et al. 2013). This may explain why sites inside the SAV bed that were not adjacent to a channel did not have measurable $^{7}$Be activity. This process creates a

local increase in sedimentation at the channel edge similar to patterns observed in subaerial floodplains (Lambert and Walling 1987) and on vegetated tidal marsh platforms (D'Alpaos et al. 2007; Palinkas and Engelhardt 2016). Thus, while the spatial heterogeneity of Flats geomorphology can explain the observed patterns, it prevents robust statistical relationships between $^{7}$Be inventory and the linear distance to the nearest channel for all sites.

*Decadal-scale geochronology and relationship with vegetation*

The nature of long-term sedimentation is revealed by core profiles of $^{210}$Pb activity. Core profiles from areas with steady-state sedimentation (relatively constant sediment supply over time) exhibit relatively uniform grain size and log-linear decreases in excess $^{210}$Pb activities with depth. In contrast, core profiles from areas with pulsed sedimentation (e.g. from flood events) have more variable grain size and $^{210}$Pb activities with depth (Jaeger et al. 1998). The former are well described by the CFCS model, which assumes steady-state sedimentation, but the latter requires a different approach, typically the CRS model. On the Flats, robust regression fits were obtained at SF1, SF4, and SF5 with the CFCS model, explaining much of the down-core variability in $^{210}$Pb activities; the weak fits at SF2 and SF3 were not statistically significant. The CRS model provides insight into the role of variable sedimentation, especially at these latter two sites, by allowing calculation of discrete sediment ages (and corresponding sedimentation rates) down cores that can be compared with potential environmental influences. On the Flats, two major influences are large flood events and historical changes in vegetation coverage.

Sediment delivery to the Flats is largely controlled by the Susquehanna River, which has had several large historical flood events (Schubel and Pritchard 1986; Gross et al. 1978). Sediment deposits from these events are an important part of the sedimentary record in the upper Chesapeake Bay (Hirschberg and Schubel 1979) and can be recognized in core profiles by layers with relatively low excess $^{210}$Pb activities and high mud content (Sommerfield et al. 1999; Palinkas et al. 2005); e.g., signatures present at ~30 cm and ~65 cm in core SF3 (Fig. 2.5a and 2.5b). Flood layers in sediment cores on the Flats correspond to several historic flood events of the Susquehanna River, especially TS Agnes in 1972 (Zabawa and Schubel 1974) and a large flood event in 1936 (Hirschberg and Schubel 1979). Flood layers corresponding to these events were found at SF1, SF2, SF3, and SF4; the absence at SF5 may reflect the relatively coarse-scale of sampling intervals or lack of obvious signature in core profiles. Anomalously low activities tend to decrease the slope (and $R^2$) of the regression fit between $^{210}$Pb activities and depth, resulting in underestimated sediment accumulation rates. This is evident by the much lower average CFCS model rates than both the average CRS model rate and $^{137}$Cs derived rates for SF2 and SF3, which were most impacted by pulsed sedimentation (lowest $R^2$ values). The CFCS and CRS average rates were more similar for sites with higher CFCS $R^2$ values (>0.5; e.g. SF4 and SF5), reflecting more steady-state sedimentation.

Abrupt changes between historical periods with and without large SAV populations on the Flats can also drive sedimentation patterns. The decline in average annual sediment accumulation on the Flats after 1971 is coincident with the precipitous decline in SAV following Agnes (Bayley et al. 1978). Similarly, the rapid

increase in average annual sediment accumulation after 2000 is consistent with the resurgence of the Flats SAV bed in the early 2000s (Gurbisz and Kemp 2014). Although sedimentation appears to gradually increase between 1980 and 1998 in Fig 2.5a, this may be an artifact due to linear interpolation between consecutive samples analyzed at relatively coarse intervals (~5 cm). The robust regression fit between total SAV bed area and average sediment accumulation rates indicates that these variables are strongly correlated, which further supports that a positive feedback mechanism exists between total SAV bed size and sediment trapping on the Flats. However, because data of SAV bed area were not available prior to 1984, and accumulation rates could only be calculated through 2008, the time-series data were not able to capture changes due to TS Lee. Based on the comparison between the historical periods with and without SAV, I expect that the decrease in bed area would also lead to a decrease in sediment accumulation rates. However, sediment load likely controls accumulation rates as well. For example, SAV bed area decreased between 2002 and 2003, and SAV bed density decreased between 2002 and 2004, while accumulation rates appear to increase over both years. In contrast, SAV bed area and density rapidly increase in both 2007 and 2008, while accumulation rates remain relatively constant. Both 2003 and 2004 were relatively wet years, while 2007 and 2008 were relatively dry years (Gurbisz and Kemp 2014), which further indicates that annual accumulation rates are sensitive to both SAV bed area and sediment supply.

**Summary**

Dense SAV beds disappeared from the Flats following TS Agnes in 1972, but recovered in the early 2000s. Because these seasonally vegetated beds are immediately downstream from the largest sediment source to the upper Chesapeake Bay, they are important for modulating the sediment input to the Chesapeake Bay. The main objective of this study was to assess how these seasonal and decadal shifts in vegetation influence sedimentation at corresponding time scales. Although variability in seasonal-scale sedimentation cannot be explained by grain size and SAV density, Susquehanna River discharge and Flats geomorphology strongly influence the spatial and temporal patterns of sedimentation; i.e. sites closest to channels had greater sedimentation. At decadal scales, variability in fluvial sediment supply and abrupt changes in SAV abundance influence sedimentation. Historical periods of SAV presence and absence generally correspond with higher and lower sedimentation rates, respectively. Additionally, the strong correlation between SAV bed area and average annual sediment accumulation on the Flats suggest a positive feedback between these variables exist.

**Tables**

Table 2.1 Average (over sample period) surficial (0-1 cm) median grain size and organic content, depth-integrated $^{7}$Be inventories, and above ground biomass (C. Gurbisz; unpublished data) for push cores. Standard errors are reported for all columns except depth-integrated $^{7}$Be inventories, for which the error is the propagated $^{7}$Be activity counting error. The (n*) under the inventory column represents the number of sites with detectable $^{7}$Be activity; inventories for sites with non-detectable $^{7}$Be were assumed to be 0 dpm cm$^{-2}$ (no deposition).

| Date | Grain size (μm) | Organic Content (%) | Inventory (dpm cm$^{-2}$) | Biomass (g m$^{-2}$) |
|---|---|---|---|---|
| Aug 2014 (n=13) | 290.5±22.6 | 2.03±0.32 | 0.71±0.21 (6*) | 254.8±111.8 |
| May 2015 (n=13) | 281.1±16.4 | 1.98±0.28 | 0.67±0.23 (4*) | 34.6±17.2 |
| Aug 2014 (n=5) | 259.6±44.8 | 2.64±0.65 | 1.52±0.33 (4*) | 339.6±291.9 |
| May 2015 (n=5) | 282.9±21.9 | 2.22±0.31 | 0.71±0.18 (1*) | 17.3±2.0 |
| Aug 2015 (n=5) | 215.0±31.7 | 3.06±1.01 | 2.23±0.52 (5*) | 163.1±68.7 |

Table 2.2 Decadal-scale sediment accumulation rate data: CFCS rate; total $^{210}$Pb inventory; core-averaged CRS rate; 1954 $^{137}$Cs depth range and corresponding average accumulation rate; 1963 $^{137}$Cs depth range and corresponding average accumulation rate; CRS-predicted 1954 and 1963 depth ranges; average CRS annual rates from1950-1972 (1950 was chosen because it was the earliest date SF2 could be dated with $^{210}$Pb), from 1972-2001, and from 2001-2008. *Indicates only rates between 1972 and 1990 could be calculated due to large surface mixed layer. NA indicates no data available.

| Site | CFCS cm $y^{-1}$ ($R^2$) | Total $^{210}Pb$ inventory dpm $cm^{-2}$ | CRS core-average cm $y^{-1}$ (g $cm^{-2}$ $y^{-1}$) | 1954 $^{137}Cs$ depth cm (cm $y^{-1}$) | 1964 $^{137}Cs$ depth cm (cm $y^{-1}$) | CRS 1954 depth range cm | CRS 1963 depth range cm | CRS rate 1950-1972 g $cm^{-2}$ $y^{-1}$ | CRS rate 1972-2001 g $cm^{-2}$ $y^{-1}$ | CRS rate 2001-2008 g $cm^{-2}$ $y^{-1}$ |
|---|---|---|---|---|---|---|---|---|---|---|
| **SF1** | 0.68 (0.71) | 1263.0 | 0.91±0.05 (1.25±0.12) | 54-56 (0.92) | 50-52 (1.00) | 52-56 | 48-52 | 1.40±0.01 | 1.60±0.03* | NA |
| **SF2** | 0.33 (0.24) | 295.5 | 0.75±0.03 (1.15±0.04) | NA | 34-36 (0.69) | 46-50 | 36-40 | 1.24±0.002 | 1.07±0.008 | 1.22±0.008 |
| **SF3** | 0.33 (0.27) | 451.4 | 0.72±0.05 (1.08±0.07) | 42-44 (0.72) | 38-40 (0.76) | 42-48 | 38-42 | 1.29±0.02 | 0.85±0.03 | 1.28±0.04 |
| **SF4** | 0.52 (0.60) | 345.0 | 0.61±0.03 (0.78±0.06) | 34-36 (0.58) | 28-30 (0.57) | 34-40 | 30-34 | 0.86±0.05 | 0.89±0.01 | 1.09±0.02 |
| **SF5** | 0.41 (0.65) | 438.6 | 0.46±0.03 (0.63±0.04) | 24-26 (0.42) | 19-20 (0.38) | 24-28 | 17-22 | 0.62±0.03 | 0.46±0.02 | 0.53±0.01 |

## Figures

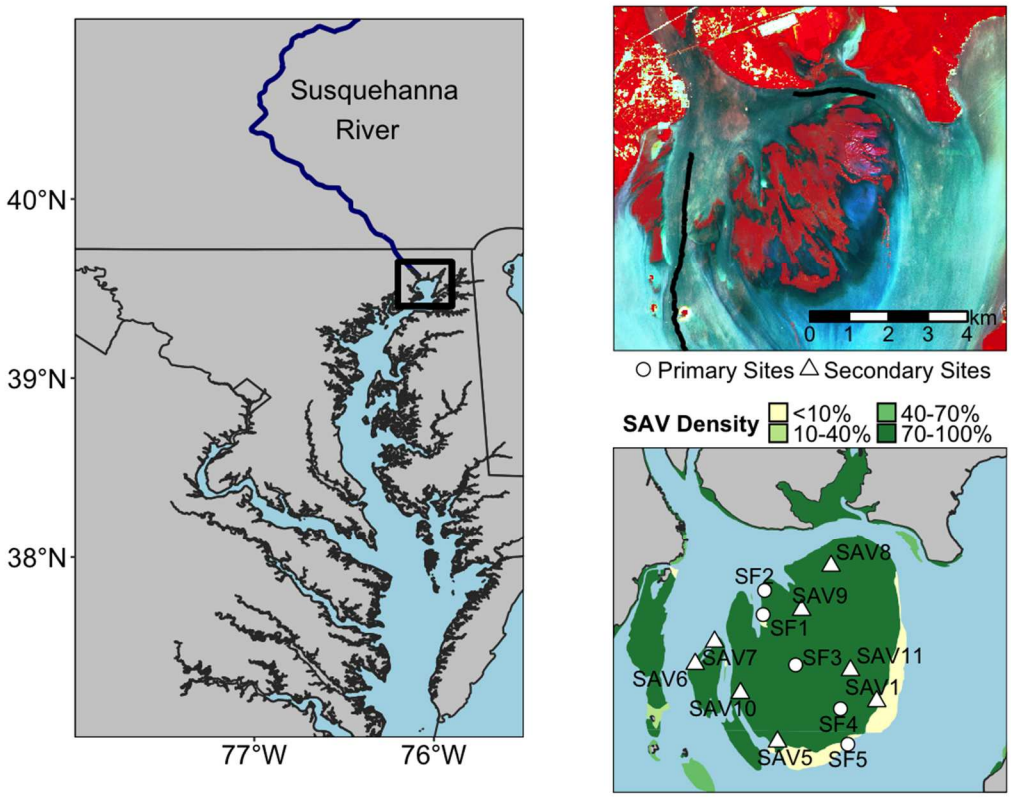


**Figure 2.1** a) Map of Chesapeake Bay and the lower portion of the Susquehanna River, with the location of Susquehanna Flats indicated by the box. b) Landsat imagery collected on August 7, 2014 near low tide. The black lines indicate the location of the main channel to the west of the bed and discontinuous channel to the north of the bed. c) Primary (circles) and secondary (triangles) coring locations superimposed over 2014 SAV density map (VIMS).

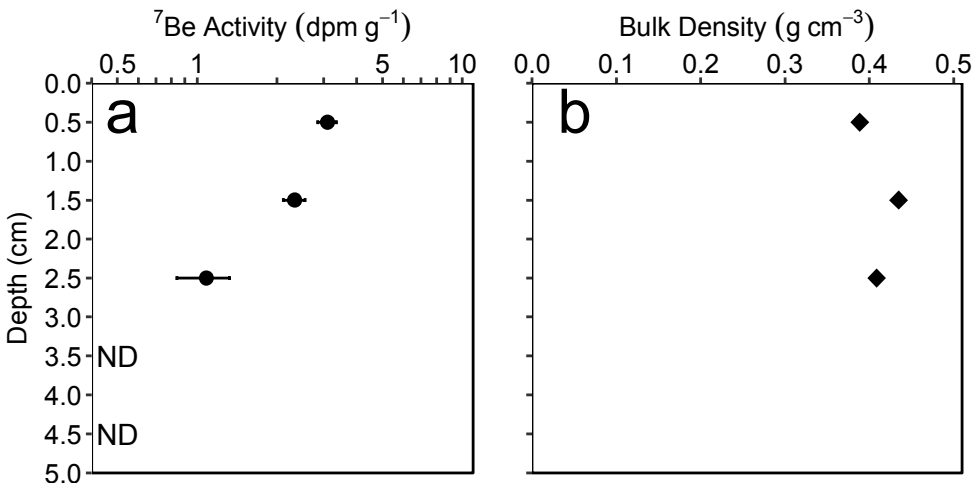


**Figure 2.2** a) Down-core $^{7}$Be activity and b) bulk density at SF3 in August 2014. $^{7}$Be inventory was calculated through equation 1, multiplying the $^{7}$Be activity of each depth interval by its bulk density and thickness (1 cm) and summing over the entire core. Inventory in this core was 2.66±0.29 dpm cm$^{-2}$. All errors were propagated from $^{7}$Be activity counting errors.

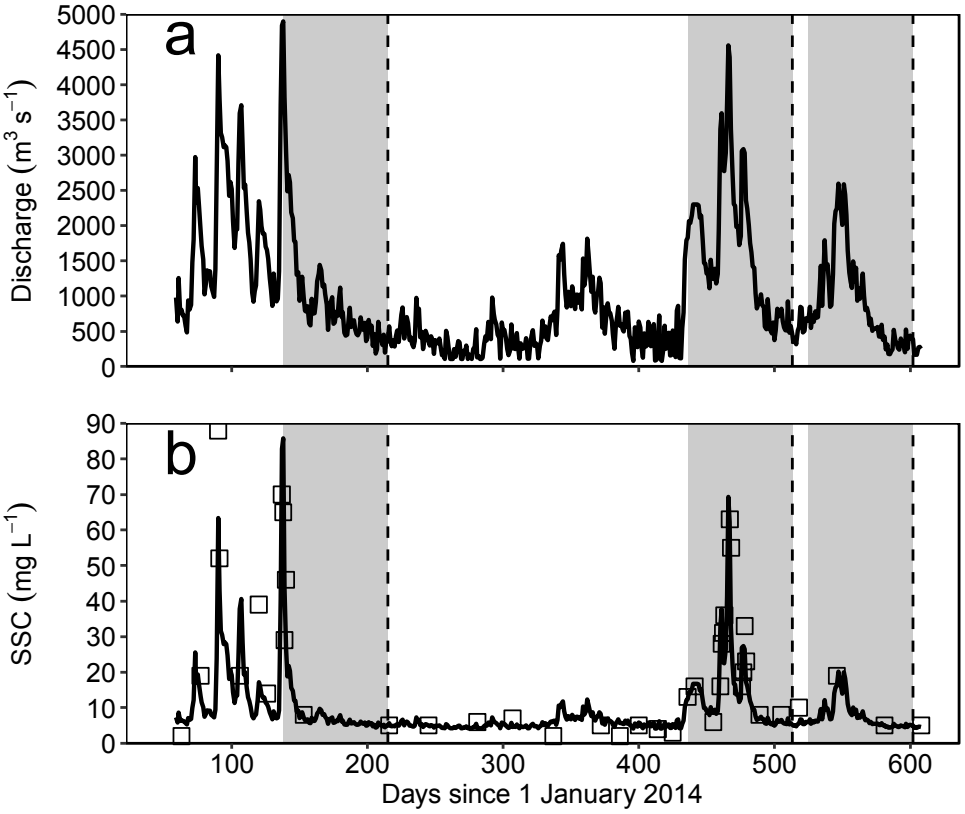


**Figure 2.3** a) Daily Susquehanna River discharge and b) calculated suspended-sediment concentration (SSC) at the Conowingo Dam between 1 March 2014 and 1 September 2015. Open squares in the SSC time series indicate measured values. In both figures, shaded regions represent the three periods over which sediment deposition was calculated, with right and left boundaries corresponding to the sampling date and the 77 days prior to sampling, respectively.

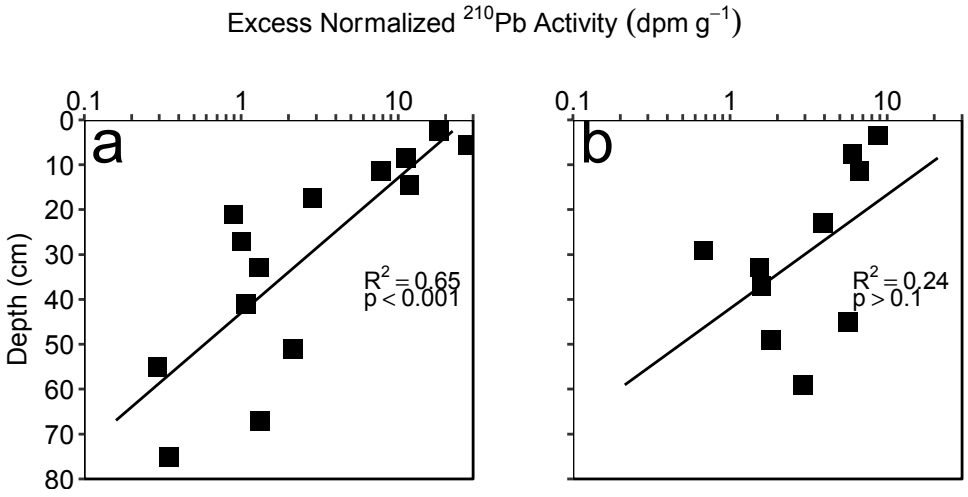


**Figure 2.4** a) SF5 depicts more steady state sedimentation, as indicated by the higher $R^2$ value, while b) SF2 depicts more non-steady state sedimentation, as indicated by the low $R^2$ value.

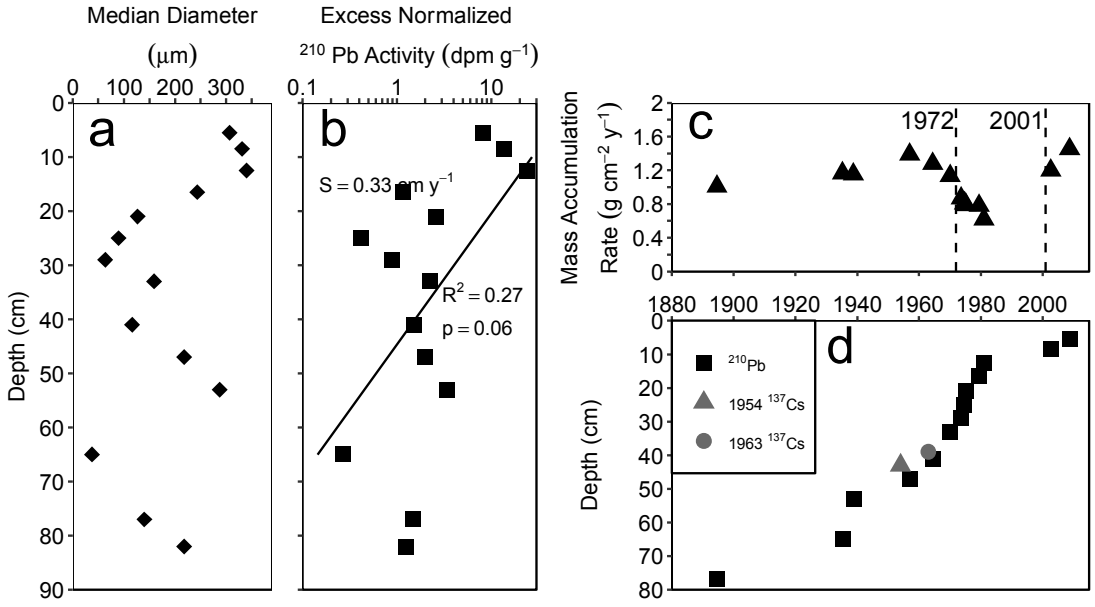


**Figure 2.5** SF3 down-core profiles of a) median diameter and b) excess normalized $^{210}$Pb activity, showing CFCS model regression fit and average accumulation rate. c) Corresponding CRS-derived mass accumulation rates over time (top right) with dashed lines indicating SAV disappearance in 1972 and reappearance in 2001. d) Down-core CRS-predicted sediment ages (black squares); the grey triangle and circle indicate horizons associated with 1954 and 1963, respectively, by $^{137}$ Cs data.

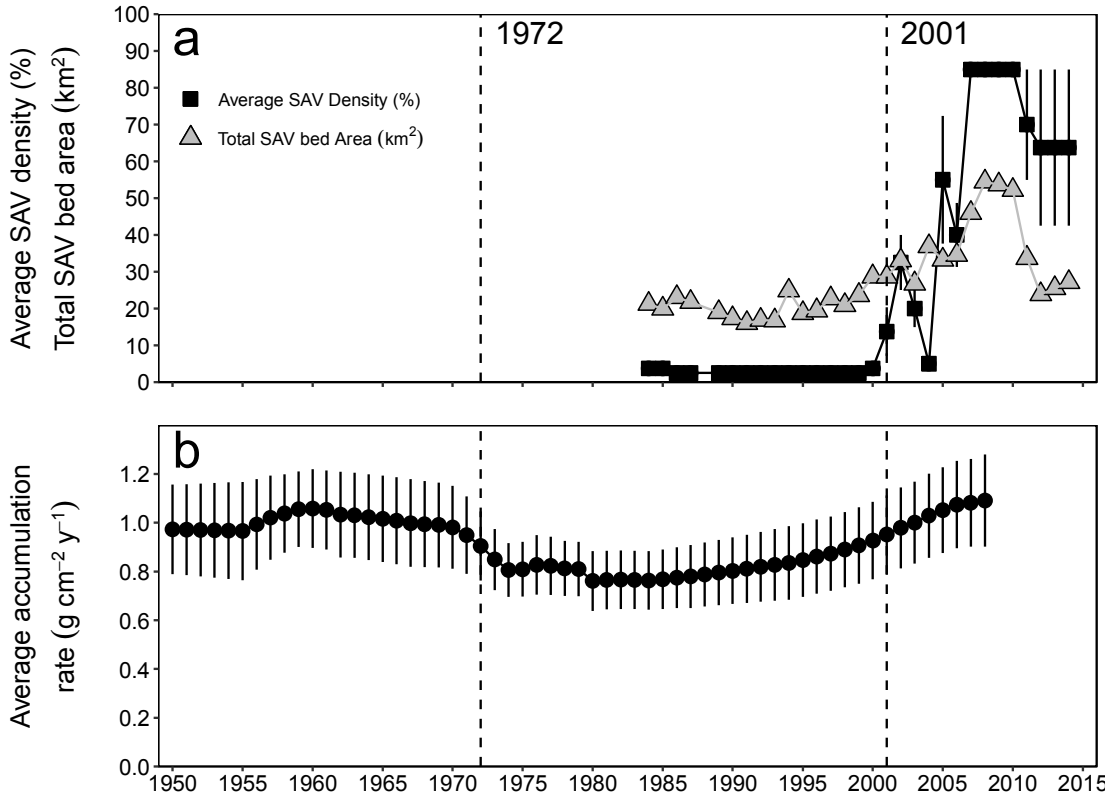


**Figure 2.6** a) Time series of average SAV density across sites SF2-SF5 (Orth et al. 2016) and total SAV bed area (Gurbisz and Kemp 2014) and b) average annual accumulation rates across sites SF2-SF5. The dashed lines indicate years of SAV disappearance (1972) reappearance (2001).

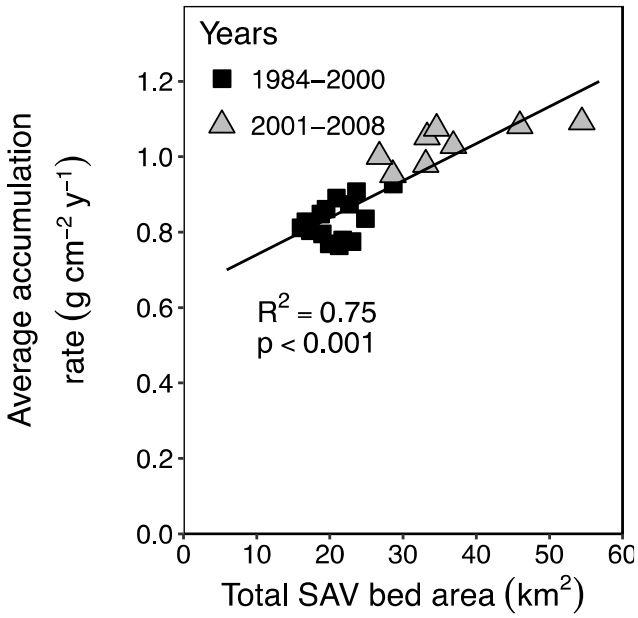


**Figure 2.7** Linear regression between total SAV bed area and average annual accumulation rate across sites SF2-SF5 between 1984 and 2008. Years before SAV resurgence (1984-2000) indicated by black squares and years after SAV resurgence (2001-2008) indicated by grey triangles.

# Chapter 3 : Sediment geochemical patterns and provenance in upper Chesapeake Bay

**Abstract**

Geochemical patterns in upper Chesapeake Bay sediments can reflect a variety of important processes. Quantifying the spatial and down-core geochemical patterns is important for understanding the underlying conservative (sediment provenance) and non-conservative (salinity, redox, anthropogenic influences) processes driving these patterns. It is particularly important to distinguish between conservative and non-conservative processes in order to quantify sediment sources, which will help developing management strategies to limit excess sedimentation in estuaries. In this study, elemental concentrations were measured via inductively coupled plasma emission/mass spectroscopy (ICP-ES/MS) and analyzed using principal component analysis. The sediment geochemistry data were then applied to evaluate contributions of Susquehanna River and shoreline erosion to bottom sediments in the upper Bay using a sediment-provenance analysis. Elements associated with aluminosilicate minerals, which were sensitive to grain-size changes, and rare earth elements, which were sensitive to salinity changes, explained the most variability in the dataset. Variability in heavy metal concentrations demonstrated changes in anthropogenic input over time. The results from the sediment-provenance analysis indicated that the Susquehanna River is the dominant source of fine sediment in the upper Bay.

## Introduction

Spatial patterns of geochemical signatures in estuarine sediments reflect a variety of important processes, depending on element behavior. For example, conservative geochemical tracers, such as Al, Li, and ratios of rare earth elements (REEs), reflect sediment provenance (Loring 1991; Windom et al. 1989; Munksgaard et al. 2003), while non-conservative tracers, such as organic matter, Fe and Mn, total REE concentrations, and heavy metals reveal changes in salinity, redox conditions, and/or anthropogenic influences (Sholkovitz and Elderfield 1988; Bricker 1993; Owens and Cornwell 1995; Guo et al. 1997; Zimmerman and Canuel 2000; Spencer et al. 2003). Elements can also behave differently depending on environmental context, such as Fe and P, which behave conservatively in fresh water under oxidizing conditions but non-conservatively in salt water under hypoxic conditions (Guo et al. 1997; Jordan et al. 2008). Therefore, it is important to analyze as many parameters as possible and interpret them within a specific environmental context.

Historically, analytical constraints have limited the number of samples and/or elements considered by individual studies, hindering interpretation of the geochemical record preserved in sediment cores. For example, most previous studies have been restricted to a specific group of elements (i.e. trace elements, heavy metals, or rare earth elements) and have limited scope, focusing on either spatial patterns of surface sediments or down-core changes at individual sites (e.g. previous work in Chesapeake Bay by Sinex and Helz 1981; Sholkovitz and Elderfield 1988; Owens and Cornwell 1995; Zimmerman and Canuel 2000). Recent advancements in analytical techniques, particularly inductively coupled plasma mass spectroscopy

(ICMPS), now allow analysis of >50 elements on small amounts of sediment for a relatively low cost, greatly expanding datasets needed for robust understanding of geochemical patterns in space and time.

These datasets often have high dimensionality and contain co-varying elements, making statistical analyses challenging; however, techniques such as correlation and principal component analyses reduce dimensionality and highlight underlying relationships in the data (Reid and Spencer 2009; Hannigan et al. 2010; Prajith et al. 2016). These advances allow the competing influences of conservative (sediment provenance) and non-conservative (salinity, redox, anthropogenic influence) processes on sediment geochemistry to be untangled, which is critical for using these data to address many scientific and management issues. For example, reducing sediment inputs is a major management focus in coastal and estuarine areas, as excess fine sediment is one of the main pollutants degrading water quality (Thrush et al. 2004; US EPA 2010; USACE 2015). Sediment-provenance analyses, which quantify sediment contributions from distinct sources, provide the data needed to develop effective sediment-management strategies (Mukundan et al. 2012). Sediment-provenance analyses employ a suite of geochemical parameters (i.e. trace metals, nutrients, radioisotopes, and stable isotopes) to produce a characteristic signature for individual sediment sources. These signatures can then be used to quantify the relative contributions of source materials to suspended or bottom sediments. For example, sediment-provenance analyses have been used to quantify source contributions from surface and subsurface sediments in river (Walling 2005) and deltaic floodplains (Jalowska et al 2017), and to determine contributions of

different land uses (Gellis and Noe 2013; Voli et al. 2013) and physiographic provinces (Devereux et al. 2010) to suspended-sediment loads.

Understanding the fate of sediment sources in the Chesapeake Bay is critical for developing targeted sediment-management approaches, especially with respect to recent total maximum daily load (TMDL) sediment reduction goals (US EPA 2010). Sediment-provenance analyses can potentially differentiate between sediments delivered from the Bay's main tributary, the Susquehanna River, and those eroded from shorelines, but these analyses require conservative element changes. There is limited information from previous studies on the geochemical character of sediments from the Susquehanna River, shoreline sediments, and upper Bay. Thus, the first step in determining provenance of Bay sediments is to identify the most prevalent elements and whether they are conservative or non-conservative in the estuary. This study takes advantage of relatively new analytical and statistical analyses of sediment geochemistry to take this first step and move forward to applying the results to a sediment-provenance analysis, providing a foundation for future work. Specifically, the objectives are to: 1) identify the most prevalent conservative and non-conservative elements in upper Bay sediments; 2) describe spatial patterns in surficial sediments and with depth in cores; 3) determine the underlying processes driving the observed patterns; and 4) evaluate the potential for results to quantify relative contributions of Susquehanna River and shoreline sediments to upper Bay sediments.

## Methods

*Study Site*

The upper Chesapeake Bay is the ~100 km section between the Susquehanna River and Choptank River mouths (Fig. 3.1). Here, the Bay varies in width between 5 km and 20 km. Although the narrow main stem Bay channel reaches depths up to 53 m south of Annapolis, the average depth of this portion of the Bay is only 4 m due to broad shallow shoals flanking the main channel (https://www.ngdc.noaa.gov/mgg/bathymetry/estuarine/). The tidal range increases from 0.3 m near Annapolis to 0.6 m at the head of the Bay. Tidal currents are also lowest near Annapolis at 0.13 m $s^{-1}$, increase to 0.6 m $s^{-1}$ near Baltimore, then decrease north of Baltimore to 0.2 m $s^{-1}$ at the head of the Bay (Zhong and Li 2006). Significant wave heights in the upper Bay are typically <1 m with a mean period <2.5 s (https://buoybay.noaa.gov/). These waves are generally fetch-limited and generated by winds (Sanford 1994).

There are three salinity regions in the upper Bay: tidal freshwater (0-0.5), from the Susquehanna River mouth to Turkey Point; oligahaline (0.5-5), from Turkey Point to the Patapsco River mouth; and mesohaline (5-18), from the Patapsco River mouth to the Potomac River estuary mouth (http://eyesonthebay.dnr.maryland.gov/). These salinity regions are largely influenced by freshwater discharge from the Susquehanna River, which delivers >80% of the total freshwater to the upper Bay (Schubel and Pritchard 1986). River discharge is generally highest during the spring, pushing the saltwater front farther seaward, and lowest during the summer, allowing the saltwater front to migrate farther landward (Schubel and Pritchard 1986).

The Susquehanna River is also the primary source of sediment to the upper Bay, supplying ~$2x10^6$ t annually (Langland 2015). Much of this sediment is trapped northward of 39°10' N (~40 km from the Susquehanna River mouth) in the estuarine turbidity maximum (ETM) (Biggs 1970; Schubel and Pritchard 1986; Donoghue et al. 1989). Shoreline erosion is another significant source to the upper Bay, contributing ~$1.0x10^6$ t $y^{-1}$, and becoming the dominant sediment source south of the ETM (Fig.3.1; Schubel 1968; Biggs 1970; calculated after applying dry bulk density correction factor from Langland and Cronin (2003)). This value reflects fastland erosion (erosion above mean high water (MHW), and was used interchangeably with shoreline erosion in this study) but not nearshore erosion, which can more than double this value when included (Langland and Cronin 2003). Sediment grain sizes in the upper Bay range from sandy-silts to silty-clays, although shorelines are predominately sandy (Kerhin 1988).

Previous research of sediment geochemistry in the upper Bay focused on surficial sediments, showing that several elements (Mn, Fe, Co, Ni, and Cu) decrease with distance from the Susquehanna River and that heavy metals (Zn, Cd, and Pb) are enriched due to anthropogenic influences (Sinex and Helz 1981). Also, analysis of particulate Fe revealed that the Susquehanna River contributes 85% of the material in the upper Bay, with shoreline erosion supplying 15% (Helz et al. 1985a). Lastly, while dissolved concentrations of rare earth elements (La, Ce, Pr, Nd, Sm, Eu, Gd, Dy, Y, Er, Yb) were studied, few reports of sediment concentrations exist (Sholkovitz and Elderfield 1988).

*Field and Laboratory Methods*

Sediments cores were collected at seven sites in the upper Bay, four of which were sampled via box cores on 11 August 2015 (Fig. 3.1; Table A.3). Box cores were subcored onsite using 6 cm inner diameter core liners (20 cm long); subcores were immediately extruded and sectioned into 1-cm intervals before returning to the laboratory for analysis. All sites were sampled via gravity cores (1.5 m long, 7 cm diameter) on 28 April 2016. Intact gravity cores were returned to the laboratory, where they were sectioned into 1-cm (top 20 cm) and 2-cm (20 cm-end of core) increments. Sediments from all cores were analyzed for grain size and elemental composition.

Field samples were also collected to characterize Susquehanna River and shoreline sediment sources (Fig. 3.1; Table A.3). Suspended sediment from the Susquehanna River was collected on 6 April 2015 at the Conowingo Dam outlet during high flow (4474 $m^3$ $s^{-1}$), using a 20 L carboy. Physical constraints prevented additional water collection at the Conowingo Dam outlet; surface sediments (0-1 cm) from the Conowingo Reservoir with detectable $^{7}Be$ activity (tracer of recently eroded watershed sediment; Olsen et al. 1986), collected in 2015-2016 (Palinkas 2017) were assumed to represent Susquehanna River sediment (n=13). Sediment from the three sites closest to the Dam was used. Surface grab samples were taken from unprotected, erosive shorelines to represent shoreline sediments (Fig. 3.1; n=16).

Grain size was analyzed by wet-sieving samples at 63 μm to separate the fine (silt+clay; <63 μm) and coarse (sand; >63 μm) fractions. The fine fraction was disaggregated with 0.05% sodium metaphospate in an ultrasonic bath and then

analyzed using a Sedigraph 5120. The coarse fraction was dry-sieved through a standard set of 13 sieves, from 500 μm to 64 μm (at ¼-phi size intervals; phi=-$\log_2$(particle diameter, mm)). The fine and coarse data were joined to calculate median diameters of the bulk sample; median diameters were also calculated for the fine fraction only.

For elemental analysis, two-gram aliquots were taken from the dried surface sediment (0-1 cm) of all box and gravity cores. Seven to nine additional aliquots were taken from dried sediment at ~5-cm increments within gravity cores, for a total of 61 aliquots. Elemental analyses were also performed on Susquehanna River and shoreline sediments. Each aliquot was sieved at 63 μm; the <63 μm fraction was transferred into a 20-mL plastic scintillation vial. Vials were sent to Bureau Veritas Commodities Canada Ltd. (Vancouver, Canada) for analysis via inductively coupled plasma emission and mass spectroscopy (ICP-ES/MS). For these analyses, 0.25 g sediment split was dissolved using microwave-assisted multi-acid digestion ($HNO_3$, $HClO_4$, HF, HCl), following the methods of Totland et al. (1995) to determine concentrations for 59 elements. Standard reference materials (NIST 1646a, estuarine sediment; OREAS 25a, ferruginous soil; OREAS 45e, lateritic soil) and replicates were analyzed to determine accuracy and precision, respectively. Elements with >10% error (19 of the original 59) were omitted from further consideration.

*Statistics*

All statistical analyses were performed in R version 3.3.2, considering surface (uppermost 1 cm) and core-averaged (>1 cm deep in cores) elemental compositions

separately; surface compositions were further divided into spring and summer. Core-averaged element concentrations $\overline{(C_e)}$ were calculated using a weighted average approach, based on differing interval thicknesses. For core n,

$$\overline{C_e} = \sum_{e,i=1}^{N} C_{e,i} \cdot \frac{h_i}{H} \qquad (1)$$

where $C_{e,i}$ is the concentration of element e in interval i, $h_i$ is the thickness of interval i, and H is the total core thickness.

Inter-element correlations were quantified using a correlation matrix. Principal component analysis (PCA) was run to reduce the dimensionality of the data and determine which elements explained the most variability across all cores. PCA generates principal components, which are uncorrelated variables made up of linear combinations of the original variables. For each principal component, a loading is assigned to each of the original variables, determined by correlation between the original variable and the principal component. The correlation matrix and PCA were run on all 61 samples (surface and down-core) in order to identify spatial and temporal patterns driving data variability. Simple linear models were developed to compare element concentrations (spring surface, summer surface, and core-averaged values) with distance from the Susquehanna River mouth; p-values $<0.05$ were considered significant.

Element concentrations were also normalized to those in Susquehanna River surficial sediment. This places all elements on a similar scale and directly compares upper Bay element concentrations to Susquehanna River values without affecting the underlying geochemical patterns. Because silt and clay differences can impact

element concentrations, an enrichment factor ($EF_{Al}$) was calculated that normalizes elemental concentrations to Al (Schropp et al. 1990).

$$EF_{Al} = \left[\frac{Element}{Al}\right]_{sample} / \left[\frac{Element}{Al}\right]_{Susq} \quad (2)$$

In Eq. 2, $[Element/Al]_{sample}$ is the Al-normalized element concentration of the sediment sample, and $[Element/Al]_{Susq}$ is the Al-normalized element concentration of the surficial Susquehanna River sample. The $EF_{Al}$ was only calculated for elements that were correlated with grain size.

A sediment-provenance analysis was then performed, in which source contributions from the Susquehanna River and shoreline erosion were quantified on target (upper Bay) sediments using the United State Geological Survey (USGS) Sediment Source Assessment Tool (Sed_SAT; Gorman-Sanisaca et al. 2017). Differences in element concentrations between Susquehanna River (metamorphic rocks such as schist, gneiss and quartzite, and felsic and mafic igneous intrusions) and shoreline sediment sources (unconsolidated clastic sediments like quartz) were assumed to reflect differences in underlying geology (Markewich et al. 1990). The Sed_SAT tool runs a series of statistical tests to remove outliers, eliminate non-conservative elements, and select a group of elements that best discriminates among different sources. All elements that were correlated with grain size were normalized to Al in both the source and target datasets. Elements that behaved conservatively with a normal distribution were passed into a Forward Stepwise Linear Discriminant Function Analysis (DFA), which selects a combination of elements that best differentiates between the source samples by minimizing the Wilks' lambda variable (Collins et al. 1997; Gellis and Noe 2013). A Wilks' lambda close to 1 means the

sources cannot be distinguished, while a value closer to 0 means the sources are significantly different. A mixing-model analysis using Monte Carlo simulations was then applied, minimizing the following equation:

$$\sum_{i=1}^{n}\{[C_i - (\sum_{i=1}^{m} P_s S_{si})]/C_i\}^2 W_i; with \sum_{s=1}^{n} P_s = 1 \quad (2)$$

"where $C_i$ is the concentration of tracer I in the target sample, $P_s$ is the optimized percentage of source type (s); $S_{si}$ is the mean concentration of tracer i in source s; $W_i$ is the weighting factor applied to tracer i; n is the number of tracers in the optimum composite fingerprint; and m is the number of sediment source types" (Gorman-Sanisaca et al. 2017). All elements were included in the first Sed_SAT model run; the second model run excluded elements with non-conservative behavior in the upper Bay.

## Results

### *Correlation Matrix*

Individual values of core-averaged bulk grain size, fine-fraction grain size, and element concentrations varied widely in the upper Bay (Table 3.1). The down-core data were combined with those from spring and summer surficial sediments (Table 3.2) to calculate a correlation matrix for the 40 elements (Fig. 3.2). Several of the 40 elements were positively correlated ($R^2$ values > 0.5) across all study sites (Fig. 3.2). There were 2 main groups of similarly correlated elements. Group 1 was composed of Li, Mg, Al, K, Sc, V, Cr, Fe, Ga, As, Rb, Tl, and Bi. Most $R^2$ values for

this group were >0.75, but Cr, As, and Bi had lower values of 0.52-0.81. Group 2 was composed of Th, U, and the rare-earth elements (REEs) La, Ce, Pr, Nd, Sm, Eu, Gd, Dy, Y, Er and Yb. $R^2$ values in this group ranged from 0.50 to 0.97, with the highest values occurring between the light REEs (La, Ce, Pr, and Nd) and Th.

Other correlations between elements with $R^2$ values > 0.5 were present: Na had a positive correlation with Mg ($R^2$=0.60) and P ($R^2$=0.58) and a negative correlation with La, Ce, Pr, Th, and Zr ($R^2$=0.51-0.58); Zr was negatively correlated with Li, Mg, and Tl (0.50-0.54); Zn was positively correlated with Cr ($R^2$=0.63) and Bi ($R^2$=0.53); and Sr was positively correlated with Al ($R^2$=0.50) and Rb ($R^2$=0.52). Correlations between median grain size of the fine fraction and the 40 elements were also evaluated. Although all $R^2$ values were <0.5 for all elements, group 1 elements tended to have a negative relationship with median grain size ($R^2$ values 0.37-0.48). $R^2$ values between median grain size and group 2 elements were < 0.1.

*Element concentrations and enrichment factors*

Concentrations of group 1 elements (e.g. Li, Sc, V) in surficial sediments generally increased with distance from the Susquehanna River in both spring and summer as did core-averaged concentrations (Fig. 3.3a; see Tables 1 and 2 for concentration data). After normalizing to Al, enrichment factors for K, Sc, Ga, Rb, and Tl showed no trend in either spring or summer, with values ~1, while the other elements significantly increased with distance downstream ($p<0.01$; $R^2$ = 0.49-0.98). Core-averaged enrichment factors for K, Sc, Fe, Ga, Rb, and Tl were ~1 and had no relationship with distance downstream. However, enrichment factors for Li, Mg, and

As increased downstream ($R^2$ = 0.55, 0.54, 0.74, respectively; Fig. 3.3b). For V and Bi, the core-averaged $EF_{Al}$ increased between Lee7 and Lee5, decreased at Lee2.5, and increased through LeeS2 (Fig. 3.3b); for Cr, the core-averaged $EF_{Al}$ decreased between Lee7 and Lee0, and increased slightly at LeeS2.

Because REEs tend to behave similarly over the salinity gradient (Sholkovitz and Szymczak, 2000), total REE concentration was used to assess changes in group 2 elements across study sites (Fig. 3.4a). Although Th and U were not included, they generally show a similar spatial pattern in both core-averaged and surficial concentrations to the other REEs. Total REE in surface sediments generally decreased with distance downstream, even though there was a slight increase at Lee2 in spring. The core-averaged total REE was relatively uniform between Lee7 and Lee5 (191.01-193.71 ppm), increased to a maximum at Lee2.5 (221.58 ppm), decreased to a minimum at Lee0 (145.45 ppm), and then increased again to 189.24 PPM at LeeS2. REE ratios were also analyzed by comparing the sum of light REEs (LREE; La, Ce, Nd, Pr) to the sum of heavy REEs (HREE; Er, Yb). The LREE and HREE concentrations of each sample were normalized to the LREE and HREE concentrations from Susquehanna River sediment, respectively. There was a slight decrease in surficial (spring and summer) and core-averaged LREE to HREE ratios with distance downstream (Fig. 3.4b).

For elements not in groups 1 or 2, spatial patterns of surficial sediments were generally similar in spring and summer (see Table 3.2). For example, Na and P increased downstream while Zr decreased; surficial Mn increased between Lee7 and Lee2.5 and then decreased at LeeS2. However, surface Mn concentrations at Lee2.5

were nearly two times higher in summer than in spring. The core-averaged concentrations of these elements were more spatially variable (see Table 3.1): Na and P concentrations increased from Lee7 to Lee0, and decreased at LeeS2; Zr increased from Lee7 and Lee5, and then decreased through Lee0. Mn concentrations increased between Lee7 and Lee2, then decreased through LeeS2.

Core-averaged values were used in the preceding analyses, because elemental values did not vary considerably down individual cores. There were some exceptions: group 1 elements As and Bi varied by a factor of 2.5; and group 2 elements varied by up to a factor of 1.5 at Lee0 and LeeS2. And, distinct concentration peaks were present in the heavy-metal down-core data profiles, particularly for Co, Ni, Cu, Mo, and Pb. For example, peaks in Pb occurred between 30-32 cm at Lee6 (123.07 ppm) and 12-13 cm at Lee2.5 (96.48 ppm); the Pb concentrations then declined towards the surface of the cores (Fig. 3.5).

*PCA*

Principal Component Analysis (PCA) showed that 75.4% of the variability across all samples (surface and down-core) was explained by the first three principal components (38.6%, 29.6%, and 7.2% for PC1, PC2 and PC3, respectively). Elements of group 1 projected strongly onto PC1 (i.e. elements from group 1 had large PC1 loadings relative to PC2), while the elements of group 2 projected strongly onto PC2 (Fig. 3.6). Grain size also projected strongly onto PC1, but in the opposite direction of the group 1 elements, reflecting negative correlations with these elements. Strontium and Zn projected more strongly onto PC1, while Zr, P and Na

had similar PC1 and PC2 loadings. Calcium, Ti, Mn, Co, Ni, Cu, Mo, Ba and Pb had relatively small loadings in both PC1 and PC2, and therefore did not contribute much to the overall variability on these principal components. Heavy metals Co, Ni, Zn, Mo, and Pb projected strongly onto PC3 (not shown in Fig. 3.6).

Surface (summer 2015 and spring 2016) and core-averaged element concentrations were transformed using the PC1 and PC2 loadings of each element and projected onto the first 2 principal components (Fig. 3.7). Minimum and maximum PC1 values occurred at Lee7 and LeeS2, respectively, in both summer 2015 and spring 2016 surface sediments. Both spring and summer PC1 values significantly increased with increased distance from the Susquehanna River (p-values 0.03 for both linear regression models), although spring PC1 values at Lee2.5 and Lee0 were outliers. In contrast, summer and spring PC2 values significantly decreased with distance from the Susquehanna River (p-values 0.01 and 0.001 for respective linear regression models). Direct comparisons between spring and summer surficial sediments were possible at Lee7, Lee5, Lee2.5, and LeeS2. In both spring and summer, minimum PC1 values and maximum PC2 values occur at Lee7, and maximum PC1 values and minimum PC2 values occur at LeeS2. However, summer surficial PC1 values were lower at Lee5 than at Lee2.5, but spring values were lower at Lee2.5 than at Lee5. PC2 values were similar between seasons at all sites except LeeS2, where values were lower in summer.

Core-averaged PC1 values showed a similar pattern to the surficial sediments, with values generally increasing with distance downstream (p-value=0.003), but over a much larger range. Core-averaged PC1 values at each site were also higher than

corresponding surficial PC1 values. Core-averaged PC2 values gradually increased from Lee7 and Lee5, reached a maximum at Lee2.5, and then decreased to a minimum at Lee0 (Fig. 3.7). Core-averaged and surficial PC2 values at each site, except at LeeS2, where surficial PC2 values were much lower. Core-averaged PC2 values were significantly higher in the oligohaline (Lee7-Lee2.5) than in the mesohaline (Lee2-LeeS2) regions of the Bay ($p<0.001$). Down-core variability was highest at Lee2.5, Lee0, and LeeS2 and lowest at Lee7, Lee6, Lee5, and Lee2.

*Sediment-provenance analysis*

Elemental concentrations in shoreline sediments generally varied more widely than concentrations in Susquehanna River sediments (Table 3.3). Of the 40 elements in the source (Susquehanna River and shoreline sediments) and target (upper Bay) geochemical datasets, only Li, Co, Ti, and Zr behaved non-conservatively in the first Sed_SAT model run, which included all elements, and were discarded from further analysis. In that run, the group of tracers that best distinguished between sources included As, Tl, Fe, and Ce and correctly classified 96.88% of source sediments; only 1 shoreline site was misclassified as Susquehanna River source. Using this group, sediment-source contributions to upper Bay sediments generally showed Susquehanna influence decreasing with distance downstream, from a core-averaged value of 95.7±0.12% at Lee7 to 75.8±0.90% at LeeS2. Susquehanna sources at Lee2 and Lee0 were outliers from this trend, having comparable values to those at Lee5 (Fig. 3.8). Down-core percentages did not vary by more than 20%, with the most variability occurring at Lee5, Lee0, and LeeS2.

Because the statistical analyses above identified several elements with non-conservative behavior in the upper Bay due to environmental variability (e.g. salinity, oxygen), the second Sed_SAT model run excluded all non-conservative elements. In this model run, the group of selected elements (Tl and Fe) correctly classified 90% of the source samples, with 3 shoreline sites misclassified as Susquehanna River sites. The Susquehanna River was again the dominant source to upper Bay sediments (Fig. 3.8), ranging from 89.53±1.57% at Lee5 to 98.32±1.33% at Lee0. Susquehanna River contribution was significantly higher (p-value <0.01) in the second run at all sites except Lee7 and Lee5 (p-value >0.3). The Susquehanna River contribution slightly decreased between Lee7 and Lee5, then slightly increased between Lee5 and Lee0, and again decreased to LeeS2. All cores displayed little down-core variability in the second model run.

## Discussion

### *Influences on element concentrations in surficial and core-averaged sediments*

Correlation matrices and PCA are common techniques for analyzing multivariate sediment geochemistry datasets. They have been applied previously to describe sediment provenance, anthropogenic influence, and changes due to salinity in estuarine sediments (Li et al. 2000; Reid and Spencer 2009; Prajith et al. 2016). Although both techniques are useful for grouping elements with similar patterns, in this study only PCA revealed underlying relationships in the data that explained the total variance.

Elements that are grouped together (i.e. similar $R^2$ values or PCA loadings) have a common source. For example, in this study, group 1 elements (e.g. Li, Sc, V) accounted for the most variance in PCA. These elements tend to be associated with aluminosilicate clay minerals (Loring 1991; Reid and Spencer 2009), such as illite, chlorite, kaolinite, and montmorillontite. These minerals are prevalent in the Chesapeake Bay (Goldberg et al. 1978), with changing concentrations along the salinity gradient that reflect changes in source (i.e. fluvial or marine) (Feuillet and Fleischer 1980). Although clay mineralogy was not evaluated in this study, the changing concentrations of group 1 elements could be a proxy for changing influence of fluvial versus marine sources; i.e. more fluvial influence near the Susquehanna River. However, while both surface and core-averaged element concentrations increased with distance downstream, these trends are likely driven by differences in grain size, which decreases from silts at Lee7 (most upstream site) to clays at LeeS2 (most downstream site). As grain size decreases, surface area and adsorption efficiency increases (Schropp et al. 1990), resulting in an apparent increase of adsorbed elements. Thus, grain-size effects must be separated from differences in mineralogy through a grain-size correction, such as granulometric or geochemical normalization (Reid and Spencer 2009; Sun et al. 2018). In this study, grain-size influence was removed via enrichment factors (EFs; normalization to Al), which also help discriminate between different sources of elements, such as terrigenous or anthropogenic sources (Reid and Spencer 2009; Prajith et al. 2016). The EFs were calculated relative to Susquehanna River surficial sediments, so an EF > 1 suggests an additional source of these elements, likely anthropogenic pollution (Sinex and Helz

1981; Prajith et al. 2016). In contrast, an EF ≤1 suggests no or minimal pollution and/or another sediment source with lower concentrations of these elements (Sinex and Helz 1981; Prajith et al. 2016).

While analyzing only the fine fraction of samples minimizes this variability (Sinex and Helz 1981), differences in silt and clay composition can still influence observations. Indeed, the lack of significant trend in the core-averaged $EF_{Al}$ for K, Sc, Ga, Rb, and Tl with distance downstream indicates that differences in silt and clay composition, not differences in sources of these elements, control observed spatial patterns. In contrast, the enrichment of core-averaged $EF_{Al}$ for Mg, As, and Li with increased distance downstream suggests that there is an additional source of these elements. For example, increased Mg can reflect increasing salinity (Elbaz-Poulichet et al. 1984), while increases in As can be due to changing redox condition – under reducing conditions As can co-precipitate with $FeS_2$ (Morse and Luther 1999) or become associated with insoluble humic complexes (Guo et al. 1997). Higher As concentrations may also reflect anthropogenic sources (Sanders 1985; Gupta and Karuppiah 1996). Lithium, however, is not typically influenced by anthropogenic sources or biogeochemical processes, but it is highly sensitive to grain-size changes and is sometimes used to correct for grain-size effects (Loring 1991). It is possible that Li concentration changes reflect a shift in dominant sediment source, such as decreasing influence of Susquehanna River sediments and increasing contributions of eroded shoreline sediment (Biggs 1970; Donoghue et al. 1989). Because shoreline sediments have lower Li concentrations than Susquehanna River sediments (Table 3.3), Li concentrations should decrease downstream; however, the opposite trend was

observed. The most likely explanation is that grain-size effects were not fully removed when normalizing to Al, and the decreasing normalized Li concentrations (Loring 1991). The non-linear trend of $EF_{Al}$ for V, Cr, and Bi suggest that these elements do not behave conservatively in upper Bay sediments. Changes in surficial and core-averaged V and Cr concentrations could reflect changes in redox conditions, since V tends to precipitate under reducing conditions (Shiller and Mao 1999) and Cr tends to co-precipitate with metal oxides. Changes in Bi concentrations could reflect anthropogenic inputs, since peaks in Bi occur near industrial areas (Baltimore and Annapolis).

Although Na and P were generally not correlated with group 1 elements, they had similar spatial patterns as Mg. The increase in surficial and core-averaged Na with distance downstream could reflect a change in sediment-source contributions and/or the increase in salinity and thus major seawater cations, like Mg (Elbaz-Poulichet et al. 1984). Unlike Na and Mg, P is not a major ion found in seawater but can still vary with changing salinity and redox conditions. A large portion of particulate P is bound to Fe in freshwater but is released at higher salinities and under more reducing conditions (Jordan et al. 2008). This release of P from Fe explains the relatively strong correlation of P and Fe between Lee7 and Lee2 ($R^2$=0.68) and the lack of relationship at Lee0 and LeeS2. Manganese is also sensitive to redox conditions; high surficial and core-averaged concentrations between Lee5 and Lee2 likely reflect the presence of Mn oxides under oxidizing conditions, and the subsequent decrease between Lee0 and LeeS2 reflects the reduction of Mn to dissolved form under reducing conditions (Guo et al. 1997).

The significant difference between core-averaged PC2 values in the mesohaline and oligohaline reflects the sensitivity of REEs to changes in salinity. At low salinities, REEs are removed from the water column and adsorbed to sediments due to the salt-induced coagulation of riverine colloids (Sholkovitz and Elderfield 1988). As salinity increases, REEs are released from sediments and resupplied to the water column (Sholkovitz and Szymczak 2000). My results are consistent with these patterns – enrichment of core-averaged REEs at Lee2.5 likely due to salt-induced coagulation of riverine particles, and the subsequent decline at the mesohaline sites suggesting desorption of REEs at higher salinities. Previous work showing a positive linear trend between salinity and water-column REE concentrations implies that there should be a corresponding negative linear trend between salinity and sediment REE concentrations (Sholkovitz and Szymczak 2000). Although core-averaged REE concentrations generally follow this pattern between Lee2.5 and LeeS2, REE concentrations at Lee0 are much lower than expected. REE concentrations are depleted by up to 30% at Lee0, and subsequently increase by ~20% at LeeS2, suggesting either a significant release of REEs from the sediment particles followed by adsorption downstream, or dilution of these sediments by REE-poor sediments (Elderfield et al. 1990; Prajith et al. 2015). Lee0 has REE concentrations that are <10% of the core-averaged REE concentrations measured in Susquehanna River sediments (Table S3). This site is located at the mouth of the Chester River, whose watershed is entirely within the Coastal Plain physiographic province, so its low REE concentrations at Lee0 may result from dilution by Chester River sediments and/or shoreline erosion. The decrease in LREE to HREE ratios downstream could either

indicate REE fractionation or changes in dominant sediment source. Previous research has shown that HREEs are preferentially released from sediments at mid- to high salinities (Sholkovitz and Szymczak 2000), which would increase LREE:HREE. Therefore, the decreasing trend in my data more likely represents changing sediment sources, supporting the use of REEs for assessing sediment provenance (Munksgaard et al. 2003) even though they behave non-conservatively. However, since average LREE:HREE in Susquehanna River and shoreline source sediments were not significantly different, REE ratios were not used for the provenance analyses discussed below.

*Temporal changes in element concentrations*

Differences in the spring and summer datasets highlight seasonal shifts in estuarine processes. For example, the differences in PC1 values at Lee5 and Lee2.5 between spring and summer (i.e. PC1 values were lower at Lee2.5 in spring than at Lee5, but were higher at Lee2.5 than at Lee5 in summer) likely reflect seasonal migration of the estuarine turbidity maximum (ETM) (Sanford et al. 2001). In spring, Susquehanna River discharge is high, and the ETM is farther seaward near Lee2.5; in summer, river discharge is lower and the ETM is nearer the head of the Bay and Lee5 (Schubel and Pritchard 1986). In spring, PC1 values of surficial sediments at Lee2.5 are lower than at Lee5, suggesting that fluvial sediment was transported farther downstream (Fig. 3.7). In summer, surficial PC1 values increase with distance downstream, similar to core-averaged patterns. The only other notable seasonal difference occurs in Mn at Lee2.5. Because this site is near the northern limit of the

seasonal anoxic zone (Officer et al. 1984b; Gavis and Grant 1986), the high Mn concentrations observed in summer surficial sediments likely represents Mn accumulation at the redox boundary, where dissolved Mn are precipitated as oxides (Burdige 1993).

Differences over longer, decadal time scales are reflected in concentration changes with depth in sediment cores. Generally, there was not much variability with depth in group 1 or 2 elements, which suggests that the sources of these elements and/or estuarine processes impacting these elements have been consistent over the past ~100 years. However, the slight variability in As and Bi may reflect anthropogenic sources (Gupta and Karuppiah 1996). Heavy metals, included in the third principal component, were the most variable with depth in cores and usually had a distinct peak in the depth profile. These peaks likely represent anthropogenic pollution such as those documented in the Chesapeake Bay (Goldberg et al. 1978; Owens and Cornwell 1995) and other estuaries with significant industrial and population growth throughout the late 19$^{th}$ and 20$^{th}$ centuries (Bricker 1993; Spencer et al. 2003). However, several pollution control measures have been adopted since the late 20$^{th}$ century that reduced heavy metal inputs. These changes are preserved in the sediments; for example, the removal of Pb from gasoline is well documented in previous studies and results in peak concentrations at depths corresponding to the late 1970s in sediment cores (Bricker 1993; Owens and Cornwell 1995; Spencer et al. 2003). These peaks were observed in upper Bay cores, at depth horizons consistent with the late 1970s using accumulation rates from Russ and Palinkas (in prep). Thus,

the down-core profiles of heavy metals likely reflect temporal shifts in anthropogenic inputs.

*Sediment-provenance application*

I expected to decreasing influence of Susquehanna River sediments with distance downstream in the upper Bay, as well as a corresponding increase in shoreline influence. The results from the first Sed_SAT mixing model run (all elements) support this hypothesis. However, the second run of the Sed_SAT mixing model (conservative elements only) indicated unexpectedly high contributions from the Susquehanna River at downstream sites. The differences between the model results using the first (As, Tl, Fe, and Ce) and second (Tl and Fe) groups of elements underscore how sensitive the model is to different groups of elements.

The results of the first model run are consistent with previous results based on Fe con centration data (Helz et al. 1985a), in which ~85% of bottom sediments in the upper 50 km of the Bay come from the Susquehanna River. Because most of the Susquehanna River sediment is trapped within the ETM (north of Lee2.5) (Donoghue et al. 1989), I expected shoreline erosion to contribute most of the sediments south of Lee2.5. However, Susquehanna River sediment was dominant throughout these cores. It is important to note that the sediment-provenance results in this study represent the source contribution of the fine fraction. And so, one explanation for the relatively high Susquehanna input in my results is that my sites received more fine Susquehanna River sediment than fine shoreline sediment. Susquehanna River source sediments were generally fine (ballpark %sand), but shoreline source sediments were

predominately sandy (>90% sand). Indeed, <35% of upper Bay shoreline sediments are composed of fine particles (Schubel 1968) that can be transported into deeper water (Halka 2000). Most of the larger, sand-sized shoreline sediments are deposited along shallow shoals immediately adjacent to the shoreline, with relatively little transport beyond nearshore zones. My results are consistent with these ideas, showing that Susquehanna River sediments contribute more fine sediment in the deeper portions of the upper Bay than shorelines, with increasing contributions from fine shoreline sediments downstream.

Although the results from the first model run agree with previous results, the mixing-model analysis included elements with non-conservative behavior in the Bay (As and Ce), as determined by this study. The Sed_SAT tool determines conservative behavior through a range test (i.e. target sediment element concentrations are within the minimum and maximum element concentrations of source sediments) (Mukundan et al. 2012), without consideration of environmental influence on elemental concentrations. Thus, it is critical to identify in a particular study area prior to using Sed_SAT as was done in the second model run. However, the results from this second run were unexpected in that Susquehanna River influence increased downstream, contrasting previous work showing dominance of shoreline sediments in the mesohaline Bay (Biggs 1970). Although the elements selected for the second run behaved conservatively in the upper Bay, these elements did not show any downstream trend after normalizing to Al, which likely explains why source contributions were similar between all sites. A possible explanation for unexpectedly low shoreline-source contributions in this model is the wide variability in Tl and Fe

concentrations in shoreline sources (Table 3.3). The mixing model uses the mean element concentration of each source to quantify its contribution to the target sediments; a wide range in element concentrations results in a mean concentration that may not appropriately represent source sediments. In this case, Fe concentrations (normalized to Al) ranged between 556-680 (average 611) in Susquehanna River sediments and between 545-3114 (average 1453) in shoreline sediments. Target sediment Fe concentrations (normalized to Al), which ranged between 537-782, closer to average Susquehanna River concentration than to average shoreline concentration, resulting in source contributions that indicate greater Susquehanna River influence.

Regardless of the differences between the two model runs, it is clear that the Susquehanna River is the dominant source of fine material near the main channel of the upper Bay, including at downstream sites. While quantifying exact contributions throughout the study area, as well as expected future changes due to natural and anthropogenic activities (climate change, dam infilling) remain fruitful areas for future research, identifying the main source(s) of fine material to the upper Bay is a critical, immediate management need. Sediment-provenance analyses have been applied in freshwater environments to better manage excess sediment inputs (i.e. Walling 2005; Gellis et al. 2009; Devereux et al. 2010; Mukundan et al. 2012); however, it has not, to my knowledge, been applied as a management tool in estuarine environments since one of the main challenges to performing these analyses in estuaries, versus freshwater environments, is that estuarine biogeochemical processes (i.e. changes in salinity, redox condition) alters sediment geochemistry. Excess fine

sediment is one of the main pollutants contributing to water quality degradation in the Chesapeake Bay (USEPA 2015), and has been linked to benthic habitat degradation in the Chesapeake Bay, such as oyster reef mortality due to burial (Rothschild et al. 1994; Colden and Lipcius 2016) and loss of submersed aquatic vegetation (SAV) communities as a result of both burial and reduced light availability (Bayley et al. 1978; Dennison et al. 1993). Excess sediments also carry particulate nutrients, which enhance eutrophication by fueling algal blooms that reduce water clarity and lead to oxygen depletion in the water column and/or harmful algal blooms (Kemp et al. 2005). Recent studies have demonstrated that the nutrients associated with sediment particles have more of a deleterious effect on water quality than sediment alone (USACE 2015; Cerco and Noel 2016), and Susquehanna River sediments contain higher nutrient concentrations than shoreline sources (Marcus and Kearney 1991). Sediment-provenance analyses therefore offer a useful tool for quantifying sediment, and by association particulate nutrient, inputs from different sources.

**Summary**

To my knowledge, this is the first study to report synoptic spatial and downcore geochemical patterns of trace elements, REEs, and heavy metals in bottom sediments of the upper Chesapeake Bay. Statistical analyses on this large dataset reveal element correlations and processes affecting sediment composition. Two groups of elements explain most of the observed geochemical variability; i.e. aluminosilicate minerals and REEs reflect grain-size effects and salinity changes, respectively. Heavy metals also influence geochemical variability and were linked to

changes in anthropogenic loading. Sediment provenance was evaluated by comparing geochemical compositions in upper Bay sediments to Susquehanna River and shoreline sediments, and indicated that the Susquehanna River is the dominant source of fine sediment.

## Tables

**Table 3.1** Core-averaged mean (standard error) of grain size (first 2 rows) and concentrations of 40 elements at each site. Units in PPM unless specified otherwise in left hand column.

| | **Lee7** | **Lee6** | **Lee5** | **Lee2.5** | **Lee2** | **Lee0** | **LeeS2** |
|---|---|---|---|---|---|---|---|
| Grain size (μm) | 20.75 | 4.04 | 2.68 | 2.72 | 0.94 | 0.73 | 0.60 |
| | (2.51) | (0.68) | (0.75) | (0.36) | (0.14) | (0.25) | (0.08) |
| Grain size <63 | 9.31 | 3.14 | 2.26 | 2.21 | 0.91 | 0.67 | 0.55 |
| (μm) | (1.16) | (0.42) | (0.39) | (0.23) | (0.11) | (0.23) | (0.10) |
| Li | 42.01 | 47.57 | 54.57 | 66.6 | 72.09 | 70.44 | 82.11 |
| | (0.88) | (1.94) | (1.81) | (3.43) | (1.7) | (3.51) | (2.71) |
| Mg (%) | 0.46 | 0.54 | 0.61 | | 0.92 | 0.89 | 0.93 |
| | (0.01) | (0.01) | (0.02) | 0.7 (0.03) | (0.01) | (0.03) | (0.01) |
| Al (%) | 4.17 | 4.72 | 4.94 | | 6.88 | 6.44 | 7.08 |
| | (0.08) | (0.14) | (0.12) | 5.9 (0.35) | (0.14) | (0.39) | (0.33) |
| K (%) | 1.39 | 1.56 | 1.69 | 1.81 | 2.27 | 2.14 | |
| | (0.02) | (0.04) | (0.02) | (0.05) | (0.05) | (0.10) | 2.2 (0.04) |
| Sc | 8.02 | 8.83 | | 11.4 | 12.91 | 11.93 | 13.51 |
| | (0.18) | (0.33) | 9.4 (0.26) | (0.62) | (0.27) | (0.78) | (0.69) |
| V | 62.45 | 74.04 | 82.5 | 86.69 | | | |
| | (1.09) | (1.51) | (2.49) | (3.61) | 105.19 | 105.43 | 121.91 |
| | | | | | (1.96) | (5.17) | (3.69) |
| Cr | 59.77 | 64.15 | 67.5 | 69.67 | 79.29 | 74.36 | 91.56 |
| | (2.98) | (1.58) | (2.05) | (2.32) | (1.23) | (2.24) | (2.37) |
| Fe (%) | 2.62 | 3.07 | 3.48 | 3.83 | 4.35 | 3.91 | 4.59 |
| | (0.05) | (0.10) | (0.14) | (0.19) | (0.08) | (0.26) | (0.10) |
| Ga | 11.84 | 13.56 | 14.46 | 15.37 | 18.53 | 17.49 | 19.63 |
| | (0.31) | (0.49) | (0.32) | (0.58) | (0.34) | (0.86) | (0.51) |
| As | 6.31 | 8.98 | | 14.39 | 14.19 | 12.64 | 20.39 |
| | (0.37) | (0.33) | 9.5 (0.85) | (1.17) | (0.63) | (0.44) | (1.43) |
| Rb | 67.32 | 75.39 | 84.55 | | | | |
| | (1.05) | (1.98) | (1.79) | 102.51 | 117.10 | 102.89 | 115.20 |
| | | | | (5.77) | (2.20) | (7.11) | (6.44) |
| Tl | 0.46 | 0.53 | 0.57 | 0.61 | 0.73 | 0.71 | 0.77 |
| | (0.01) | (0.02) | (0.02) | (0.02) | (0.02) | (0.03) | (0.02) |
| Bi | 0.22 | 0.29 | 0.32 | | 0.43 | 0.38 | 0.48 |
| | (0.01) | (0.01) | (0.02) | 0.3 (0.02) | (0.01) | (0.02) | (0.03) |
| La | 35.39 | 34.81 | 33.93 | 38.24 | 33.3 | 24.75 | 32.23 |
| | (0.75) | (0.52) | (0.64) | (1.37) | (0.81) | (1.86) | (2.97) |
| Ce | 70.95 | 71.51 | 70.87 | 80.62 | 70.44 | 52.19 | 68.87 |
| | (1.09) | (1.35) | (1.35) | (2.93) | (1.53) | (3.98) | (5.98) |
| Pr | 9.11 | 9.03 | 9.12 | 10.09 | 8.87 | 6.62 | 8.68 |
| | (0.15) | (0.15) | (0.16) | (0.38) | (0.16) | (0.50) | (0.71) |
| Nd | 34.09 | 33.8 | 34.51 | 40.64 | 35.01 | 26.27 | 33.21 |
| | (0.55) | (0.52) | (0.66) | (1.93) | (0.66) | (1.95) | (2.77) |
| Sm | 6.77 | 6.84 | | 8.34 | 6.99 | 5.60 | 7.23 |
| | (0.13) | (0.13) | 7.2 (0.16) | (0.45) | (0.21) | (0.40) | (0.55) |
| Eu | 1.29 | 1.33 | 1.42 | 1.58 | 1.37 | 1.06 | 1.38 |
| | (0.03) | (0.04) | (0.04) | (0.09) | (0.04) | (0.06) | (0.11) |
| Gd | 5.34 | 5.89 | 6.09 | 6.97 | 6.16 | | 6.08 |
| | (0.17) | (0.21) | (0.19) | (0.44) | (0.14) | 4.7 (0.22) | (0.51) |
| Dy | 4.10 | 4.58 | 4.79 | 5.20 | 4.87 | 3.73 | 4.87 |
| | (0.10) | (0.16) | (0.16) | (0.30) | (0.13) | (0.18) | (0.36) |
| Y | 19.64 | 20.55 | 20.83 | 23.95 | 20.97 | 16.45 | 21.48 |
| | (0.56) | (0.63) | (0.52) | (1.52) | (0.58) | (0.62) | (1.60) |
| Er | 2.12 | 2.32 | 2.39 | 3.01 | 2.57 | 2.09 | 2.73 |
| | (0.06) | (0.04) | (0.09) | (0.13) | (0.07) | (0.09) | (0.19) |
| Yb | 2.21 | 2.35 | 2.55 | 2.92 | 2.47 | 2.02 | 2.47 |

| | | | | | | | |
|---|---|---|---|---|---|---|---|
| | (0.05) | (0.06) | (0.08) | (0.14) | (0.05) | (0.06) | (0.16) |
| Th | | 9.82 | 10.13 | 10.24 | 9.44 | 7.88 | 9.97 |
| | 9.8 (0.19) | (0.14) | (0.2) | (0.26) | (0.16) | (0.52) | (0.81) |
| U | 2.97 | 3.42 | 3.42 | 3.91 | 2.88 | 2.34 | 3.65 |
| | (0.06) | (0.10) | (0.07) | (0.14) | (0.07) | (0.13) | (0.34) |
| Na (%) | 1.03 | 1.13 | 1.19 | 1.27 | 2.03 | 2.65 | |
| | (0.03) | (0.04) | (0.04) | (0.05) | (0.04) | (0.18) | 1.8 (0.27) |
| P (%) | 0.53 | 0.66 | 0.75 | 0.81 | 1.00 | 1.27 | 0.88 |
| | (0.05) | (0.05) | (0.06) | (0.07) | (0.07) | (0.14) | (0.07) |
| Ca (%) | 0.24 | 0.31 | 0.22 | 0.35 | 0.27 | 0.26 | 0.38 |
| | (0.01) | (0.03) | (0.01) | (0.05) | (0.03) | (0.01) | (0.09) |
| Ti (%) | 0.32 | 0.37 | 0.39 | 0.35 | 0.34 | | 0.34 |
| | (0.03) | (0.01) | (0.01) | (0.01) | (0.00) | 0.3 (0.01) | (0.01) |
| Mn | 934.14 | 1039.96 | 1531.27 | 1348.14 | 1720.21 | 1074.6 | 695.84 |
| | (83.19) | (112.32) | (101.11) | (292.19) | (75.58) | (66.91) | (26.84) |
| Co | 35.18 | 39.16 | 39.48 | 35.3 | 37.65 | 34.94 | 43.08 |
| | (2.62) | (2.68) | (2.37) | (5.51) | (1.90) | (7.31) | (3.14) |
| Ni | 52.42 | 55.03 | 60.68 | 52.65 | 56.86 | 45.15 | |
| | (3.09) | (2.83) | (2.79) | (4.06) | (2.03) | (1.8) | 55 (2.34) |
| Cu | | | | | | | 85.63 |
| | 124.07 | 116.55 | 126.17 | 142.93 | 71.99 | 97.33 | (4.53) |
| | (7.31) | (10.47) | (13.02) | (6.37) | (14.44) | (15.91) | |
| Zn | 185.77 | 211.65 | 219.53 | 200.79 | 249.20 | 205.96 | 304.14 |
| | (13.14) | (15.1) | (11.43) | (19.05) | (4.10) | (4.01) | (28.62) |
| Sr | 64.91 | 78.46 | 73.62 | 92.00 | 96.24 | 84.69 | |
| | (1.31) | (3.10) | (1.30) | (3.47) | (1.73) | (3.35) | 95.06 (7) |
| Zr | | | | | 93.48 | 84.82 | 86.67 |
| | 119.40 | 125.13 | 131.74 | 120.32 | (1.25) | (3.58) | (1.11) |
| | (9.03) | (3.98) | (3.94) | (3.19) | | | |
| Mo | 1.45 | 1.14 | 1.11 | 1.54 | 1.14 | 1.42 | 2.25 |
| | (0.19) | (0.18) | (0.14) | (0.10) | (0.07) | (0.14) | (0.14) |
| Ba | 337.64 | 362.08 | 345.46 | 350.67 | 395.64 | 324.57 | 234.25 |
| | (7.92) | (14.13) | (4.67) | (13.26) | (6.04) | (23.10) | (20.83) |
| Pb | 46.44 | 67.23 | 58.93 | 67.21 | 66.91 | 57.06 | |
| | (3.99) | (7.55) | (4.53) | (6.61) | (1.45) | (6.17) | 108.41 |
| | | | | | | | (8.75) |

**Table 3.2** Surficial spring (top) and summer (bottom) of grain size (first 2 rows) and concentrations of the 40 elements at each site. Units in PPM unless otherwise stated

| | Lee7 | Lee6 | Lee5 | Lee2.5 | Lee2 | Lee0 | LeeS2 |
|---|---|---|---|---|---|---|---|
| Grain size (μm) | 27.23 | 4.72 | 3.10 | 2.08 | 1.93 | 2.56 | 0.97 |
| | 21.69 | | 8.13 | 2.27 | | | 1.32 |
| Grain size <63 | 6.49 | 3.35 | 2.99 | 1.51 | 1.49 | 2.34 | 0.96 |
| (μm) | 9.61 | | 3.00 | 1.78 | | | 1.29 |
| Li | 38.3 | 41.5 | 46.2 | 46.4 | 56.7 | 48.3 | 75.1 |
| | 41.9 | | 43.4 | 47.8 | | | 69.4 |
| Mg (%) | 0.5 | 0.6 | 0.66 | 0.57 | 0.81 | 0.67 | 0.91 |
| | 0.49 | | 0.57 | 0.67 | | | 0.99 |
| Al (%) | 4.21 | 4.76 | 4.52 | 4.11 | 5.84 | 4.11 | 5.46 |
| | 4.09 | | 4.37 | 4.43 | | | 5.43 |
| K(%) | 1.41 | 1.7 | 1.62 | 1.48 | 1.91 | 1.65 | 2.1 |
| | 1.44 | | 1.64 | 1.76 | | | 2 |
| Sc | 7.8 | 8.6 | 9 | 8 | 10.9 | 7.8 | 9.7 |
| | 7.7 | | 7.7 | 8.3 | | | 9.7 |
| V | 64 | 72 | 75 | 68 | 89 | 81 | 113 |
| | 61 | | 70 | 81 | | | 96 |
| Cr | 55 | 63 | 64 | 57 | 75 | 60 | 86 |
| | 47 | | 58 | 62 | | | 78 |
| Fe (%) | 2.51 | 2.88 | 3.02 | 2.61 | 3.64 | 2.93 | 4.27 |
| | 2.49 | | 2.83 | 2.99 | | | 3.85 |
| Ga | 11.79 | 13.28 | 13.13 | 11.67 | 15.57 | 12.76 | 18.07 |
| | 10.99 | | 12.82 | 14.02 | | | 16 |
| As | 5.5 | 7.9 | 8.8 | 7.6 | 10.1 | 10.1 | 16.2 |
| | 6.6 | | 6.7 | 8.7 | | | 11.2 |
| Rb | 66 | 75.9 | 78.1 | 73.2 | 98.9 | 75.6 | 94.9 |
| | 68.3 | | 78.4 | 81.3 | | | 66.7 |
| Tl | 0.43 | 0.45 | 0.5 | 0.44 | 0.61 | 0.54 | 0.69 |
| | 0.43 | | 0.47 | 0.55 | | | 0.66 |
| Bi | 0.16 | 0.24 | 0.35 | 0.27 | 0.36 | 0.53 | 0.38 |
| | 0.16 | | 0.19 | 0.21 | | | 0.31 |
| La | 40.4 | 35.4 | 34.8 | 32.4 | 34.1 | 25.8 | 18.2 |
| | 37.5 | | 35.7 | 31.2 | | | 13.9 |
| Ce | 75.42 | 71.75 | 68.96 | 67.1 | 69.68 | 53.74 | 40.94 |
| | 73.63 | | 71.4 | 64.7 | | | 31.12 |
| Pr | 9.7 | 9.2 | 8.5 | 8.3 | 8.4 | 6.6 | 5.3 |
| | 9.3 | | 9.1 | 8.1 | | | 4.1 |
| Nd | 36.4 | 35.3 | 33.4 | 32 | 34.3 | 25.4 | 20.7 |
| | 35.5 | | 36.6 | 30.6 | | | 16.1 |
| Sm | 6.9 | 6.5 | 7 | 6.5 | 6 | 5.1 | 4.5 |
| | 6.6 | | 6.9 | 5.7 | | | 3.7 |
| Eu | 1.4 | 1.4 | 1.2 | 1.2 | 1.3 | 1 | 0.8 |
| | 1.2 | | 1.3 | 1 | | | 0.8 |
| Gd | 5.1 | 4.5 | 5.1 | 4.9 | 5.2 | 4.7 | 3.7 |
| | 5.4 | | 5.5 | 4.8 | | | 3.6 |
| Dy | 3.6 | 4 | 4.1 | 3.3 | 4.3 | 3.1 | 3.5 |
| | 3.4 | | 3.7 | 4 | | | 2.6 |

| | | | | | | | |
|---|---|---|---|---|---|---|---|
| Y | 18.5 | 18 | 19.2 | 16.7 | 17.8 | 14.7 | 13.9 |
| | 17 | | 18 | 16.5 | | | 11.9 |
| Er | 2.3 | 2.3 | 2.2 | 2.2 | 2.5 | 1.8 | 1.9 |
| | 2 | | 2.2 | 2.1 | | | 1.5 |
| Yb | 2.3 | 2.2 | 1.9 | 2.3 | 2.1 | 1.9 | 1.7 |
| | 2.2 | | 2.4 | 2.1 | | | 1.5 |
| Th | 10.5 | 9.9 | 9.5 | 9 | 9 | 7.7 | 6 |
| | 10.6 | | 9.6 | 8.6 | | | 4.6 |
| U | 3.1 | 2.9 | 3 | 3 | 2.7 | 2.2 | 2.3 |
| | 3.1 | | 3.2 | 3.2 | | | 1.2 |
| Na (%) | 0.987 | 1.048 | 1.515 | 1.359 | 2.134 | 2.311 | 2.51 |
| | 0.972 | | 1.25 | 1.506 | | | 3.851 |
| P (%) | 0.379 | 0.364 | 0.464 | 0.436 | 0.811 | 0.729 | 1.185 |
| | 0.375 | | 0.649 | 0.579 | | | 1.123 |
| Ca (%) | 0.32 | 0.38 | 0.27 | 0.23 | 0.25 | 0.26 | 0.26 |
| | 0.28 | | 0.26 | 0.23 | | | 0.31 |
| Ti (%) | 0.459 | 0.446 | 0.401 | 0.379 | 0.341 | 0.321 | 0.329 |
| | 0.386 | | 0.358 | 0.327 | | | 0.286 |
| Mn | 1048 | 1438 | 2014 | 1987 | 1538 | 697 | 686 |
| | 1382 | | 1083 | 3734 | | | 627 |
| Co | 22.8 | 24.1 | 27.5 | 23.2 | 30.1 | 20.8 | 25.4 |
| | 23.7 | | 22.1 | 29.5 | | | 30.4 |
| Ni | 41.5 | 43.2 | 46.6 | 41 | 46.6 | 36.2 | 47 |
| | 40.7 | | 39.5 | 45.9 | | | 43.8 |
| Cu | 144.2 | 145 | 84.7 | 154.2 | 210.4 | 211.7 | 84 |
| | 125 | | 124.8 | 164 | | | 84.4 |
| Zn | 142 | 145 | 161.7 | 167 | 219.4 | 184.2 | 254 |
| | 131.4 | | 134.6 | 187.9 | | | 215.2 |
| Sr | 71 | 95 | 84 | 83 | 94 | 76 | 73 |
| | 71 | | 77 | 81 | | | 65 |
| Zr | 163.7 | 142.9 | 141.2 | 133.9 | 97.6 | 112.4 | 85.2 |
| | 135.7 | | 141.7 | 117.8 | | | 78.7 |
| Mo | 0.59 | 1.09 | 0.92 | 1.07 | 1.03 | 1.27 | 1.64 |
| | 0.57 | | 0.57 | 1.13 | | | 1.66 |
| Ba | 337 | 393 | 365 | 357 | 368 | 305 | 310 |
| | 353 | | 353 | 369 | | | 261 |
| Pb | 31.74 | 59.08 | 50.49 | 40.97 | 65.83 | 103.86 | 57.77 |
| | 32.6 | | 38.83 | 44.84 | | | 65.86 |

**Table 3.3** Average concentration (standard error) of 40 elements at Susquehanna River and shoreline sites.

| Element | Susquehanna River | Shoreline |
|---|---|---|
| Li | 55.39 (1.9) | 30.7 (2.74) |
| Mg | 0.8 (0.13) | 0.71 (0.1) |
| Al | 5.53 (0.21) | 3.93 (0.34) |
| K | 2.05 (0.06) | 1.5 (0.18) |
| Sc | 9.98 (0.41) | 8.72 (0.82) |
| V | 81.31 (3.37) | 108.56 (13.06) |
| Cr | 51.92 (2.88) | 110.44 (21.3) |
| Fe | 3.39 (0.15) | 5.33 (0.64) |
| Ga | 16.27 (0.72) | 12.06 (1.02) |
| As | 7.31 (0.27) | 23.54 (2.9) |
| Rb | 102.91 (3.87) | 63.48 (9.81) |
| Tl | 0.65 (0.03) | 0.36 (0.03) |
| Bi | 0.29 (0.02) | 0.28 (0.03) |
| La | 37.38 (1.39) | 30.59 (2.7) |
| Ce | 78.19 (3.14) | 66.48 (6.24) |
| Pr | 8.98 (0.37) | 7.58 (0.67) |
| Nd | 37.12 (1.6) | 30.09 (2.55) |
| Sm | 7.37 (0.34) | 6.16 (0.55) |
| Eu | 1.41 (0.07) | 1.26 (0.11) |
| Gd | 6.18 (0.37) | 5.32 (0.46) |
| Dy | 4.78 (0.26) | 4.38 (0.38) |
| Y | 21.45 (1.06) | 20.73 (1.84) |
| Er | 2.52 (0.12) | 2.31 (0.21) |
| Yb | 2.48 (0.13) | 2.14 (0.2) |
| Th | 9.38 (0.37) | 6.94 (0.55) |
| U | 2.72 (0.09) | 3.11 (0.23) |
| Ca | 0.88 (0.58) | 0.68 (0.11) |
| Ti | 0.21 (0.03) | 0.15 (0.02) |
| Mn | 1485.77 (80.06) | 2259.5 (398.86) |
| Co | 33.49 (1.92) | 24.65 (4.23) |
| Ni | 57.24 (2.19) | 61.89 (9.52) |
| Cu | 95.21 (6.82) | 299.94 (46.01) |
| Zn | 207.62 (9.07) | 203.33 (23.85) |
| Sr | 106.46 (23.43) | 105.12 (6.84) |
| Zr | 69.04 (7.6) | 34.29 (8.56) |
| Mo | 0.93 (0.05) | 3.02 (0.36) |
| Ba | 475.77 (31.02) | 311.19 (35.07) |
| Pb | 38.51 (3) | 71.88 (16.09) |

## Figures

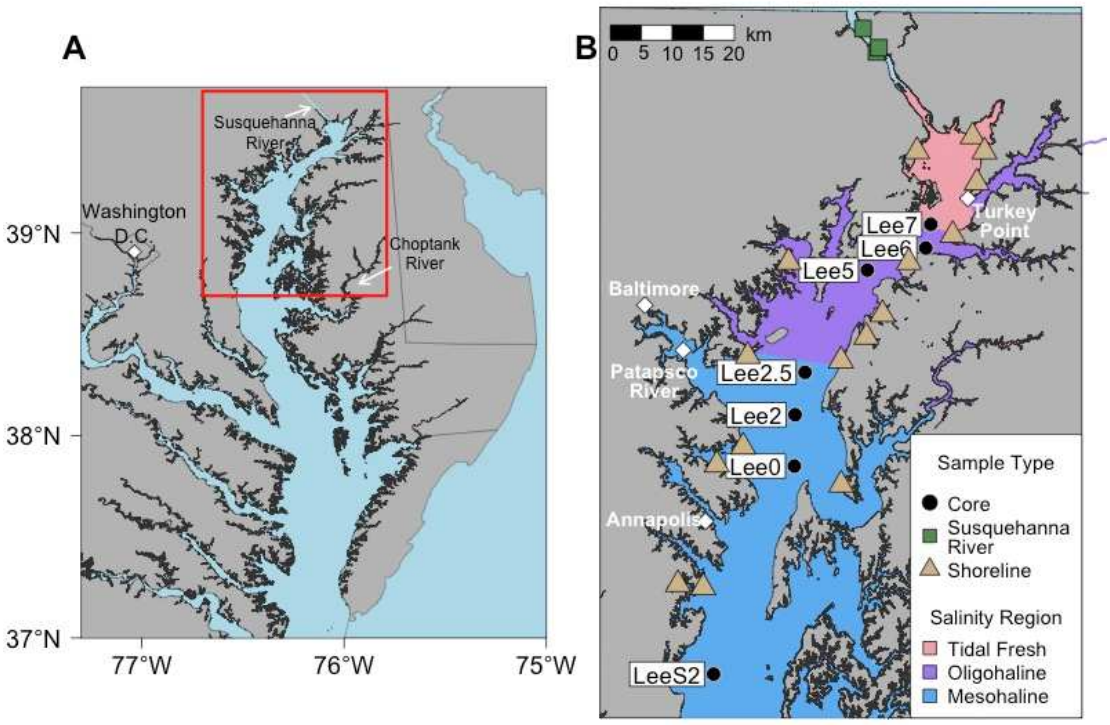


**Figure 3.1** (A) Map of Chesapeake Bay; the red box outlines the area shown in B. (B) Location and names of cores (black circles) and location where Susquehanna River (green squares) and shoreline sediments (tan triangles) were collected. White diamonds indicate the locations of places noted in the text. The major salinity regions are shown in the shading indicated by the legend.

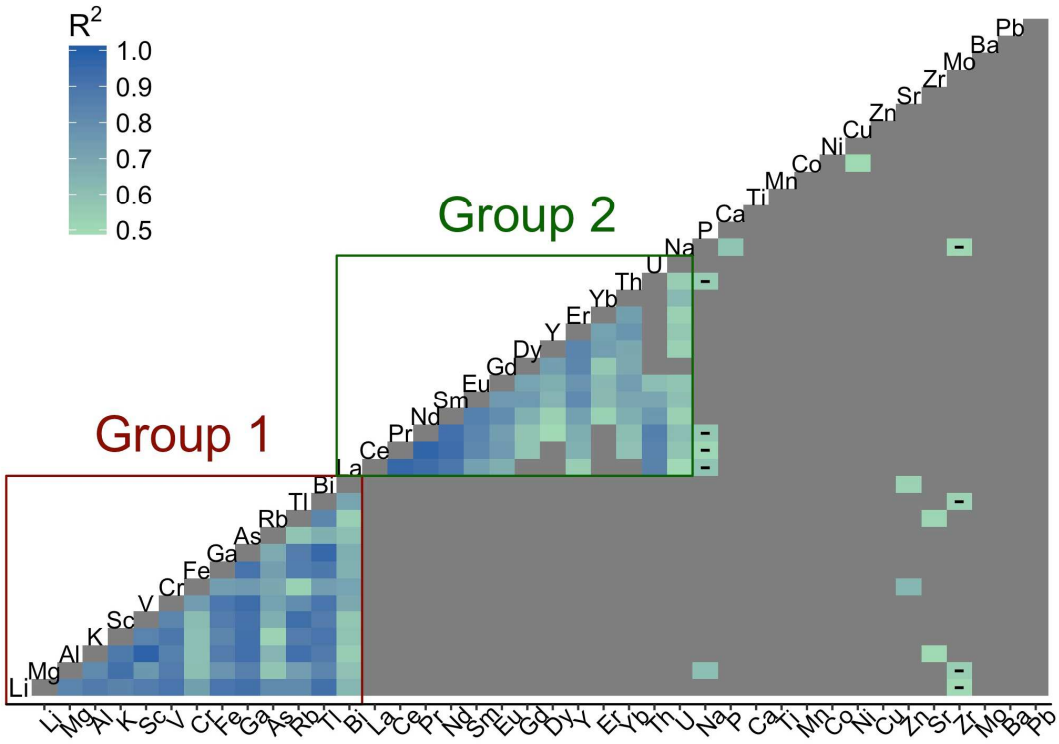


**Figure 3.2** Correlation matrix of 40 elements measured across all upper Bay samples (n=63). To aid in visual interpretation, elements have been organized into groups with similar correlations (red box=group 1; green box= group 2). Black dashes indicate negative correlations (e.g. Na and Zr), and the shading represents the $R^2$ value for correlations with $R^2$ >0.5 as noted in the legend (gray indicates $R^2$<0.5). The x- and y- axes labels correspond to column and row, respectively.

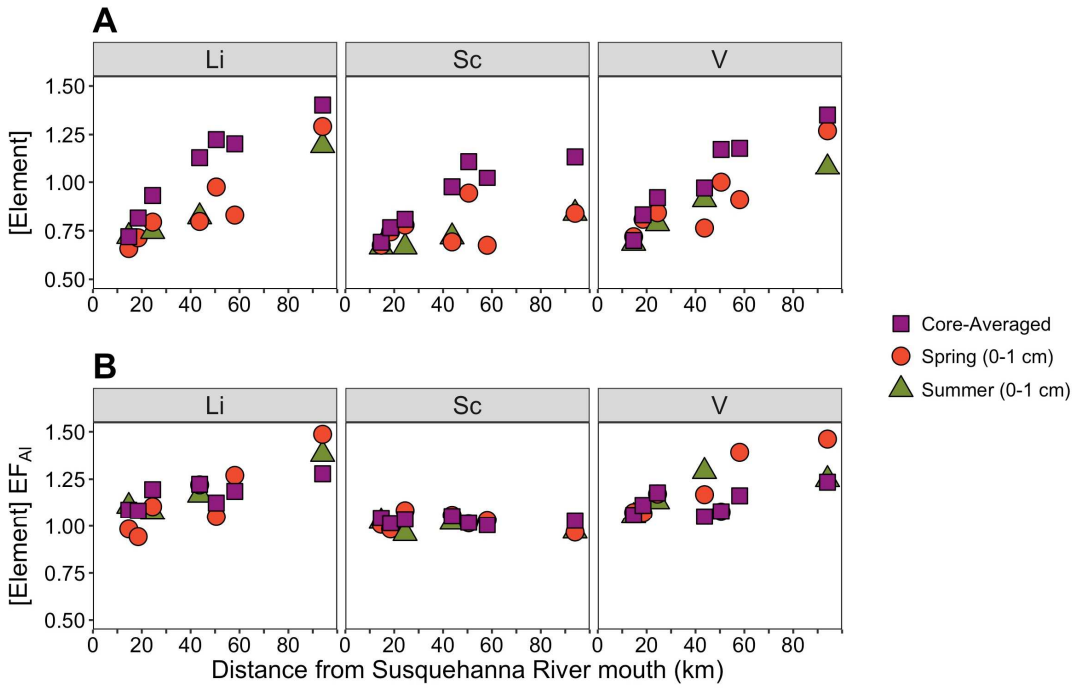


**Figure 3.3** Examples of observed trends in elements concentrations (Li, Sc, and V) with distance from the Susquehanna River mouth. A) Core-averaged (squares), spring (0-1 cm) samples (circles), and summer (0-1 cm) samples (triangles) element concentrations with distance downstream. B) Core-averaged, spring, and summer sample enrichment factors (normalized to Al) with distance downstream. For visual clarity, the element concentrations have been normalized to surficial Susquehanna River sediment concentrations in order to be placed on the same scale.

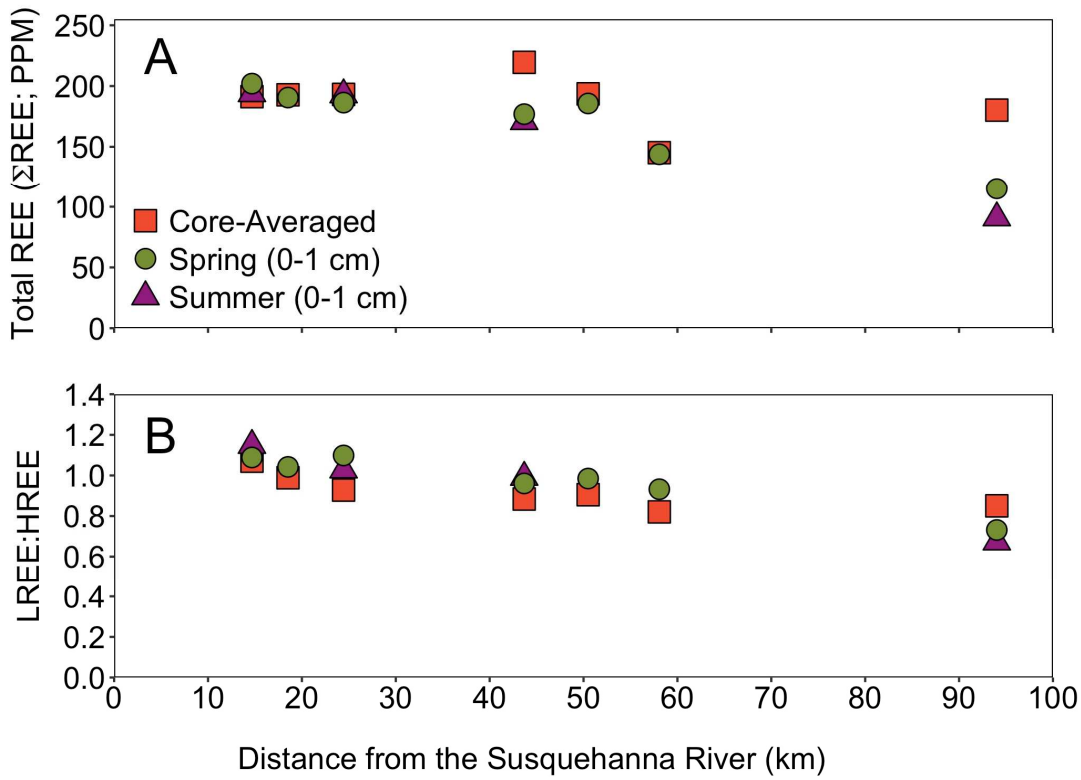


**Figure 3.4** Core-averaged (squares), spring (0-1 cm) samples (circles), and summer (0-1 cm) samples (triangles) total REE concentrations (ΣREE) (La, Ce, Pr, Nd, Sm, Eu, Gd, Dy, Y, Er, Yb) in PPM with distance from Susquehanna River sediments (A) and LREE:HREE (ΣLa, Ce, Pr, Nd:ΣEr, Yb (B).

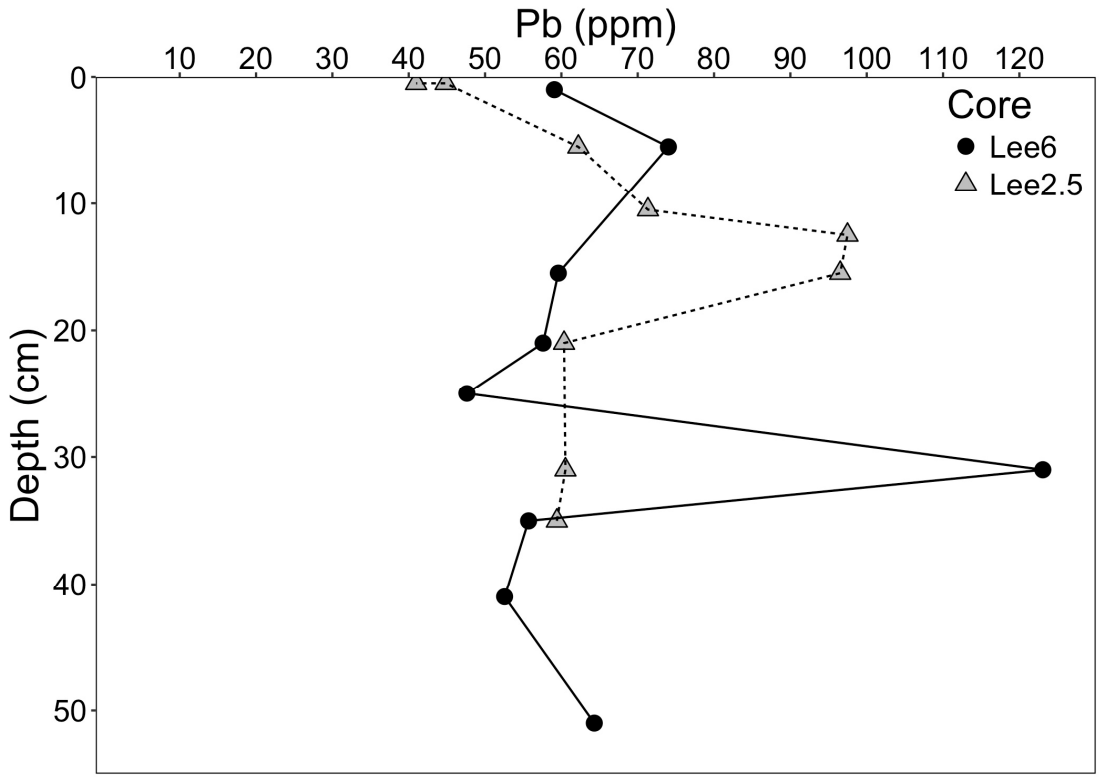


**Figure 3.5** Down-core Pb concentration profile. Black circles and gray triangles represent Lee6 and Lee2.5 profiles, respectively.

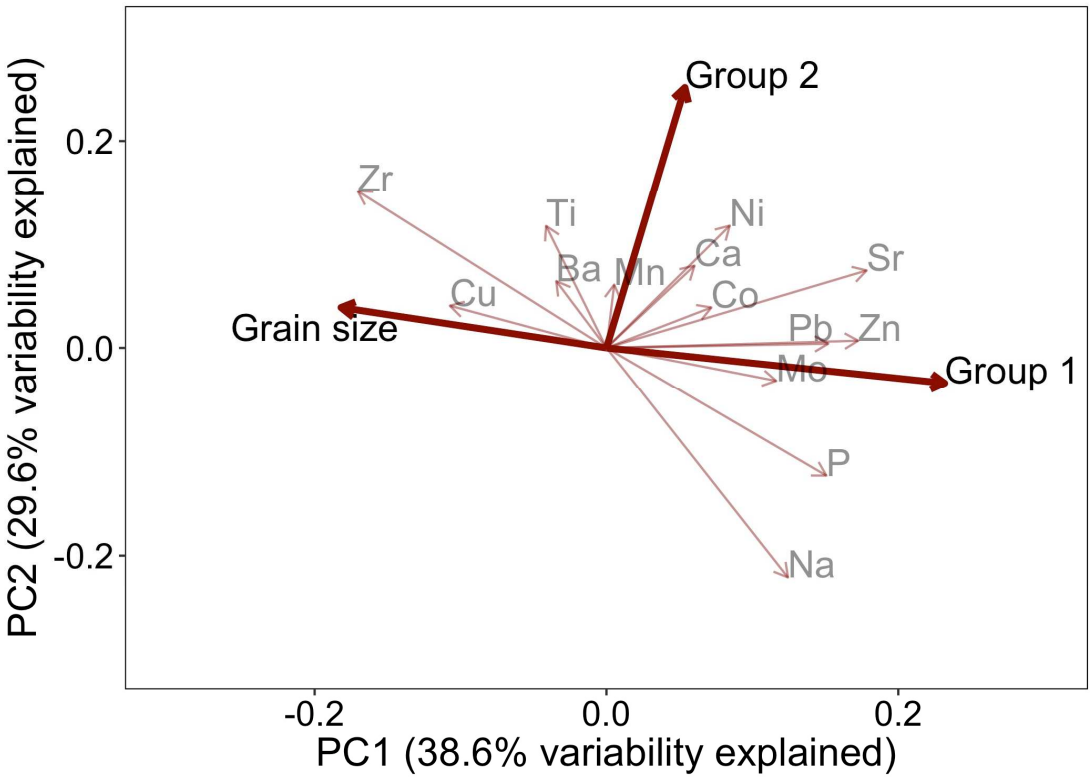


**Figure 3.6** Relative loadings of elements and grain size on the first two principal components. Elements from group 1 and group 2 have been averaged into single vectors (bolded arrows, black text) because of significant overlap among elements in these groups. Vectors for the non-correlated variables (thin arrows, gray text) are also plotted.

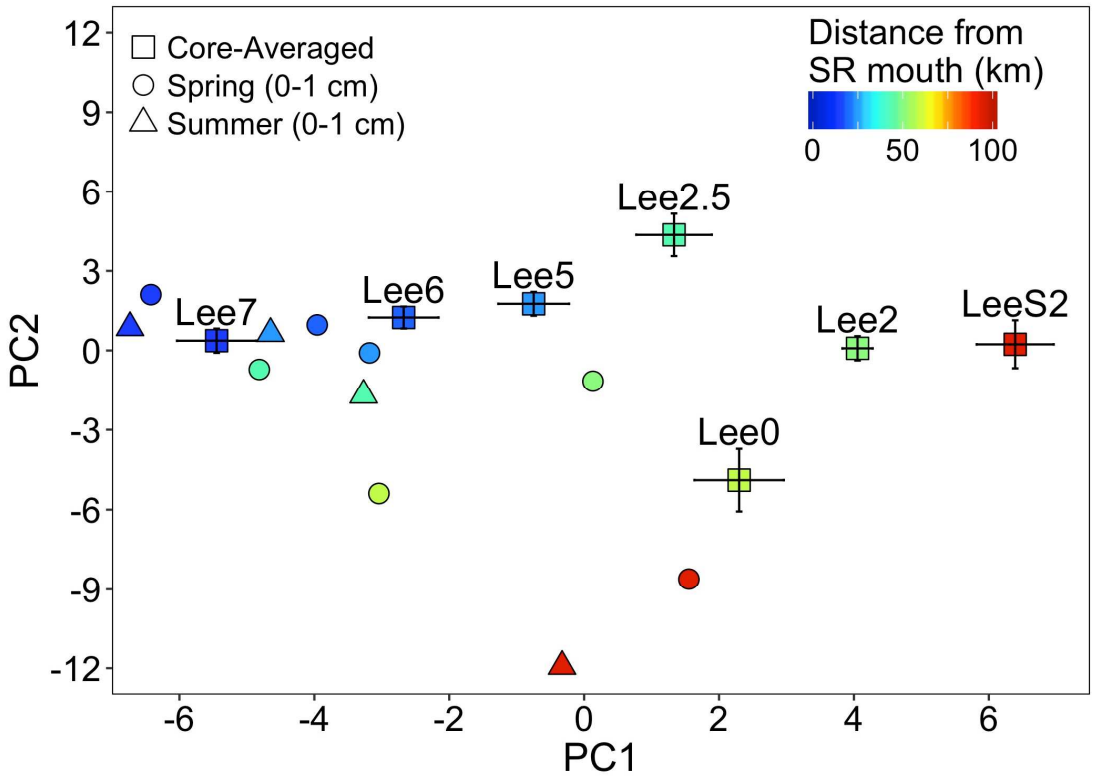


**Figure 3.7** Core averaged (squares), spring (0-1 cm) samples (circles), and summer (0-1 cm) samples (triangles) PC1 and PC2 values across upper Bay sites. Error bars represent standard error of both PC1 (horizontal) and PC2 (vertical) for the core-averaged values.

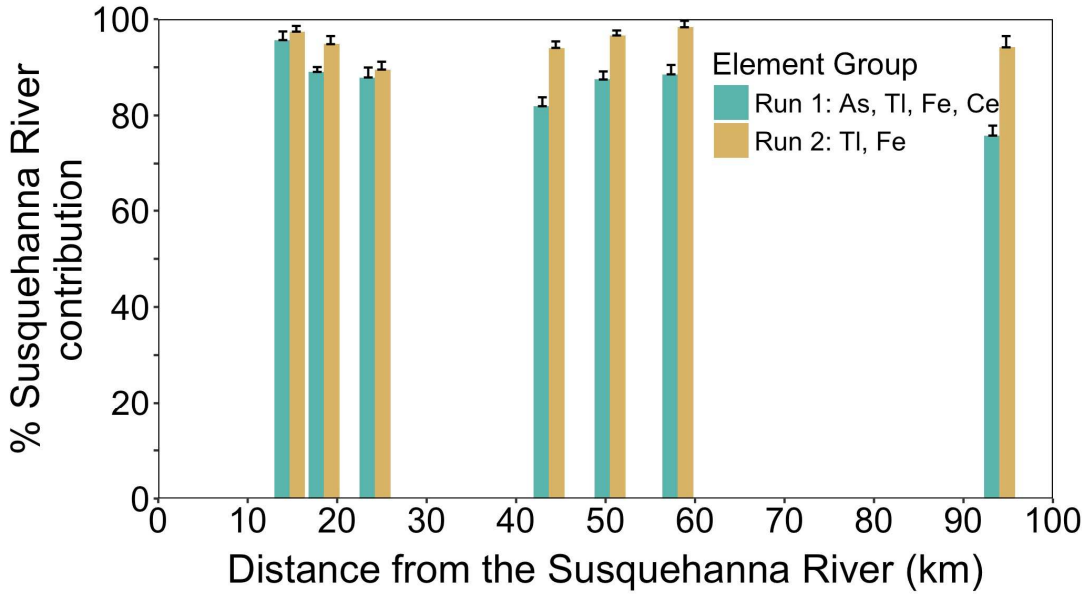


**Figure 3.8** Average percent Susquehanna River source contribution (with error bars) with distance downstream in the first Sed_SAT model run (A) using As, Tl, Fe, and Ce to determine provenance and the second Sed_SAT model run (B) using Tl and Fe.

# Chapter 4 : Sediment dynamics in upper Chesapeake Bay

**Abstract**

The upper Chesapeake Bay is an important sediment sink for fluvial and shoreline erosion sediment sources; however, evolving sediment dynamics such as increases in sediment-conservation activities, trapping behind large dams, and increased shoreline protection have altered sediment loads. Sediment budgets are important tools for quantifying sediment dynamics through identifying sources, sinks, and transport pathways. The most recent upper Bay sediment budget was developed >25 years ago and does not reflect the evolution of sediment delivery. The objective of this study is to develop an updated sediment budget through quantitative analysis of sediment sources (Susquehanna River and shoreline erosion) and sinks (Susquehanna Flats and mainstem sediment-accumulation rates) in upper Chesapeake Bay. Results indicate that Susquehanna River input to upper Bay has decreased during low flows due to implementation of conservation-management strategies; however sediment delivery has increased during high flows as a result of sediment infilling of the Conowingo Reservoir. Inputs from shoreline erosion have decreased due to increased shoreline stabilization. Mass accumulation rates in the upper Bay generally decrease with distance downstream, but elevated sedimentation rates occur in deeper water, likely due to sediment focusing in the channels. Susquehanna River and shoreline erosion sediment input from both will likely increase with changing climate due to increases in precipitation, storminess, and sea-level rise. However, shoreline erosion may be reduced due to increased shoreline stabilization, which will likely lead to changes in sediment character.

## Introduction

Estuaries often form the interface between terrestrial and marine environments, facilitating exchange and storage of materials derived from watershed and coastal sources. Estuaries are also locations with intense human development and disturbance, and every estuary in the US has been impacted by some level of human activity (Bricker et al. 1999). These activities have resulted in estuarine ecosystem changes such as increased eutrophication (Nixon 1995; Cloern 2001; Paerl 2006; Brush 2009), hypoxia (Diaz and Rosenberg 2008; Rabalais et al. 2010), and heavy metal contamination (Bricker 1993; Owens and Cornwell 1995; Spencer et al. 2003). In particular, human activities have altered sediment delivery in contrasting ways. For example, land-use changes often increase fluvial sediment loads; e.g. conversion of forests to agriculture during European settlement along the US Atlantic coast (Brush 2009; Kirwan 2011), or relatively recent increases in mining and deforestation in Papua New Guinea and Indonesia (Wolanski and Spagnol 2000; Syvitski et al. 2005). Conversely, dam construction decreases sediment delivery to estuaries and the coastal ocean (Syvitski et al. 2005; Walling 2006), leading to sinking deltas (i.e. Yangtze River; Yang et al. 2006) and rapid land loss (i.e. coastal Louisiana; Templet and Meyer-Arendt 1988; Blum and Roberts 2009). These deficits are compounded by those induced by shoreline-protection structures (e.g. bulkheads, seawalls, riprap) that disconnect natural exchange at the land-water interface (Dugan et al. 2011; Gittman et al. 2015). Since estuaries effectively trap sediments from a variety of sources (e.g. rivers, shoreline erosion, and ocean input), determining the net result of these impacts to specific sediment sources and sinks is important for resource management.

Sediment budgets offer a simple box-model approach to identify sediment sources and sinks, as well as likely transport pathways. Budgets can also help evaluate how a system responds to natural and anthropogenic sediment forcing (Eulie et al. 2018) and inform engineering project designs (Rosati 2005).

These issues have come to the forefront in Chesapeake Bay, the largest estuary in the United States. Humans have altered the main sources of sediment to the upper Chesapeake Bay, Susquehanna River and shoreline erosion, for >300 years, although the greatest impacts occurred after industrialization (Brush 2009). Susquehanna River watershed sediment loads were high between the mid-19$^{th}$ and early 20$^{th}$ century as humans cleared forests to support intensive agriculture and mining activities, but loads declined following farm abandonment and the implementation of conservation-management practices in the mid-20$^{th}$ century (Brush 1984). Historically, up to 75% of the annual Susquehanna sediment load was trapped within the Lower Susquehanna River Reservoir system, which spans the lower 50 km of the river and includes three sequential hydroelectric dams and their associated reservoirs (in downstream order: Lake Clarke, Lake Aldred, and Conowingo Reservoir; Langland 2009; Langland 2015). The sediment-trapping capacity of these reservoirs has decreased over time due to sediment infilling, and Lakes Clarke and Aldred reached dynamic equilibrium (i.e. sediment inputs and outputs are approximately equal over long time scales; Langland 2009) in the 1950s-1960s. Recent work indicates that the last reservoir, upstream of the Conowingo Dam, has also reached this state, increasing sediment loads to the Bay (Hirsch 2012; Zhang et al. 2013; Langland 2015).

Humans have also modified shoreline inputs to the Chesapeake Bay, exacerbating land loss from increasing rates of sea-level rise (Kearney and Stevenson 1991; Boesch 2008) and intense storms (Hennessee and Halka 2005) through increased shoreline development (Hardaway and Byrne 1999). To protect development and prevent further land loss, more than 500 km (300 miles) of stabilization structures, such as seawalls and bulkheads, were installed between 1978 and 1997 (Titus 1998; Hardaway and Byrne 1999; Halka et al. 2005). Although these structures can reduce fastland erosion (above mean low water (MLW); used interchangeably with "shoreline erosion" here) and turbidity caused by fine-grained particles, nearshore erosion (below MLW) can be enhanced by decreasing sand supply to adjacent habitats and/or through reflecting, rather than dampening, wave energy (Hardaway and Byrne 1999; Halka et al. 2005).

Several sediment budgets have been previously developed for the Chesapeake Bay (Biggs 1970; Officer et al. 1984a; Donoghue et al. 1989; Hobbs et al. 1992) to evaluate sediment dynamics. However, the most recent sediment budget (Hobbs et al. 1992) was developed >25 years ago and does not reflect recent changes in sediment delivery to the Bay. Specifically, increased sediment loads from the Susquehanna due to reservoir infilling (Hirsch 2012; Zhang et al. 2013), and increased (from climate change and relatively rapid sea-level rise; Boesch 2008) or decreased (from increased shoreline stabilization; Titus 1998; Gittman et al. 2015) inputs from shoreline erosion. Furthermore, sediment accumulation on the Susquehanna Flats, the subaqueous delta of the Susquehanna that lies between the Susquehanna and upper Bay, has never been explicitly included in a sediment budget. The Susquehanna Flats contain the largest

submersed aquatic vegetation (SAV) bed in the upper Bay; it was decimated following the passage of Tropical Storm (TS) Agnes in 1972 but returned in the early 2000s (Gurbisz and Kemp 2014). This resurgence has increased sediment trapping on the Flats, modulating sediment delivery of Susquehanna River sediments to the upper Bay (Russ and Palinkas 2018). Thus, the overall goal of this study is to develop an updated sediment budget through quantitative analysis of sediment sources (Susquehanna River and shoreline erosion) and sinks (Susquehanna Flats and mainstem sediment-accumulation rates) in upper Chesapeake Bay. The insights gained from this study directly inform sediment management in the upper Bay, especially within the context of the Chesapeake Bay Total Maximum Daily Load (TMDL), that seeks to reduce fine-sediment input by 20% in 2025 (US EPA 2010). The findings from this study are also broadly applicable to other fluvial-estuarine systems, particularly those with dams approaching dynamic equilibrium.

## ***Methods***

### *Study Site*

In this study, the upper Chesapeake Bay is defined as the 100 km section extending from the Susquehanna River mouth to the Choptank River mouth (Fig. 4.1a). The Susquehanna River is the only Bay tributary that discharges directly into the Bay, rather than into a sub-estuary, supplying 85% of the total freshwater flow (average annual discharge of 1100 $m^3$ $s^{-1}$; Schubel and Pritchard 1986) and ~60% of the sediment input (Officer et al. 1984a). Sediment delivery from the Susquehanna is controlled by river discharge, which is generally highest in the spring, due to

snowmelt and precipitation, and lowest in the summer (Schubel and Pritchard 1986); 50-60% of the annual sediment load is typically delivered during the spring freshet (Gross et al. 1978). However, large storm events can contribute sediment loads that are an order of magnitude higher than average annual sediment loads (e.g. $30x10^6$ from Tropical Storm Agnes in 1972; Gross et al. 1978; 6-$19x10^6$ from Tropical Storm Lee in 2011; Hirsch 2012; Palinkas et al. 2014). These immense storm loads include scoured sediments from three sequential reservoirs along the lower portion (last 50 km) of the Susquehanna.

Shoreline erosion is the other main sediment source to the upper Bay, supplying ~$1x10^6$ t $y^{-1}$ between the mouths of the Susquehanna River and the Potomac River estuary (Fig. 4.1; Schubel 1968; Biggs 1970; Langland and Cronin 2003). Shoreline erosion around the Bay varies spatially and depends on shoreline orientation, fetch, bathymetry, sediment composition, and land use (Langland and Cronin 2003). Shoreline-change rates range from -3 to +3 m $y^{-1}$ (Sanford and Gao 2018), with ~70% of the shoreline classified as eroding (Hennessee et al. 2006). Much of the coarse material from shoreline erosion is deposited adjacent to shore in depths <3 m, while the fine fraction is transported into deeper water (Halka 2000). While biogenic production and oceanic input contribute sediment to the Bay, their input is only significant in the southern Bay, well downstream of the study area (Hobbs et al. 1992).

Historic sedimentation rates in the upper Bay range from 0.1 to 1.2 g $cm^{-2}$ $y^{-1}$ (Officer et al. 1984a). Although the variability is wide, sedimentation rates are generally highest in the upper 20-40 km of the Bay, within the estuarine turbidity

maximum (ETM) (Sanford et al. 2001), and decrease to a minimum between 100-150 km (Biggs 1970; Officer et al. 1984a; Schubel and Pritchard 1986; Donoghue et al. 1989). Previous sediment budgets indicate that between $1x10^6$ t $y^{-1}$ (Biggs 1970) to $3x10^6$ t $y^{-1}$ (Officer et al. 1984a) sediment is buried in the upper Chesapeake Bay annually. Approximately 70% of this material comes from the Susquehanna River and the remaining ~30% from shoreline erosion (Officer et al. 1984a). However, Susquehanna River sediment makes up ~80% of the material buried in the upper 40 km of the Bay, but <30% south of 40 km (Biggs 1970).

*Susquehanna River sediment load*

Susquehanna River discharge ($m^3$ $s^{-1}$) and suspended-sediment concentrations (SSCs; mg $L^{-1}$) at the Conowingo Dam between 1 January 1978 (earliest date of SSC data collection) and 31 December 2017 were used to quantify Susquehanna River sediment loads. Average daily discharge and instantaneous SSC were obtained from the USGS National Water Information System (https://waterdata.usgs.gov/nwis; site 01578310). SSC data were collected 1-2 times per month, depending on flow conditions, and assumed to represent daily SSC. An exponential model ($R^2$=0.79, p-value<0.001) was fit to average daily discharge on days with corresponding SSC following the methods of Russ and Palinkas (2018):

$$SSC = 21.74 \times \exp(2.68 \times 10^{-4} \times discharge) - 18.73 \quad (1)$$

This model was used to fill gaps in the SSC record; daily SSC was then multiplied by daily average discharge to calculate daily sediment load. The annual sediment load was calculated by summing up the daily loads for each year (Russ and Palinkas

2018). This model assumes that the relationship between discharge and SSC is constant over the 40-year record. However, recent work indicates that this relationship has evolved due to land-use changes and reservoir infilling (Langland 2015; Zhang et al. 2016a; Palinkas et al. submitted). Therefore, additional exponential models of discharge and SSC (in the same format as eq. 1; Table A.6) were developed for each decade to account for possible changes in sediment loads (Fig. 4.2).

For this budget, the Susquehanna is assumed to be the major source of fluvial sediments to the Bay, neglecting contributions from other, smaller tributaries in this region. The fluvial loads of these tributaries are at least an order of magnitude smaller than the Susquehanna River fluvial load (i.e.0.0014-0.1x$10^6$ t $y^{-1}$; Yarbro et al. 1983; Marcus and Kearney 1991; Langland and Cronin 2003), and most sediment is retained in tributary estuaries under normal conditions (Schubel and Carter 1977).

*Shoreline-change calculation*

All shoreline-change data were calculated from existing spatial datasets using Python 3.7.0 and the GeoPandas library (http://geopandas.org/). The most recent shapefiles of shoreline-stabilization structures (2004) and bank heights (2002-2006) from the Comprehensive Coastal Inventory Program, Center for Coastal Resources Management (Virginia Institute of Marine Science (VIMS), and shoreline-change transects (1970s shorelines versus 1990s or 2000s shorelines, except Talbot, which used 1942 and 1992 shorelines) from the Maryland Geological Survey (MGS) were obtained from http://data.imap.maryland.gov/. Average annual shoreline-change rates

from the MGS were calculated using the Digital Shoreline Analysis System (DSAS) (Thieler et al. 2009) by dividing the distance of shoreline change over shore-normal transects by the number of years between shoreline surveys. Average annual shoreline area (change in area between shoreline surveys) and volume change were calculated using the shoreline-change transects, stabilization structures, and bank heights shapefiles. Shoreline sediments were assumed to come from unprotected shorelines, and so only unprotected shorelines (as of 2004) were included in the shoreline-change calculations. However, many shoreline stabilization structures around the Bay were installed within the past 30 years, presumably in areas with high erosion rates (e.g. Palinkas et al. 2018). Therefore, both protected and unprotected shorelines were included to estimate maximum shoreline change; rates of change along protected shorelines were obtained from the shore-change transect shapefile. Only shorelines along the mainstem of the upper Bay were included, which assumes that tributaries retain shoreline sediments eroded within them (Schubel and Carter 1977).

All shapefiles were imported into GIS and used to quantify shoreline area and volume change for the counties surrounding the upper Bay (Fig. 4.1). Shapefiles for shoreline-stabilization structures, shoreline-change transects, and bank heights were spatially joined. Note that bank heights in the shapefile were reported as ranges (e.g. 0-1.5m, 1.5-3m, etc.); mean values (0.75 m, 2.25 m, etc.) of these ranges were used for volume-change calculations. Shoreline change could not be calculated along all upper Bay shorelines due to missing bank-height data. For example, these data were not publically available for ~80% of Harford County shorelines, which include Aberdeen Proving Grounds, a US Army facility in southeastern Harford County.

Total shoreline length, length of shoreline analyzed (sometimes shorter than the total length due to missing data), area change, and volume change were then calculated for unprotected only as well as protected and unprotected shorelines. Shoreline area and volume change were calculated along shoreline segments (i.e. continuous segments of unprotected shoreline). Shoreline positions in the shoreline-structures shapefile were assumed to represent the most current shoreline locations, since they were most recently surveyed (2004). The location of these shorelines after 1 year was determined by projecting the annual shoreline-change rate along shoreline transects. Area change was the change in area between the current and projected shoreline positions, with negative and positive values indicating erosion and accretion, respectively. Annual volume change was calculated by multiplying the average bank height along each shoreline segment by the change in area. An example of these calculations is illustrated in Fig. 4.3b. Repetition of this process for every shoreline in the counties of interest yields the total annual change in shoreline area and volume around the upper Bay. The change in volume was multiplied by 1.5 g $cm^{-3}$, the average bulk density for Maryland shoreline sediments (Langland and Cronin 2003), to determine the mass of sediment derived from shorelines.

*Sediment-accumulation rates*

Sediment cores were collected using a gravity core (~1.5m long; 7 cm diameter) at seven sites in the upper Bay (Table 4.1, Fig. 4.1b) on 28 April 2016. Intact gravity cores were returned to the laboratory and sectioned into 1-cm (0-20 cm

depth in core) and 2-cm increments (20-end of the core) for grain size and geochronological analyses.

Grain size was analyzed by wet-sieving samples at 64 μm to separate the mud (silts and clays; <64 μm) and sand (>64 μm) fractions. The mud fraction was disaggregated with 0.05% sodium metaphospate in an ultrasonic bath and then analyzed using a Sedigraph 5120. The sand fraction was dry-sieved through a standard set of 13 sieves, from 500 μm to 64 μm (at ¼-phi size intervals; phi=-log2(particle diameter, mm)). The mud and sand data were joined to calculate median diameters. Bulk density was assumed to be a function of porosity, calculated from water loss after drying at 60°C until constant sediment weight was reached, assuming sediment density of 2.65 g $cm^{-3}$.

Sediment accumulation rates were determined using $^{210}Pb$ (half-life 22.3 years) geochronology and verified with an independent geochronometer, $^{137}Cs$ (half-life 30.17 years). $^{210}Pb$ is primordial, and part of the $^{238}U$ decay series, so all sediment particles have supported $^{210}Pb$ activity due to decay of its effective parent $^{226}Ra$ ("supported activity"). $^{210}Pb$ is also supplied to the water column through precipitation and runoff; watershed sediments delivered to the upper Bay scavenge $^{210}Pb$ as they settle through the water column ("excess activity"; Koide et al. 1972; Nittrouer et al. 1979). $^{137}Cs$ is an anthropogenic radioisotope that was introduced to the atmosphere through nuclear testing, beginning in 1954 and reaching a peak in 1963 (Walling and He 1997).

Total $^{210}Pb$ (half-life 22.3 y) activities were measured using alpha spectroscopy and following the procedures of Palinkas and Engelhardt (2016). $^{226}Ra$-

supported $^{210}$Pb activity was assumed to be equal to the activity at the bottom of each core and was calculated via gamma spectroscopy from a weighted average of the $^{214}$Pb energies (295 and 352 keV) and $^{214}$Bi photopeak (609 keV). Excess $^{210}$Pb activities for each core were calculated by subtracting the corresponding supported $^{210}$Pb activity from total $^{210}$Pb activities. If the core was not long enough to reach a constant, low $^{210}$Pb activity indicative of the supported value, and the $^{210}$Pb profile had a relatively steady logarithmic decrease with depth characteristic of steady-state accumulation, its supported $^{210}$Pb activity was estimated by calculating the remaining activity of the total $^{210}$Pb activity at the top of the core (below the surface mixed layer, if present) after five half-lives (assumed limit of detectability). All measured activities were decay-corrected to the time of collection; excess activities were normalized to the corresponding measured mud fraction, because $^{210}$Pb preferentially adsorbs to fine particles (Nittrouer et al. 1979; Goodbred and Kuehl 1998).

Sedimentation rates were calculated using the constant flux/constant sedimentation (CFCS) model, which assumes a constant supply of unsupported $^{210}$Pb to the sediment and steady-state sedimentation (Appleby and Oldfield, 1978). This model was chosen since most (5 of 7) profiles exhibited steady-state behavior (Fig. 4.4a). Linear sedimentation rates (cm $y^{-1}$) were calculated from the slope of the linear regression fit between the log of excess $^{210}$Pb activity and depth. Mass accumulation rates (g $cm^{-2}$ $y^{-1}$) were calculated by multiplying the sedimentation rate by the core-averaged dry bulk density. For the 2 profiles with variable $^{210}$Pb with depth, characteristic of non-steady-state sedimentation (Fig. 4.4b), minimum sedimentation

rates were calculated by dividing the maximum depth of excess $^{210}$Pb by 100 years (the assumed limit of detectability; Jaeger et al. 1998).

The total amount of sediment buried in the upper Bay was calculated by extrapolating these mass accumulation rates across its area. The upper Bay was sectioned into 1-km long (from north to south) compartments in R (version 3.3.3), generated by intersecting a series of 100 equal-sized rectangles with a polygon of the upper Bay (Fig. 4.5a). A single mass accumulation rate was calculated for each compartment by linearly interpolating the mass accumulation rate between the nearest sites. The rates were multiplied by the compartment area and summed together to obtain annual sediment burial. Because upper Bay sedimentation displays much spatial variability likely not captured by the cores collected for this study, $^{210}$Pb accumulation from previous studies were added to the dataset (Table A.7) to obtain another estimate of sediment burial in the upper Bay. The complete dataset was also used to generate a predictive multiple-linear-regression model of accumulation rate with distance from the Susquehanna River mouth and water depth. A third estimate of sediment accumulation was quantified by applying this model to raster datasets of bathymetry and distance from the Susquehanna River mouth.

## Results

*Sediment sources: Susquehanna River and shoreline erosion*

The average annual discharge of the Susquehanna River from 1978-2017 ranged from 667.13 $m^3 s^{-1}$ (2001) to 2041.37 $m^3 s^{-1}$ (2011) with an average of 1123.4±52.3 $m^3 s^{-1}$. Average discharge in 2011 was exceptionally high due to

Tropical Storm Lee, which produced the second highest river discharge recorded at the Conowingo Dam outlet on 9 September 2011 (22000 $m^3 s^{-1}$; Palinkas et al. 2014). Other notable high-discharge events occurred in 1996 (ice dam melt) and 2004 (remnants of Hurricane Ivan), which had average annual discharges of 1797.2±98.6 $m^3 s^{-1}$ and 1855.8±81.5 $m^3 s^{-1}$, respectively. Measured suspended-sediment concentration (SSC) values from 1978-2017 (~1000 samples) varied from 1 mg $L^{-1}$ (2 February 1982) to 3680 mg $L^{-1}$ (20 September 2004) with a median of 13 mg $L^{-1}$ and average of 39.7±5.3 mg $L^{-1}$. Approximately 6% of all measured SSC were above 100 mg $L^{-1}$.

Annual suspended-sediment loads calculated from eq. 1, which includes all years, ranged from 0.3-15.7x$10^6$ t $y^{-1}$, with an average annual load of 1.7±0.4x$10^6$ t $y^{-1}$. However, there were differences in the relationship of discharge and SSC among the 4 decadal time periods evident in Fig. 4.2. For example, calculated SSCs were lower in 2008-2017 than 1978-1987 at discharges below 3500 $m^3 s^{-1}$, while SSCs were higher in 2008-2017 than 1978-1987 at discharges above 3500 $m^3 s^{-1}$. Using separate equations for each decade of measurement (Table A.6), average annual sediment loads were 1.5±0.3 t $y^{-1}$ for 1978-1987, 1.3±0.4 t $y^{-1}$ for 1988-1997, 1.8±0.8 t $y^{-1}$ for 1998-2007, and 2.9±2.2 t $y^{-1}$ for 2008-2017, with an average of 1.9±0.6 t $y^{-1}$. Note that all of these time periods include high-flow events. For flows above ~11,300 $m^3 s^{-1}$ (400,000 cfs), scoured sediment from reservoir bottoms joins with eroded watershed sediments to produce exceptionally high sediment loads (Gross et al. 1978; Hirsch 2012; Palinkas et al. 2014). This is especially apparent in 1996, 2004, and

2011, for which >70 % of the annual sediment load occurred during individual events.

Erosion, rather than accretion, dominates shoreline change in the upper Bay as indicated by the net negative change in shoreline area and volume (Table 4.2). Annual shoreline area change ranged from $+1.9 \times 10^3$ $m^2$ in Baltimore County to $-12.9 \times 10^3$ $m^2$ in Kent County, for a total land loss of $22.0 \times 10^3$ $m^2$ $y^{-1}$ along unprotected shorelines. Total sediment volume eroded from unprotected upper Bay counties was $64.4 \times 10^3$ $m^3$ $y^{-1}$, which is equivalent to $0.10 \times 10^6$ t $y^{-1}$. When protected shorelines were included in the calculations, the annual sediment loss from upper Bay counties nearly doubled ($0.19 \times 10^6$ t $y^{-1}$). However, this is a conservative estimate because elevation data were not available for ~35% of shorelines (unprotected and protected). The missing mass of sediment can be estimated by multiplying the calculated change in area along each county by the average bank height in each county and sediment bulk density, increasing the total loss to 0.24 t $y^{-1}$.

*Sediment sinks: sediment accumulation rates and net burial*

Sediments in upper Bay cores were dominantly muddy (grain sizes <63 μm), with core-averaged mud fractions ranging from a minimum of 69±1.0% at Lee6 to a maximum of 99±0.2% at LeeS2 (Table 4.3). Median diameters were relatively uniform with depth in all cores, and core-averaged median diameter generally decreased with distance downstream from silt-sized (20.65±2.62 μm) in the north (Lee7) to clay-sized (0.49±0.06 μm) in the south (LeeS2). Core-averaged bulk

densities ranged from 1.14±0.10 g $cm^{-3}$ at the northernmost site (Lee7) to 0.35±0.01 g $cm^{-3}$ at a southern site (Lee0).

Most cores had relatively strong CFCS model fits ($R^2$ = 0.71-0.91; p-values < 0.01), exemplified by the $^{210}$Pb profile for Lee2.5 (Fig. 4.4a). However, there was no significant relationship between depth and excess $^{210}$Pb activity at Lee2 and Lee0 (e.g. Fig. 4.4b) indicating non-steady-state sedimentation; minimum sedimentation rates (0.81 cm $y^{-1}$) were calculated for these cores by dividing the maximum depth of excess $^{210}$Pb (base of the cores) by 100 years. Lee2 and Lee0 are closer to the main channel (<0.5 km) and in deeper water than the other sites (13.5 m) (Table 4.1), suggesting depositional processes are different in deeper water. Sediment accumulation rates increased between Lee7 (0.34 cm $y^{-1}$) and Lee5 (1.20 cm $y^{-1}$), then decreased to the south (minimum of 0.26 cm $y^{-1}$ at LeeS2). The minimum rates at Lee2 and Lee0 are higher than those at the adjacent up- and down-stream sites, suggesting higher accumulation in deeper waters of the main channel.

Sediment horizons corresponding to 1954 and 1963 were identified from the $^{137}$Cs profile (first appearance and maximum activity, respectively) for all cores except Lee5, where maximum $^{137}$Cs activity occurred at the base of the core. The $^{137}$Cs-derived sedimentation rates at Lee7, Lee6, Lee2.5, and LeeS2 were within 20% of CFCS derived rates (0.26-0.84 cm $y^{-1}$ for $^{210}$Pb vs 0.29-0.85 cm $y^{-1}$ for $^{137}$Cs). At Lee5, $^{137}$Cs, the activity at the bottom of the core was similar to the activity of the assumed 1963 peaks in the other cores (~1.00 dpm $g^{-1}$). Assuming the base of Lee5 corresponds to ~1963, the $^{137}$Cs-derived rate was 1.11 cm $y^{-1}$, similar to the CFCS-derived rate of 1.20 cm $y^{-1}$. The $^{137}$Cs-derived sedimentation rate at Lee2 (0.87 cm $y^{-}$

$^{-1}$) is consistent with the minimum sedimentation rate from $^{210}$Pb; however, at Lee0, the rates differed by a factor of >2.5 (0.30 cm y$^{-1}$ for $^{137}$Cs and 0.81 cm y$^{-1}$ for $^{210}$Pb).

Net sediment burial was calculated using mass accumulation rates (linear $^{210}$Pb-derived rates multiplied by the corresponding core-averaged bulk density; Table 4.3). Assuming uniform sedimentation in each 1-km compartment, 3.50x10$^{6}$ t y$^{-1}$ is buried in the 1071 km$^{2}$ area between Lee7 and LeeS2 (Fig. 4.5a). When the mass accumulation rates from previous studies are included (Table A.7; Fig. 4.5b), 4.42x10$^{6}$ t y$^{-1}$ is buried in the upper Bay. Lastly, spatial predictors for sedimentation rates were assessed through linear relationships with distance downstream and water depth (Table 4.1 and Table A.7). Mass accumulation rate was not linearly correlated with depth ($p>0.1$) but was weakly correlated with distance downstream ($R^2=0.17$; $p<0.02$). Mass accumulation rates were best predicted from a multiple linear regression model that included both distance downstream (km) and depth (m) ($R^2=0.62$; $p<0.001$). Using this model on raster grids of bathymetry and distance downstream, 4.04x10$^{6}$ t of sediment is buried in the upper Bay each year (Fig. 4.6).

To these totals, sedimentation on the Susquehanna Flats (upstream of Lee7) can be added by extrapolating accumulation rates from Russ and Palinkas (2018), which ranged from 0.63 g cm$^{-2}$ y$^{-1}$ to 1.25 g cm$^{-2}$ y$^{-1}$ and averaged 0.99±0.12 g cm$^{-2}$ y$^{-1}$. Since sedimentation on the Flats is controlled by both plant presence and spatial focusing (see Discussion), net burial in this area was calculated by multiplying the average SAV bed area size between 1984 and 2016 (28.02±2.01; Gurbisz et al. 2014; Orth et al. 2016) by the maximum and minimum sedimentation rate, yielding a range

of 0.18-0.35x$10^6$ t $y^{-1}$. Adding this to the upper Bay yielded a total sediment burial of 3.68-4.77 t $y^{-1}$ buried.

## Discussion

A sediment budget provides a useful framework for evaluating current sediment sources and sinks, as well as discussing possible future changes relevant to sediment management. The text below discusses uncertainties of calculations within the context of previous work, as well as broader implications and relevance to management.

### *Sediment sources*

In upper Chesapeake Bay, the two dominant sediment sources are fluvial input and shoreline erosion. In this study, I evaluated fluvial delivery only from the Bay's main tributary, the Susquehanna River, and calculated an annual average load of 1.7-1.9x$10^6$ t $y^{-1}$. This load agrees well with previous load estimates (1-2x$10^6$ t $y^{-1}$; Gross et al. 1978; Langland 2015), even though the relationship of suspended-sediment concentration (SSC) to river discharge has changed over time (Zhang et al. 2013; Palinkas et al. submitted). These changes are evident in the decadal-scale rating curves (Fig. 4.2), highlighting the role of "normal" versus event (high-flow) river discharges. In particular, lower SSCs at discharges <3000 $m^3$ $s^{-1}$ in recent years indicate reduced sediment supply at lower discharges over time. This decrease in

sediment loading has been attributed to recent changes in land use and implementation of erosion control/soil conservation best-management practices (BMPs) in the Susquehanna River watershed (Langland 2015; Zhang et al. 2016a; Palinkas et al. submitted). In contrast, recent increases in SSC at high river discharges are consistent with increased scouring due to infilling of the Conowingo Reservoir (Hirsch 2012; Zhang et al. 2013; Palinkas et al. submitted). Although infrequent, these flood events deliver enormous volumes of sediment to the upper Bay, greatly outweighing contributions from normal flows (e.g. up to 80% of the 2011 load was delivered by TS Lee) and influencing the shape of rating curves (Zhang et al. 2016b). The lower end of my range in annual Susquehanna sediment load was derived from equation 1, which uses data from 1978-2017; in contrast, Gross et al. (1978) and Langland (2015) used data from 1966-1976 and 1928-2012, respectively to calculate previous sediment loads. The higher end ($1.9 \times 10^6$ t $y^{-1}$) was calculated using discrete decadal equations, which include events, and most likely represents the "true" Susquehanna sediment load ("best estimate" in Table 4.4). Note that neither of these values includes sediment from other rivers. This potential input is poorly characterized, but the few studies that exist indicate that most tributaries retain their sediment and even import sediment from the Bay (Schubel and Carter 1977; Palinkas and Cornwell 2012), although sediment transport during high-flow events has not been studied.

My calculations of sediment load from shoreline (fastland) erosion range from $0.10 \times 10^6$ t $y^{-1}$ to $0.24 \times 10^6$ t $y^{-1}$, depending on treatment of protected shorelines. It is important to note the average bank height was used in my calculations; using

maximum bank heights yields greater shoreline contributions (between $0.14x10^6$ t $y^{-1}$ and $0.31x10^6$ t $y^{-1}$), while using minimum bank height yields lower shoreline contributions (between $0.06x10^6$ t $y^{-1}$ to $0.12x10^6$ t $y^{-1}$). The lower estimate of shoreline sediment load ($0.10x10^6$ t $y^{-1}$) is more representative of shoreline erosion within the past 15 years, since only unprotected shorelines as of 2004 are considered; the upper estimate ($0.24x10^6$ t $y^{-1}$) is probably more representative of shoreline erosion >15 years ago, since it includes both protected and unprotected shorelines. Therefore, the best estimate of decadal-scale shoreline erosion is likely between my low and high calculations, assumed to be the average ($0.17x10^6$ t $y^{-1}$), since shoreline erosion has varied over time due to increased shoreline stabilization. My calculations are 1.5-4 times lower than previous estimates of shoreline erosion ($0.39x10^6$ t $y^{-1}$ Schubel 1968; Biggs 1970), likely due to increased shoreline protection. Many seawalls and bulkheads were installed in the Chesapeake Bay following World War II to protect recently built coastal structures (Hardaway and Byrne 1999), and continued to increase, especially between the 1970s and 1990s (Titus 1998). Recently "green" stabilization techniques have increased following the implementation of the Living Shorelines Protection Act enacted by Maryland state law in 2008 (http://dnr.maryland.gov/ccs/Documents/ls/2008_LSPA.pdf).

Taking the best estimates together, the Susquehanna River and shoreline erosion deliver $2.07x10^6$ t $y^{-1}$ to the upper Bay. An important sediment source not considered by this study is nearshore erosion (erosion below MLW), because shoreline-change rates only consider changes in shoreline position. This source can contribute up to 1.5 times more sediment than fastland shoreline erosion (Langland

and Cronin 2003) and assumed to be $0.32 \times 10^6$ t $y^{-1}$. When added to the other terms, the total sediment input to the upper Bay is $2.39 \times 10^6$ t $y^{-1}$.

*Sediment Sinks*

Mass accumulation rates from the Susquehanna Flats through the upper Bay range over an order of magnitude, 0.13-1.25 g $cm^{-2}$ $y^{-1}$, similar to previous studies (see Table S2). Most cores exhibited steady-state sedimentation, as indicated by the strong log-linear relationship between $^{210}$Pb activity and depth, and sedimentation rates decreased with distance downstream. However, observations at Lee2 and Lee0 deviated from these trends; rates were higher at these sites and $^{210}$Pb profiles showed non-steady-state behavior. One explanation for the variability in $^{210}$Pb profiles is pulsed sedimentation during flood events (Hirschberg and Schubel 1979), in which large sediment loads are transported farther downstream than during normal flow conditions. Typically flood events can be distinguished in sediment profiles by relatively low $^{210}$Pb activities and high mud content (e.g. Russ and Palinkas et al. 2018); however, the mud content was relatively uniform within these cores, making it unclear whether variable $^{210}$Pb activities reflect flood events. Another explanation for these observations is sediment focusing due to the proximity of these sites to the main channel (Officer et al. 1984a; Sanford et al. 2001). Sedimentation rates in the channel are somewhat unknown, since the channel is dredged to allow ship passage to Baltimore Harbor (Halka et al. 1991; Sanford et al. 2001). Dredging not only removes sediment but also causes slumping (Officer et al. 1984a) that would result in variable $^{210}$Pb activities observed at these sites.

Using the mass accumulation rates from the 7 upper Bay sites from this study and those from the Susquehanna Flats from Russ and Palinkas (2018), total sediment burial along the entire dispersal system ranges 3.68-3.85x$10^6$ t $y^{-1}$. These results agree well with the burial estimates from Officer et al. (1984), but are 2-4 times higher than those from Biggs (1970) and Hobbs et al. (1992). Some of the discrepancy may be due to different calculation methods for sediment-accumulation rates (i.e. mass balance on inputs and outputs, radioisotope geochronology, and volumetric differences between bathymetry surveys for Biggs 1970, Officer et al. 1984a, and Hobbs et al. 1992, respectively). However, more of the discrepancy probably arises from extrapolating measurements from a small number of cores over large areas. While there are no other coring studies on the Flats to my knowledge, there have been many previous studies in the upper Bay. To avoid potential methodological differences, only data from previous $^{210}$Pb measurements were added to the dataset from literature (Table S2); this expanded dataset yielded total burial of 4.42x$10^6$ t $y^{-1}$ for the upper Bay, and thus 4.60-4.77x$10^6$ t $y^{-1}$ for the Flats-Bay dispersal system. Statistical models offer another approach to calculating sediment burial, predicting sedimentation rates from site-location characteristics like water depth and distance downstream. Each of these parameters reflect some of the spatial variability, including enhanced sedimentation in the ETM (Sanford et al. 2001), but neither could explain the variability alone. Instead, a multiple-linear regression model using both parameters was significant ($R^2$=0.62, p-value=2x$10^6$), and was used to predict sedimentation given site-location characteristics. Using this model, 4.22-4.39x$10^6$ t $y^{-1}$ of sediment is buried in the upper Bay-Flats dispersal system. Spatial variability

with both distance and depth is better captured in this model, and is therefore my best estimate for total sediment burial. This model predicts that sedimentation is higher in deeper water, indicating sediment focusing in channels. Since spatial variability with both distance and depth is better captured in this model, it is considered the best estimate for total sediment burial. However, note that it considerers the entire upper Bay to be depositional, contrasting with the assertion of Hobbs et al. (1992) that only 52% of the Bay is net depositional, and thus likely overestimating actual burial in the upper Bay. Also, dredging is an important sediment sink not included in any of these calculations; nearly $1x10^6$ $m^3$ of sediment is removed from the upper Bay annually, which is equivalent to $0.57x10^6$ t $y^{-1}$, assuming a dry bulk density of 0.57 g $cm^{-3}$ (Sanford et al. 2001; Halka 2000). Therefore, the total burial in the upper Bay (including the Susquehanna Flats) is between $4.25x10^6$ t $y^{-1}$ and $5.34x10^6$ t $y^{-1}$.

*Implications and relevance to management*

This sediment budget connects sediment transport from the lower Susquehanna River to the upper Bay. Sediment dynamics in this system have changed over time and are likely to continue evolving in the future due to both natural and anthropogenic processes. These changes often have contrasting influences. For example, land-use changes in the Susquehanna River watershed have decreased watershed supply of sediment to the Bay in normal flows. Similar soil-conservation practices have led to decreasing sediment loads in many rivers around the world, such as the Yellow River (Wang et al. 2007). Additional sediment reductions from the Susquehanna River watershed are expected in the future because one of the main

goals of the Chesapeake Bay total maximum daily load (TMDL) is to reduce sediment loads by 20% by 2025 (USEPA 2010). In contrast, dam construction decreases sediment supply from rivers to estuaries due to retention of sediment behind reservoirs (Syvitski et al. 2005; Walling 2006). However, this retention capacity decreases once reservoirs reach dynamic equilibrium, as is the case for the three reservoirs on the lower Susquehanna. In particular, infilling of the Conowingo Reservoir has led to a lower scour threshold, such that more sediment can be resuspended at lower discharges than in the past, and thus an increase in suspended-sediment concentrations during high flows (Hirsch 2012). Understanding the impacts to downstream ecosystems from this increase in sediment supply is an important management issue for many river-estuarine systems, including Chesapeake Bay (Palinkas et al. submitted). Indeed, many reservoirs in the US were designed to have a >100 year life span, but this has been shortened due to sedimentation (Hargrove et al. 2009). Because many reservoirs were built in the 1940s-50s, understanding sediment-load changes due to reservoir infill will be even more important in the coming years.

Susquehanna River sediment loads may also increase in the future as a result of increased precipitation in the Mid-Atlantic, particularly during winter and spring, which will likely increase watershed erosion and streamflow (Boesch 2008; Najjar et al. 2010). Increased rain also increases shoreline erosion (Boesch 2008), but rising sea level and increased storminess will likely have a greater influence on shoreline erosion (Mariotti and Fagherazzi 2010; Sanford and Gao 2018). In response, property owners are hardening shorelines everywhere (Gittman et al. 2015). Increases in “gray infrastructure” (i.e. bulk heads, seawalls) have decreased fastland erosion in the upper

Bay, but these structures increase nearshore erosion (Hardaway and Byrne 1999). Additionally, these structures do not adapt to changing environmental conditions and deteriorate over time (Sutton-Grier et al. 2015). As a result, living shorelines and other "green" approaches to shoreline stabilization have been encouraged and/or mandated in the Chesapeake Bay; these approaches stabilize shorelines and have other ecosystem benefits such as habitat creation and nutrient sequestration (Subramanian et al. 2008; Bilkovich et al. 2016; Davis et al. 2015).

One consequence of evolving sediment dynamics is the change in balance between fluvial and shoreline input, which alters sediment character. For example, Susquehanna River sediment is generally finer grained than shoreline sediments. Increases in Susquehanna River input would increase mud inputs and turbidity in the upper Bay, while decreases in shoreline erosion decrease sand supply. Reducing sand availability, along with coincident increases in mud, is detrimental to SAV habitats along the shoals of the upper Bay (Palinkas and Koch 2012). In addition to increasing turbidity, increased fine sediment alters the biological and chemical properties at the sediment-water interface, limiting biological productivity (Cahoon et al. 1999; Duarte 2002). Another outcome of evolving sediment dynamics is the relationship of sedimentation rates to those of sea-level rise. Currently, the average linear sedimentation rate in the upper Bay (average 0.95±0.18 cm $y^{-1}$) exceeds average sea-level rise in the Bay (3-4 mm $y^{-1}$; Boesch 2008; Najjar et al. 2010). However, it is important to consider the range of sedimentation rates (0.10-4.16 cm $y^{-1}$) in predicting possible trajectories of smaller areas. For example, sedimentation rates on the Susquehanna Flats are relatively high (0.46-0.91 cm $y^{-1}$) and currently outpacing sea-

level rise, suggesting persistence of this SAV bed in the future, assuming other habitat requirements (i.e. light availability, wave environment; Koch 2001; Dennison et al. 1993) remain suitable. However, sea-level rise outpaces accretion in other areas, especially south of the ETM and in shallow waters. Indeed, the shallow margins of the upper Bay, where shoreline erosion is the main sediment source, may be most vulnerable to sea-level rise in the future, becoming deeper over time due to increases in gray shoreline protection structures that disconnect these areas from sediment sources.

**Summary**

The upper Chesapeake Bay traps sediment from the Susquehanna River and shoreline erosion; however, sediment input to the upper Bay has evolved over time as a result of natural and anthropogenic impacts. Results indicate that Susquehanna River sediment supply has decreased at low to normal river discharges due to implementation of soil conservation practices, but has increased at high river discharges due to Conowingo Reservoir infilling. Increased shoreline stabilization has reduced sediment input from shoreline erosion. Sedimentation rates are generally highest near the mouth of the Susquehanna River and decrease with distance downstream. Accumulation rates are higher in deeper water, likely due to sediment focusing into the channels. Sediment loads from both Susquehanna River and shoreline are expected increase due to increased precipitation, sea-level rise, and storminess. However, these increases in shoreline erosion may be offset by increased shoreline stabilization. These evolving sediment dynamics will likely change the

downstream sediment character, which can have important implications on benthic habitats, such as reduced light availability due to increased fine-grained sediment and subsequent reductions in suitable SAV habitat.

Tables

**Table 4.1** Study site names, coordinates, distance from Susquehanna River (SR) mouth, water depth at each site, and distance to main channel.

| Site | Coordinates | Distance from SR mouth (km) | Water Depth (m) | Distance to main channel (km) |
|---|---|---|---|---|
| Lee7 | 39.414°N, 76.079°W | 14.68 | 3 | 2.62 |
| Lee6 | 39.380°N, 76.088°W | 18.52 | 7.5 | 0.55 |
| Lee5 | 39.346°N, 76.197°W | 24.44 | 6.5 | 1.17 |
| Lee2.5 | 39.197°N, 76.311°W | 43.68 | 5.0 | 2.97 |
| Lee2 | 39.135°N, 76.328°W | 50.49 | 13.5 | 0.13 |
| Lee0 | 39.061°N, 76.328°W | 58.07 | 13.5 | 0.41 |
| LeeS2 | 38.757°N, 76.473°W | 94.02 | 11.0 | 3.72 |

**Table 4.2** Shore change information for unprotected (unprotected and protected) shorelines: total mainstem shoreline length, length of shoreline analyzed, area change, and volume change.

| County | Total Shoreline Length ($x10^5$ m) | Length shoreline analyzed ($x10^5$ m) | Area Change ($x10^3$ $m^2$) | Volume Change ($x10^3$ $m^3$) | Mass ($x10^6$ tons) |
|---|---|---|---|---|---|
| Harford | 1.29 | 0.18 | 0.04 | -2.2 | -0.003 |
| | | (0.19) | (0.07) | (-2.2) | (-0.003) |
| Baltimore | 0.29 | 0.23 | 1.9 | 2.1 | 0.003 |
| | | (0.28) | (1.9) | (2.1) | (0.003) |
| Anne Arundel | 0.83 | 0.76 | -9.0 | -8.8 | -0.01 |
| | | (0.77) | (-9.1) | (-8.9) | (-0.01) |
| Cecil | 0.54 | 0.29 | -1.8 | -11.9 | -0.02 |
| | | (0.46) | (-3.5) | (-22.2) | (-0.03) |
| Kent | 1.46 | 1.11 | -12.9 | -43.1 | -0.06 |
| | | (1.14) | (-23.4) | (-85.1) | (-0.13) |
| Queen Anne's | 0.36 | 0.13 | 1.1 | 0.3 | 0.0005 |
| | | (0.36) | (-4.3) | (-2.7) | (-0.004) |
| Talbot | 0.19 | 0.05 | -1.2 | -0.9 | -0.001 |
| | | (0.13) | (-8.7) | (-6.6) | (-0.01) |
| Total | 4.96 | 2.75 | -22.0 | -64.4 | -0.10 |
| | | (3.33) | (-47.0) | (-125.5) | (-0.19) |

**Table 4.3** $^{210}$Pb and $^{137}$Cs accumulation results of upper Chesapeake Bay: CFCS rate (cm $y^{-1}$ and g $cm^{-2}$ $y^{-1}$), 1954 $^{137}$Cs depth range and corresponding average accumulation rate; 1963 $^{137}$Cs depth range and corresponding average accumulation rate; and core-averaged mud fraction

| Site | Distance from SR mouth (km) | CFCS cm $y^{-1}$, g $cm^{-2}$ $y^{-1}$ ($R^2$) | 1954 $^{137}$Cs depth cm (cm $y^{-1}$) | 1963 $^{137}$Cs depth cm (cm $y^{-1}$) | Mud fraction |
|---|---|---|---|---|---|
| Lee7 | 14.68 | 0.34, 0.36 (0.78) | 20-22.5 (0.34) | 19-20 (0.37) | 0.73 |
| Lee6 | 18.52 | 0.84, 0.70 (0.77) | 48-50 (0.79) | 44-46 (0.85) | 0.70 |
| Lee5 | 24.44 | 1.20, 0.85 (0.71) | NA | >58 (>1.11) | 0.92 |
| Lee2.5 | 43.68 | 0.29, 0.22 (0.91) | 20-22 (0.34) | 13-14 (0.25) | 0.89 |
| Lee2 | 50.49 | >0.81, >0.37* | 54-56 (0.89) | 44-46 (0.85) | 0.98 |
| Lee0 | 58.07 | >0.81, >0.29* | 19-20 (0.31) | 15-16 (0.29) | 0.97 |
| LeeS2 | 94.02 | 0.26, 0.13(0.75) | 18-19 (0.29) | 15-16 (0.29) | 0.99 |

**Table 4.4** Sediment budget for upper Chesapeake Bay describing sources (top) and sink (bottom).

| | **Range ($x10^6$ tons $y^{-1}$)** | **Best estimate ($x10^6$ tons $y^{-1}$)** |
|---|---|---|
| **Sources** | | |
| Susquehanna River (at Conowingo Dam) | 1.70-1.90 | 1.90 |
| Shoreline (fastland) shoreline | 0.10-0.24 | 0.17 |
| Nearshore shoreline[1] | 0.32 | 0.32 |
| **Total** | **2.12-2.41** | **2.39** |
| **Sinks** | | |
| Susquehanna Flats[2] | 0.18-0.35 | 0.26 |
| Upper Bay | 3.50-4.42 | 4.04 |
| Dredging[3] | 0.57 | 0.57 |
| **Total** | **4.25-5.34** | **4.87** |

[1] Data from Langland and Cronin (2003)
[2] Data from Russ and Palinkas (2018)
[3] Data from Sanford et al. 2001; Halka 2000

Figures

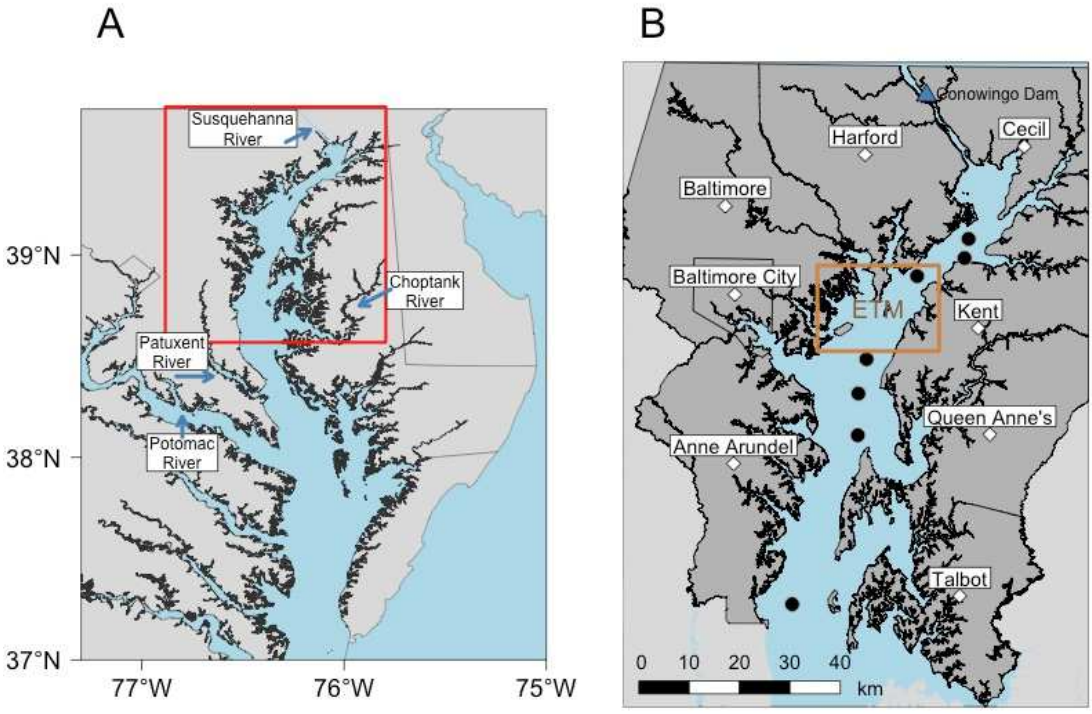


**Figure 4.1** A) Map of Chesapeake Bay, with upper Chesapeake Bay study area enclosed by red box. B) Black circles indicate core locations. Site names, from north to south, are Lee7, Lee6, Lee5, Lee2.5, Lee2, Lee0, LeeS2 (see Table 1). The upper Bay coastal counties are delineated in dark gray and the estuarine turbidity maximum (ETM) in orange.

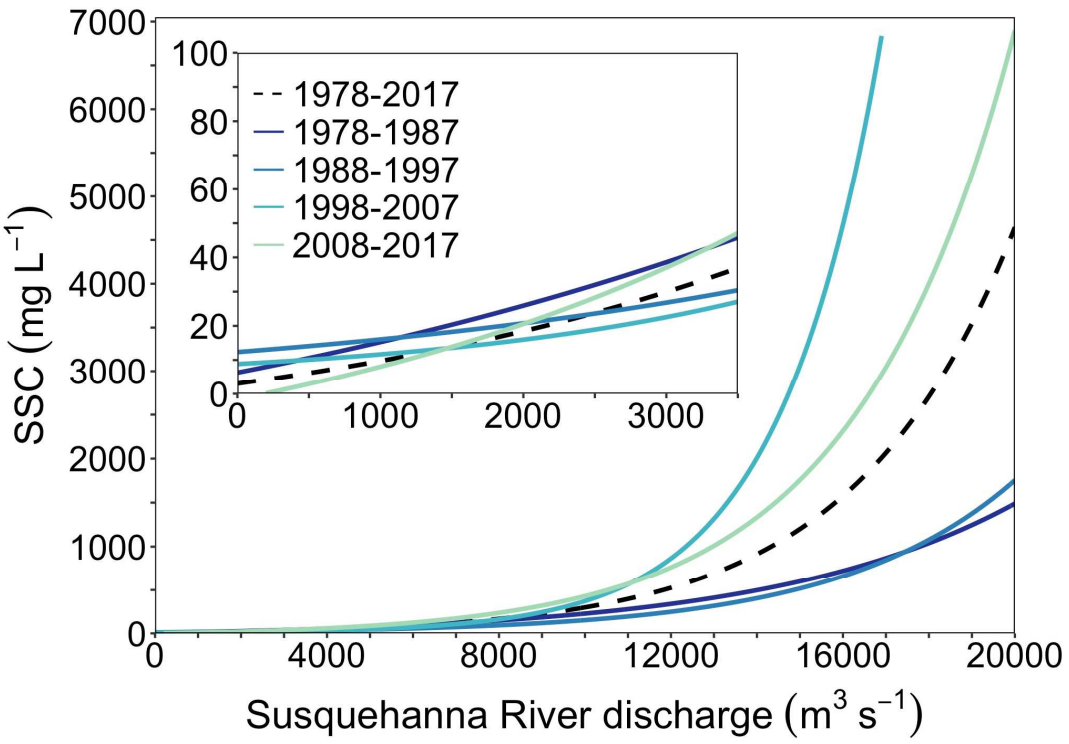


**Figure 4.2** Exponential relationship between Susquehanna River discharge and suspended-sediment concentrations including all years (dashed black line; 1978-2017; Eq. 1) and for individual decadal time periods (solid lines; see Table A.7). Dark blue is the earliest decade (1978-1987), and light green is most recent decade (2008-2017). The inset highlights differences in the relationships SSC concentrations at lower river discharges (0-3500 $m^3$ $s^{-1}$; the first flood gate opens at ~2500 $m^3$ $s^{-1}$ (Velleux and Hallden 2017)) typical of most time periods.

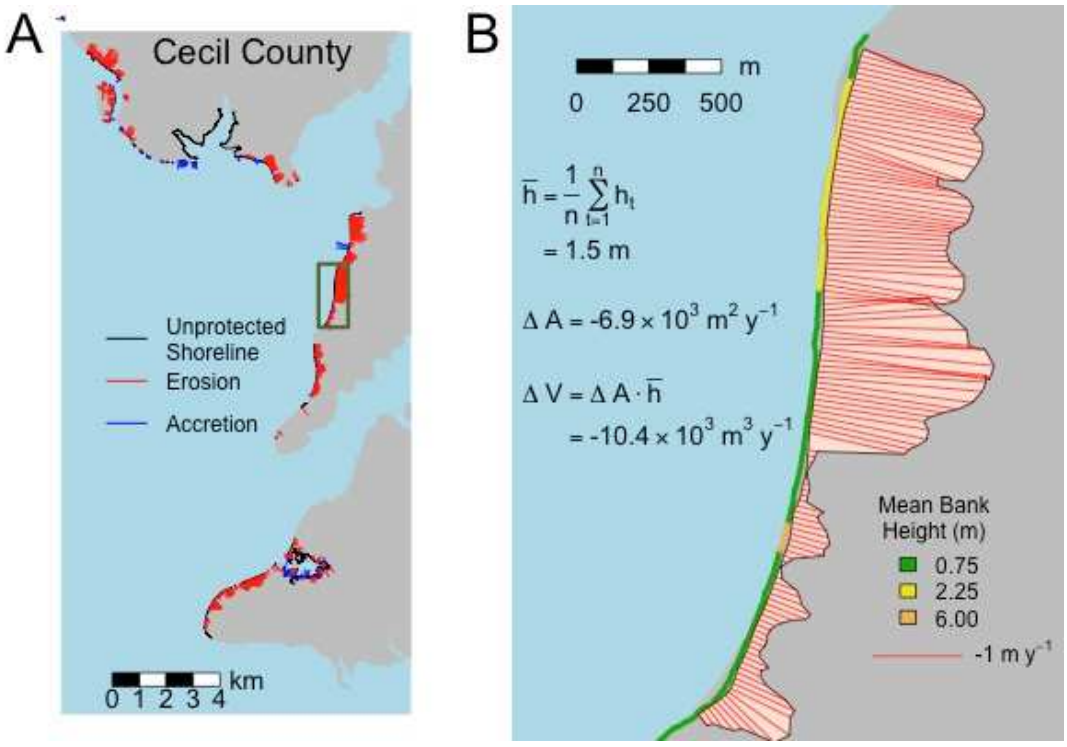


**Figure 4.3** Shoreline change example. A) Accretion (blue lines) and erosion (red lines) along unprotected shorelines in Cecil County. B) Calculation of average bank height $(\overline{h})$, area change $(\Delta A)$, and volume change $(\Delta V)$, along a shoreline segment. Average bank height $(\overline{h})$ for this shoreline segment is 1.5m, which is the average bank height of all transects ($h_t$) in this shoreline segment. Area change $(\Delta A)$ for this shoreline segment is -6.9x10$^3$ m$^2$ y$^{-1}$, and is the area of the polygon shown in pink. This polygon reflects the difference in area between the most current shoreline (2004) and the projected shoreline after 1 year using annual shoreline-change rates (red lines; length indicates the rate of change). Volume change $(\Delta V)$ for this shoreline segment calculated from multiplying the area change by average bank height is 10.4x10$^3$ m$^3$ y$^{-1}$.

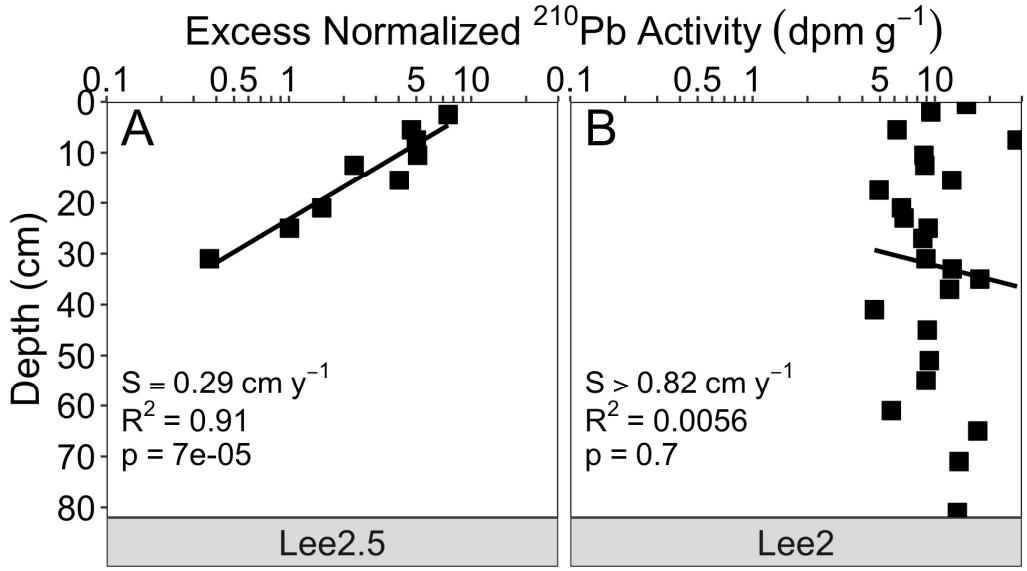


**Figure 4.4** Excess normalized $^{210}$Pb activity at (A) Lee2.5 showing steady-state sedimentation and (B) Lee2 showing non-steady-state sedimentation. Linear sedimentation rate (S), $R^2$,and p-value are included.

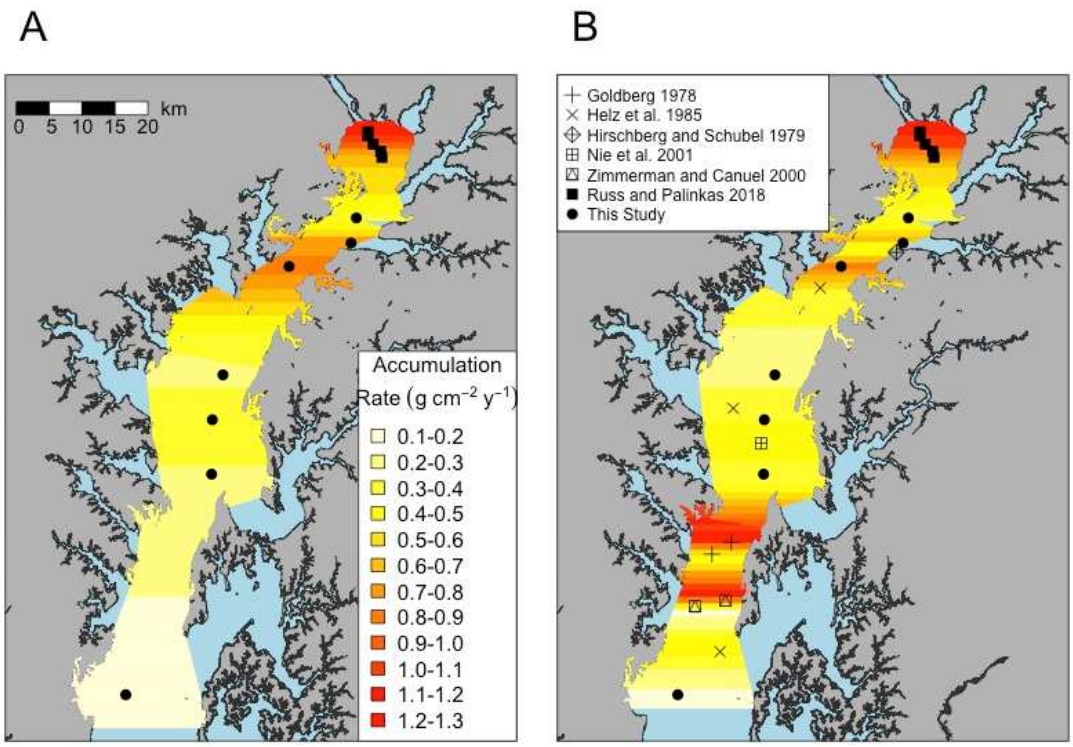


**Figure 4.5** A) Linearly interpolated mass-accumulation rates of the upper Chesapeake Bay using mass-accumulation rates from Susquehanna Flats (Russ and Palinkas 2018) as well as upper Bay. B) Linearly interpolated mass-accumulation rates using data from Table S2.

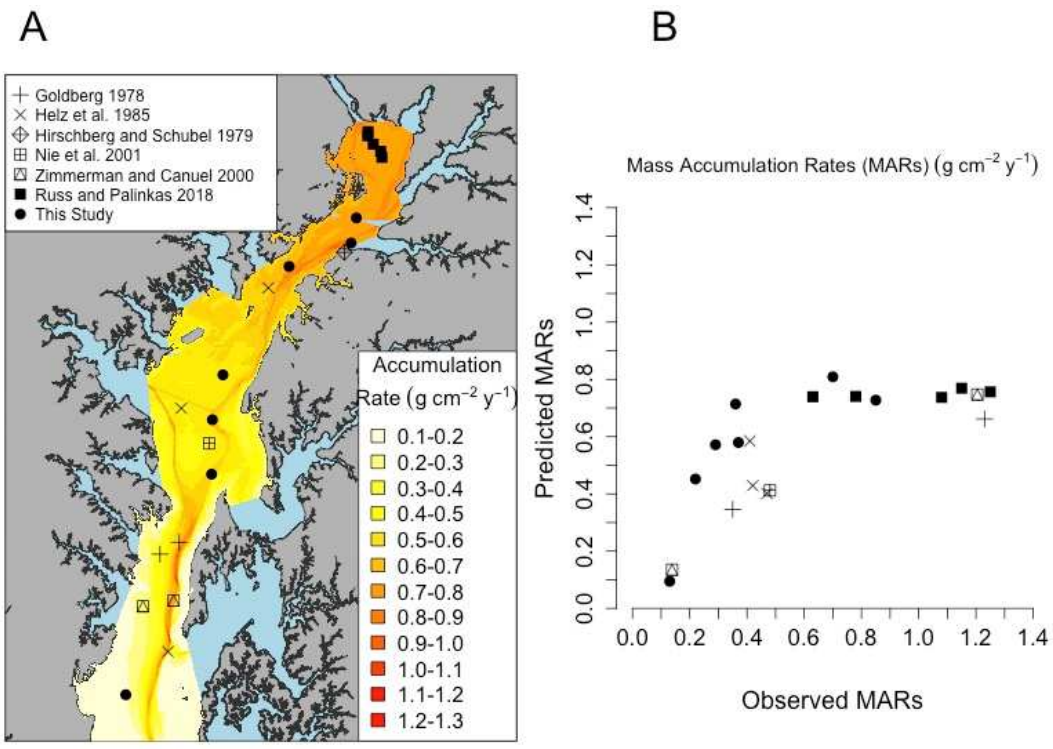


**Figure 4.6** A) Predicted mass-accumulation rates of the upper Chesapeake Bay using multiple-linear regression with depth and distance downstream on data from Table S2. B) Observed vs predicted mass-accumulation rates, following the symbology in A.

# Chapter 5 : Summary and synthesis

In the three previous chapters of this dissertation, I evaluated sediment sources, sinks, and transport pathways in the upper Chesapeake Bay through geochronological, geochemical, and spatial analyses. I have summarized the major findings of this work in the following paragraphs.

Results from Chapter 2 revealed that the dense, seasonally-vegetated beds on the subaqueous Susquehanna River delta (Susquehanna Flats) are important for modulating the sediment input to the Chesapeake Bay. Seasonal-scale variability in sediment deposition is explained by Susquehanna River discharge, sediment supply, and Susquehanna Flats geomorphology. Decadal-scale sediment accumulation variability is driven by flood events and abrupt changes in submersed aquatic vegetation (SAV) abundance. The strong positive correlation between SAV bed area and average annual sediment accumulation on the Flats suggests that a positive feedback between these variables exist.

In Chapter 3, I evaluated surficial and down-core geochemical patterns using correlation and principal component analyses. Elements associated with aluminosilicate minerals, which were sensitive to grain-size changes, and rare earth elements, which were sensitive to salinity changes, explained the most spatial variability in the dataset. Variability in heavy metal concentrations reflected changes in anthropogenic inputs over time. A sediment-provenance analysis was performed using the sediment-geochemistry data to evaluate contributions of Susquehanna River

and shoreline erosion to bottom sediments in the upper Bay. The results from the sediment-provenance analysis indicated that the Susquehanna River is the dominant source of fine sediment in the upper Bay.

Chapter 4 presented an updated sediment budget that highlighted the evolving sediment dynamics of sources and sinks in the upper Chesapeake Bay. Results revealed that the Susquehanna River input to upper Bay has decreased over the past 40 years, during low and normal flows over the past 40 years, reflecting increased soil conservation; however sediment delivery has increased during high flows, consistent with a decreasing scour threshold for bottom sediments in Conowingo Reservoir as it has filled. Inputs from shoreline erosion have decreased due to increased shoreline stabilization. Mass-accumulation rates in the upper Bay generally decreased with distance downstream, similar to previous studies; however, elevated rates were observed in deeper water near the main channel, suggesting sediment was focused into the channels.

Collectively, this research connects sediment delivery from the lower Susquehanna River through the Susquehanna Flats to its fate in upper Chesapeake Bay, highlighting major sources, sediment transport pathways, and sinks. Sediment has a dual nature in the Chesapeake Bay, acting as a pollutant in areas that receive excess fine sediment (e.g. main channel, estuarine turbidity maximum) and a resource in areas that do not receive enough sediment (e.g. eroding beaches, wetlands). Quantifying the relative contributions of sediment sources to the upper Bay is important given Susquehanna sediments are typically finer and more nutrient-rich,

thus more likely to increase turbidity and fuel algal blooms than shoreline sediments (Marcus and Kearney 1991)

Understanding the current sediment dynamics in the Chesapeake Bay is critical for developing effective sediment-management strategies. One of the main goals of the Chesapeake Bay Total Maximum Daily Load (TMDL), established by the US Environmental Protection Agency (EPA) in 2010, is to reduce excess sediment inputs by 2025 to achieve water quality standards (USEPA 2010). However, the sediment loads predicted for the TMDL report relied on models that were calibrated with historical data (1984-2005), which do not capture changes due to resurgence of SAV at the head of the Bay or infilling of the Conowingo Dam. These major changes were therefore not accounted for in the TMDL sediment reduction plans. This dissertation builds upon previous upper Bay sediment budgets and specifically discusses recent changes on the lower Susquehanna River and upper Chesapeake Bay continuum, which will help inform future sediment-management decisions.

This work also provides context for how sediment dynamics are expected to evolve in the future due to anthropogenic impacts and climate change. Susquehanna River inputs are expected to increase due to both Conowingo Reservoir infilling and increased precipitation/streamflow (Boesch 2008; Najjar et al. 2010). However, the SAV bed on the Susquehanna Flats can modulate sediment input to the upper Bay and are likely to persist in the future given sedimentation rates that are greater than sea-level rise (Russ and Palinkas 2018). Future inputs from shoreline erosion are more uncertain, as accelerated sea-level rise and increased storminess are expected to

increase shoreline erosion (Boesch 2008; Najjar et al. 2010), but increased shoreline stabilization may offset this erosion (Gittman et al. 2015). Parts of the Bay that rely on shoreline erosion may become deeper over time, if sedimentation is unable to keep up with sea-level rise.

The findings of this research address how sediment dynamics in the upper Chesapeake Bay vary over space and time due to both natural and anthropogenic processes and are broadly applicable to other fluvial-estuarine/coastal systems. Particularly, this research is relevant to systems that have reduced sediment inputs due to soil-conservation practices and dam construction, ultimately increasing SAV habitat suitability as well as systems with reservoirs approaching dynamic equilibrium, which will likely be an issue in the coming years.

# Appendix A : Supplemental Tables

**Table A. 1** Surficial (0-1 cm) median grain size in μm, % surficial organic content, depth-integrated $^{7}$Be inventories in dpm cm$^{-2}$ (propagated $^{7}$Be activity counting error), and above ground biomass from Gurbisz (unpublished data) in g m$^{-2}$ (standard error) at all push core sites during the three samplings. NA means core not collected, ND means $^{7}$Be activity not detected.

| Site | Aug-14 | May-15 | Aug-15 |
|---|---|---|---|
| *Median Grain Size (μm)* | | | |
| **SF1** | 328.6 | 326.6 | 310.1 |
| **SF2** | 375.7 | 323.6 | 236.1 |
| **SF3** | 114.1 | 287.0 | 113.1 |
| **SF4** | 243.3 | 270.6 | 210.7 |
| **SF5** | 236.1 | 206.5 | 204.8 |
| **SAV1** | 173.5 | 318.9 | NA |
| **SAV5** | 313.5 | 221.3 | NA |
| **SAV6** | 320.6 | 270.8 | NA |
| **SAV7** | 405.3 | 370.1 | NA |
| **SAV8** | 294.3 | 320.9 | NA |
| **SAV9** | 366.9 | 338.1 | NA |
| **SAV10** | 298.7 | 175.9 | NA |
| **SAV11** | 305.6 | 223.6 | NA |
| *Organic Content (%)* | | | |
| **SF1** | 0.50 | 2.04 | 0.82 |
| **SF2** | 2.29 | 1.26 | 5.18 |
| **SF3** | 3.74 | 2.51 | 5.78 |
| **SF4** | 2.46 | 2.16 | 2.04 |
| **SF5** | 4.20 | 3.15 | 1.5 |
| **SAV1** | 2.91 | 2.51 | NA |
| **SAV5** | 2.28 | 1.89 | NA |
| **SAV6** | 1.72 | 1.62 | NA |
| **SAV7** | 0.60 | 0.59 | NA |
| **SAV8** | 1.06 | 0.84 | NA |
| **SAV9** | 0.73 | 1.33 | NA |
| **SAV10** | 2.28 | 4.41 | NA |
| **SAV11** | 1.61 | 1.44 | NA |
| *Inventory (dpm cm$^{-2}$)* | | | |
| **SF1** | 2.11 (0.44) | ND | 2.64 (0.65) |
| **SF2** | ND | ND | 2.08 (0.30) |
| **SF3** | 2.66 (0.29) | ND | 1.82 (0.33) |
| **SF4** | 0.73 (.30) | ND | 1.82 (0.34) |
| **SF5** | 2.09 (0.42) | 0.71 (0.40) | 2.79 (0.78) |
| **SAV1** | ND | ND | NA |
| **SAV5** | ND | 3.53 (0.37) | NA |
| **SAV6** | ND | ND | NA |

| | | | |
|---|---|---|---|
| **SAV7** | ND | ND | NA |
| **SAV8** | 0.76 (0.11) | 2.82 (0.50) | NA |
| **SAV9** | ND | ND | NA |
| **SAV10** | ND | 1.66 (0.40) | NA |
| **SAV11** | 0.94 (0.26) | ND | NA |
| *Above Ground Biomass* | | | |
| **SF1** | NA | NA | NA |
| **SF2** | 1503.8 (268.6) | 25.7 (20.4) | 327.6 (75.7) |
| **SF3** | 112.2 (45.0) | 5.4 (3.5) | 219.8 (40.9) |
| **SF4** | 82.2 (46.1) | 43.8 (30.3) | 268.0 (74.7) |
| **SF5** | NA | NA | NA |
| **SAV1** | 11.5 (5.9) | 5.6 (1.7) | NA |
| **SAV5** | 66.5 (17.3) | 4.8 (2.1) | NA |
| **SAV6** | 257.3 (75.3) | 221.8 (211.7) | NA |
| **SAV7** | 398.7 (315.9) | 94.9 (82.4) | NA |
| **SAV8** | 239.8 (100.2) | 4.5 (2.2) | NA |
| **SAV9** | 126.2 (19.6) | 3.3 (1.8) | NA |
| **SAV10** | 452.9 (125.5) | 32.3 (11.8) | NA |
| **SAV11** | 61.1 (39.1) | 7.4 (3.6) | NA |

**Table A. 2** Statistical parameters for pairwise linear regressions; $R^2$ (p-value). None of these relationships are statistically significant after applying Bonferroni correction.

| | **August 2014** | | **May 2015** | | **August 2015** | |
|---|---|---|---|---|---|---|
| | *Grain size* | *Biomass* | *Grain size* | *Biomass* | *Grain size* | *Biomass* |
| *Inventory* | 0.30 (0.05) | 0.21 (0.15) | 0.14 (0.20) | 0.003 (0.87) | 0.32 (0.32) | 0.86 (0.25) |
| *Biomass* | 0.07 (0.42) | | 0.08 (0.40) | | 0.80 (0.29) | |

**Table A. 3** Site coordinates of upper Bay core locations and locations where surficial source sediment was collected from the Susquehanna River and upper Bay shorelines. *Indicates site was reoccupied multiple times.

| Site | Coordinates | Date |
|---|---|---|
| *Upper Bay* | | |
| Lee7 | 39.414°N, 76.079°W* | 08/2015 |
| Lee7 | 39.414°N, 76.079°W* | 04/2016 |
| Lee6 | 39.380°N, 76.088°W | 04/2016 |
| Lee5 | 39.346°N, 76.197°W* | 08/2015 |
| Lee5 | 39.346°N, 76.197°W* | 04/2016 |
| Lee2.5 | 39.197°N, 76.311°W* | 08/2015 |
| Lee2.5 | 39.197°N, 76.311°W* | 04/2016 |
| Lee2 | 39.135°N, 76.328°W | 04/2016 |
| Lee0 | 39.061°N, 76.328°W | 04/2016 |
| LeeS2 | 38.757°N, 76.473°W* | 08/2015 |
| LeeS2 | 38.757°N, 76.473°W* | 04/2016 |
| *Susquehanna River* | | |
| SR1 (Dam) | 39.661°N, 76.173°W | 04/2015 |
| SR2 | 39.697°N, 76.211°W* | 07/2015 |
| SR3 | 39.697°N, 76.211°W* | 09/2015 |
| SR4 | 39.697°N, 76.211°W* | 12/2015 |
| SR5 | 39.697°N, 76.211°W* | 04/2016 |
| SR6 | 39.663°N, 76.185°W* | 05/2015 |
| SR7 | 39.663°N, 76.185°W* | 07/2015 |
| SR8 | 39.663°N, 76.185°W* | 09/2015 |
| SR9 | 39.663°N, 76.185°W* | 12/2015 |
| SR10 | 39.663°N, 76.185°W* | 04/2016 |
| SR11 | 39.669°N, 76.181°W* | 05/2015 |
| SR12 | 39.669°N, 76.181°W* | 07/2015 |
| SR13 | 39.669°N, 76.181°W* | 04/2016 |
| *Shoreline* | | |
| Sh1 | 39.542°N, 76.003°W | 04/2017 |
| Sh2 | 39.520°N, 75.980°W | 04/2017 |
| Sh3 | 39.520°N, 76.107°W | 04/2018 |
| Sh4 | 39.475°N, 75.994°W | 03/2018 |
| Sh5 | 39.399°N, 76.038°W | 04/2017 |
| Sh6 | 39.358°N, 76.120°W | 03/2018 |
| Sh7 | 39.356°N, 76.345°W | 04/2018 |
| Sh8 | 39.283°N, 76.168°W | 04/2018 |
| Sh9 | 39.249°N, 76.197°W | 04/2018 |
| Sh10 | 39.219°N, 76.418°W | 04/2018 |
| Sh11 | 39.214°N, 76.244°W | 04/2018 |
| Sh12 | 39.087°N, 76.424°W | 04/2018 |
| Sh13 | 39.061°N, 76.473°W | 04/2018 |
| Sh14 | 39.034°N, 76.241°W | 03/2018 |
| Sh15 | 38.886°N, 76.541°W | 04/2018 |
| Sh16 | 38.882°N, 76.494°W | 04/2018 |

**Table A. 4** All element names and chemical symbol described in this manuscript

| Element | Symbol |
|---|---|
| Lithium | Li |
| Magnesium | Mg |
| Aluminum | Al |
| Potassium | K |
| Scandium | Sc |
| Vanadium | V |
| Chromium | Cr |
| Iron | Fe |
| Gallium | Ga |
| Arsenic | As |
| Rubidium | Rb |
| Thallium | Tl |
| Bismuth | Bi |
| Yttrium | Y |
| Lanthanum | La |
| Cerium | Ce |
| Praseodymium | Pr |
| Neodymium | Nd |
| Samarium | Sm |
| Europium | Eu |
| Gadolinium | Gd |
| Dysprosium | Dy |
| Erbium | Er |
| Ytterbium | Yb |
| Thorium | Th |
| Uranium | U |
| Calcium | Ca |
| Sodium | Na |
| Phosphorus | P |
| Titanium | Ti |
| Manganese | Mn |
| Cobalt | Co |
| Nickel | Ni |
| Copper | Cu |
| Zinc | Zn |
| Strontium | Sr |
| Zirconium | Zr |
| Molybdenum | Mo |
| Barium | Ba |
| Lead | Pb |

**Table A. 5** REE concentrations in Chester River suspended sediments

| Element | Concentration (PPM) |
|---|---|
| La | 1.6 |
| Ce | 3.31 |
| Pr | 0.3 |
| Nd | 1.7 |
| Sm | 0.5 |
| Eu | <0.1 |
| Gd | 0.4 |
| Dy | 0.3 |
| Y | 1.4 |
| Er | 0.2 |
| Yb | 0.1 |

**Table A. 6** Equations to calculate SSC at 10-year intervals (see Fig. 3). Calculated range and average annual sediment load.

| Decade | SSC equation | Range (x$10^6$ t $y^{-1}$) | Average (x$10^6$ t $y^{-1}$) |
|---|---|---|---|
| 1978-1987 | $47.2e^{(1.7\times10^{-4}\times Discharge)} - 40.9$ | 0.6-2.9 | 1.5±0.3 |
| 1988-1997 | $13.4e^{(2.4\times10^{-4}\times Discharge)} - 1.1$ | 0.5-3.7 | 1.3±0.4 |
| 1998-2007 | $5.4e^{(4.2\times10^{-4}\times Discharge)} - 3.4$ | 0.3-8.9 | 1.8±0.8 |
| 2008-2017 | $30.8e^{(2.7\times10^{-4}\times Discharge)} - 32.4$ | 0.4-22.7 | 2.9±2.2 |

**Table A. 7** Supplemental $^{210}Pb$ data from upper Chesapeake Bay. * Indicates only linear sedimentation rate (cm $y^{-1}$) was available in the study and the mass accumulation rate was estimated by multiplying by bulk densities from nearby sites.

| Study | Coordinates | Distance from SR mouth (km) | Water depth (m) | Distance to main channel (km) | Mass accumulation rate (g $cm^{-2}$ $y^{-1}$) |
|---|---|---|---|---|---|
| Russ et al. (2018) | 39.527°N, 76.061°W | 2.61 | 0.5 | 1.93 | 1.15 |
| Russ et al. (2018) | 39.533°N, 76.061°W | 2.15 | 0.5 | 1.89 | 1.25 |
| Russ et al. (2018) | 39.515°N, 76.051°W | 4.13 | 0.5 | 2.90 | 1.08 |
| Russ et al. (2018) | 39.505°N, 76.039°W | 5.69 | 1 | 3.89 | 0.78 |
| Russ et al. (2018) | 39.497°N, 76.036°W | 6.53 | 1 | 3.30 | 0.63 |
| Cooper and Brush (1991) | 38.650°N, 76.406°W | 103.44 | 16 | 0.88 | 0.084* |
| Cooper and Brush (1991) | 38.652°N, 76.435°W | 103.93 | 14 | 1.59 | 0.064* |
| Cooper and Brush (1991) | 38.644°N, 76.428°W | 104.61 | 14 | 0.87 | 0.049* |
| Cooper and Brush (1991) | 38.652°N, 76.486°W | 105.34 | 10 | 6.02 | 0.090* |
| Goldberg et al. (1978) | 38.967°N, 76.383°W | 69.51 | 32 | 0.48 | 1.23 |
| Goldberg et al. (1978) | 38.950°N, 76.467°W | 72.34 | 12 | 2.56 | 0.35 |
| Goldberg et al. (1978) | 38.567°N, 76.450°W | 113.38 | 12 | 1.03 | 0.30 |
| Helz et al. (1985b) | 39.317°N, 76.233°W | 28.78 | 4 | 1.34 | 0.41 |
| Helz et al. (1985b) | 39.150°N, 76.383°W | 51.25 | 5 | 5.04 | 0.42 |
| Helz et al. (1985b) | 38.817°N, 76.400°W | 85.62 | 15 | 0.37 | 0.47 |
| Hirschberg and Schubel (1979) | 39.367°N, 76.100°W | 20.01 | 5 | 1.38 | 0.37* |
| Karlsen et al. (2000) | 38.560°N, 76.427°W | 113.57 | 16.5 | 0.79 | 0.058* |
| Karlsen et al. (2000) | 38.544°N, 76.427°W | 115.27 | 24.3 | 0.12 | 0.029* |
| Nie et al. (2001) | 39.103°N, 76.333°W | 53.93 | 6.5 | 2.49 | 0.48 |
| Nie et al. (2001) | 38.367°N, 76.333°W | 132.68 | 21 | 0.91 | 0.028 |
| Zimmerman and Canuel (2002) | 38.887°N, 76.392°W | 78.05 | 26.5 | 0.23 | 1.21 |
| Zimmerman and Canuel (2002) | 38.878°N, 76.445°W | 80.62 | 7.9 | 4.14 | 0.14 |
| Zimmerman and Canuel (2002) | 38.567°N, 76.445°W | 113.18 | 15 | 0.62 | 0.48 |

# References :


Anderson, J.B., D.J. Wallace, A.R. Simms, A.B. Rodriguez, and K.T. Milliken. 2014. Variable response of coastal environments of the northwestern Gulf of Mexico to sea-level rise and climate change: Implications for future change. *Marine Geology* 352: 348–366. doi:10.1016/j.margeo.2013.12.008.

Anthony, E.J., N. Marriner, and C. Morhange. 2014. Human influence and the changing geomorphology of Mediterranean deltas and coasts over the last 6000 years: From progradation to destruction phase? *Earth-Science Reviews* 139: 336–361. doi:10.1016/j.earscirev.2014.10.003.

Appleby, P.G, and F. Oldfield. 1978. The Calculation of Lead-210 dates assuming a constant rate of supply of unsupported $^{210}$Pb to the sediment. *Catena* 5: 1–8.

Arnold, R.R., J.C. Cornwell, W.C. Dennison, and J.C. Stevenson. 2000. Sediment-based reconstruction of submersed aquatic vegetation distribution in the Severn River, a sub-estuary of Chesapeake Bay. *Journal of Coastal Research*: 188–195.

Bates, D., M. Mächler, B. Bolker, and S. Walker. 2015. Fitting linear mixed-effects models using lme4. *Journal of Statistical Software* 67: 1–48. doi:10.18637/jss.v067.i01.

Bayley, S., V.D. Stotts, P.F. Springer, and J. Steenis. 1978. Changes in submerged aquatic macrophyte populations at the head of Chesapeake Bay, 1958-1975. *Estuaries* 1: 171. doi:10.2307/1351459.

Beckett, Leah H, Andrew H Baldwin, and Michael S Kearney. 2016. Tidal marshes across a chesapeake bay subestuary are not keeping up with sea-level rise. *PloS one* 11: e0159753.

Bianchi, T.S., and M.A. Allison. 2009. Large-river delta-front estuaries as natural "recorders" of global environmental change. *Proceedings of the National Academy of Sciences* 106: 8085–8092. doi:10.1073/pnas.0812878106.

Biggs, R.B. 1970. Sources and distribution of suspended sediment in northern Chesapeake Bay. *Marine Geology* 9: 187–201. doi:10.1016/0025-3227(70)90014-9.

Bilkovic, D.M., M. Mitchell, P. Mason, and K. Duhring. 2016. The role of living shorelines as estuarine habitat conservation strategies. *Coastal Management* 44: 161–174.

Blum, M.D., and H.H. Roberts. 2009. Drowning of the Mississippi Delta due to insufficient sediment supply and global sea-level rise. *Nature Geoscience* 2: 488–491. doi:10.1038/ngeo553.

Boesch, D.F. (editor). 2008. Global warming and the Free State: Comprehensive assessment of climate change impacts in Maryland. Report of the Scientific and Technical Working Group of the Maryland Commission on Climate Change. University of Maryland Center for Environmental Science, Cambridge, Maryland.

Bouma, T.J., L.A. van Duren, S. Temmerman, T. Claverie, A. Blanco-Garcia, T. Ysebaert, and P.M.J. Herman. 2007. Spatial flow and sedimentation patterns within patches of epibenthic structures: Combining field, flume and modelling experiments. *Continental Shelf Research* 27: 1020–1045. doi:10.1016/j.csr.2005.12.019

Bricker, S.B., C.G. Clement, D.E. Pirhalla, S.P. Orlando, and Farrow. 1999. *National estuarine eutrophication assessment: effects of nutrient enrichment in the nation's estuaries*. NOAA, National Ocean Service, Special Projects Office and the National Centers for Coastal Ocean Science. Silver Spring, MD: 77pp.

Bricker, S.B. 1993. The History of Cu, Pb, and Zn Inputs to Narragansett Bay, Rhode Island as Recorded by Salt-Marsh Sediments. *Estuaries* 16: 589. doi:10.2307/1352797.

Brush, G.S. 1984. Patterns of recent sediment accumulation in Chesapeake Bay (Virginia—Maryland, U.S.A.) tributaries. *Chemical Geology* 44: 227–242. doi:10.1016/0009-2541(84)90074-3.

Brush, G.S. 2009. Historical land use, Nitrogen, and coastal eutrophication: A paleoecological perspective. *Estuaries and Coasts* 32: 18–28. doi:10.1007/s12237-008-9106-z.

Brush, G.S., and W.B. Hilgartner. 2000. Paleoecology of submerged macrophytes in the upper Chesapeake Bay. *Ecological Monographs* 70: 645–667.

Burdige, D.J. 1993. The biogeochemistry of manganese and iron reduction in marine sediments. *Earth-Science Reviews* 35: 249–284. doi:10.1016/0012-8252(93)90040-E.

Cahoon, L.B., J.E. Nearhoof, and C.L. Tilton. 1999. Sediment grain size effect on benthic microalgal biomass in shallow aquatic ecosystems. *Estuaries* 22: 735–741. doi:10.2307/1353106.

Cerco, C.F., and M.R. Noel. 2016. Impact of reservoir sediment scour on water quality in a downstream estuary. *Journal of Environment Quality* 45: 894. doi:10.2134/jeq2014.10.0425.

Cheng, P., M.Li, and Y.Li. 2013. Generation of an estuarine sediment plume by a tropical storm. *Journal of Geophysical Research: Oceans* 118: 856–868. doi:10.1002/jgrc.20070.

Christiansen, T., P.L. Wiberg, and T.G. Milligan. 2000. Flow and sediment transport on a tidal salt marsh surface. *Estuarine, Coastal and Shelf Science* 50: 315–331. doi:10.1006/ecss.2000.0548.

Cloern, J.E. 2001. Our evolving conceptual model of the coastal eutrophication problem. *Marine Ecology Progress Series* 210: 223–253. doi:10.3354/meps210223.

Colden, A.M, and R.N Lipcius. 2015. Lethal and sublethal effects of sediment burial on the eastern oyster Crassostrea virginica. *Marine Ecology Progress Series* 527: 105–117. doi:10.3354/meps11244.

Collins, A.L., D.E. Walling, and G.J.L. Leeks. 1997. Source type ascription for fluvial suspended sediment based on a quantitative composite fingerprinting technique. *CATENA* 29: 1–27. doi:10.1016/S0341-8162(96)00064-1.

Cooper, S. R., and G. S. Brush. 1991. Long-Term History of Chesapeake Bay Anoxia. *Science* 254: 992–996. doi:10.1126/science.254.5034.992.

Cotton, J.A., G. Wharton, J.A.B. Bass, C.M. Heppell, and R.S. Wotton. 2006. The effects of seasonal changes to in-stream vegetation cover on patterns of flow and accumulation of sediment. *Geomorphology* 77: 320–334. doi:10.1016/j.geomorph.2006.01.010.

D'Alpaos, A., S. Lanzoni, M. Marani, and A. Rinaldo. 2007. Landscape evolution in tidal embayments: Modeling the interplay of erosion, sedimentation, and vegetation dynamics. *Journal of Geophysical Research* 112. doi:10.1029/2006JF000537.

Dalrymple, R.W., B.A. Zaitlin, and R. Boyd. 1992. Estuarine facies models; conceptual basis and stratigraphic implications. *Journal of Sedimentary Research* 62: 1130–1146. doi:10.1306/D4267A69-2B26-11D7-8648000102C1865D.

Davis, F.W. 1985. Historical changes in submerged macrophyte communities of upper Chesapeake Bay. *Ecology* 66: 981–993. doi:10.2307/1940560.

Davis, J.L, C.A. Currin, C. O'Brien, C. Raffenburg, and A. Davis. 2015. Living shorelines: coastal resilience with a blue carbon benefit. *PLoS One* 10: e0142595.

Day, J.W., A. Yáñez-Arancibia, W.M Kemp, and B.C. Crump. 2012. Introduction to Estuarine Ecology. In *Estuarine Ecology*, ed. J.W. Day, B.C. Crump, W.M Kemp, and A. Yáñez-Arancibia, 1–18. Hoboken, NJ, USA: John Wiley & Sons, Inc.

Dennison, W.C., R.J. Orth, K.A. Moore, J.C. Stevenson, V. Carter, S. Kollar, P.W. Bergstrom, and R.A. Batiuk. 1993. Assessing water quality with submersed aquatic vegetation. *BioScience* 43: 86–94. doi:10.2307/1311969.

Devereux, O.H., K.L. Prestegaard, B.A. Needelman, and A.C. Gellis. 2010. Suspended-sediment sources in an urban watershed, Northeast Branch Anacostia River, Maryland. *Hydrological Processes* 24: 1391–1403. doi:10.1002/hyp.7604.

Diaz, R. J., and R. Rosenberg. 2008. Spreading dead zones and consequences for marine ecosystems. *Science* 321: 926–929. doi:10.1126/science.1156401.

Dibb, J.E., and D.L. Rice. 1989. Temporal and spatial distribution of beryllium-7 in the sediments of Chesapeake Bay. *Estuarine, Coastal and Shelf Science* 28: 395–406. doi:10.1016/0272-7714(89)90087-5.

Donoghue, J. F., O.P. Bricker, and C.R. Olsen. 1989. Particle-borne radionuclides as tracers for sediment in the Susquehanna River and Chesapeake Bay. *Estuarine, Coastal and Shelf Science* 29: 341–360. doi:10.1016/0272-7714(89)90033-4.

Duarte, C.M. 2002. The future of seagrass meadows. *Environmental conservation* 29: 192–206. doi:10.1017/S0376892902000127.

Dugan, J.E., L. Airoldi, M.G. Chapman, S.J. Walker, and T. Schlacher. 2011. Estuarine and coastal structures. In *Treatise on Estuarine and Coastal Science*, 17–41. Elsevier.

Elbaz-Poulichet, F., P. Holliger, W.W. Huang, and J.M. Martin. 1984. Lead cycling in estuaries, illustrated by the Gironde estuary, France. *Nature* 308: 409–414. doi:10.1038/308409a0.

Elderfield, H., R. Upstill-Goddard, and E.R. Sholkovitz. 1990. The rare earth elements in rivers, estuaries, and coastal seas and their significance to the composition of ocean waters. *Geochimica et Cosmochimica Acta* 54: 971–991. doi:10.1016/0016-7037(90)90432-K.

Eulie, D.O., D.R. Corbett, and J.P. Walsh. 2018. Shoreline erosion and decadal sediment accumulation in the Tar-Pamlico estuary, North Carolina, USA: A

source-to-sink analysis. *Estuarine, Coastal and Shelf Science* 202: 246–258. Doi:10.1016/j.ecss.2017.10.011.

Feuillet, J.P., and P. Fleischer. 1980. Estuarine circulation; controlling factor of clay mineral distribution in James River estuary, Virginia. *Journal of Sedimentary Research* 50: 267–279.

Fisk, H. N., C.R. Kolb, E. McFarlan, and L. J. Wilbert. 1954. Sedimentary framework of the modern Mississippi delta [Louisiana]. *Journal of Sedimentary Research* 24: 76–99. doi:10.1306/D4269661-2B26-11D7-8648000102C1865D.

Fonseca, M.S., and J.A. Cahalan. 1992. A preliminary evaluation of wave attenuation by four species of seagrass. *Estuarine, Coastal and Shelf Science* 35: 565–576. doi:10.1016/S0272-7714(05)80039-3.

Fonseca, M.S., and J.S. Fisher. 1986. A comparison of canopy friction and sediment movement between four species of seagrass with reference to their ecology and restoration. *Marine Ecology Progress Series* 29: 15–22.

Fonseca, M.S., J.S. Fisher, J.C. Zieman, and G.W. Thayer. 1982. Influence of the seagrass, Zostera marina L., on current flow. *Estuarine, Coastal and Shelf Science* 15: 351–364. doi:10.1016/0272-7714(82)90046-4.

French, J.R., and T. Spencer. 1993. Dynamics of sedimentation in a tide-dominated backbarrier salt marsh, Norfolk, UK. *Marine Geology* 110: 315–331. doi:10.1016/0025-3227(93)90091-9.

Gacia, E., and C.M. Duarte. 2001. Sediment retention by a Mediterranean Posidonia oceanica Meadow: The Balance between Deposition and Resuspension. *Estuarine, Coastal and Shelf Science* 52: 505–514. doi:10.1006/ecss.2000.0753.

Gambi, M.C, A.R.M. Nowell, and P.A. Jumars. 1990. Flume observations on flow dynamics in Zostera marina (eelgrass) beds. *Marine Ecology Progress Series* 61: 159–169. doi:10.3354/meps061159.

Ganju, Neil K., Matthew L. Kirwan, Patrick J. Dickhudt, Glenn R. Guntenspergen, Donald R. Cahoon, and Kevin D. Kroeger. 2015. Sediment transport-based metrics of wetland stability. *Geophysical Research Letters* 42: 7992–8000. USGS Publications Warehouse. doi:10.1002/2015GL065980.

Gavis, J., and V. Grant. 1986. Sulfide, iron, manganese, and phosphate in the deep water of the Chesapeake Bay during anoxia. *Estuarine, Coastal and Shelf Science* 23: 451–463. doi:10.1016/0272-7714(86)90003-X.

Gellis, A.C., and G.B. Noe. 2013. Sediment source analysis in the Linganore Creek watershed, Maryland, USA, using the sediment fingerprinting approach: 2008 to 2010. *Journal of Soils and Sediments* 13: 1735–1753. doi:10.1007/s11368-013-0771-6.

Gellis, A.C., C.R. Hupp, M.J. Pavich, J. M. Landwehr, W.S.L. Banks, B.E. Hubbard, M.J. Lanland, and J.C. Ritchie. 2009. *Sources, transport, and storage of sediment at selected sites in the Chesapeake Bay Watershed*. US Geological Survey Science Investigations Report 2008-5186.

Gittman, R.K, F.J. Fodrie, A.M. Popowich, D.A. Keller, J.F. Bruno, C.A. Currin, C.H. Peterson, and M.F. Piehler. 2015. Engineering away our natural defenses: an analysis of shoreline hardening in the US. *Frontiers in Ecology and the Environment* 13: 301–307. doi:10.1890/150065.

Goldberg, E.D., V. Hodge, M. Koide, J. Griffin, E. Gamble, O.P. Bricker, G. Matisoff, G.R. Holdren, and R. Braun. 1978. A pollution history of Chesapeake Bay. *Geochimica et Cosmochimica Acta* 42: 1413–1425. doi:10.1016/0016-7037(78)90047-9.

Goodbred, S.L., and S.A. Kuehl. 1998. Floodplain processes in the Bengal Basin and the storage of Ganges–Brahmaputra river sediment: an accretion study using 137Cs and 210Pb geochronology. *Sedimentary Geology* 121: 239–258. doi:10.1016/S0037-0738(98)00082-7.

Gorman-Sanisaca, L.E., A.C. Gellis, and D.L. Lorenz. 2017. *Determining the sources of fine-grained sediment using the Sediment Source Assessment Tool (Sed_SAT)*. U.S. Geological Survey Open-File Report 2017-1062.

Gottschalk, L.C. 1945. Effects of soil erosion on navigation in upper Chesapeake Bay. *Geographical Review* 35: 219. doi:10.2307/211476.

Gross, M.G., M. Karweit, W.B. Cronin, and J.R. Schubel. 1978. Suspended sediment discharge of the Susquehanna River to northern Chesapeake Bay, 1966 to 1976. *Estuaries* 1: 106–110. doi:10.2307/1351599.

Guo, T, R.D. DeLaune, and W.H. Patrick Jr. 1997. The influence of sediment redox chemistry on chemically active forms of arsenic, cadmium, chromium, and zinc in estuarine sediment. *Environment International* 23: 305–316. doi:10.1016/S0160-4120(97)00033-0.

Gupta, G., and M. Karuppiah. 1996. Heavy metals in sediments of two Chesapeake Bay tributaries — Wicomico and Pocomoke Rivers. *Journal of Hazardous Materials* 50: 15–29. doi:10.1016/0304-3894(96)01773-6.

Gurbisz, C., W.M. Kemp, L.P. Sanford, and R.J. Orth. 2016. Mechanisms of storm-related loss and resilience in a large submersed plant bed. *Estuaries and Coasts* 39: 951–966. doi:10.1007/s12237-016-0074-4.

Gurbisz, C., and W.M. Kemp. 2014. Unexpected resurgence of a large submersed plant bed in Chesapeake Bay: Analysis of time series data. *Limnology and Oceanography* 59: 482–494. doi:10.4319/lo.2014.59.2.0482.

Hainly, R.A., L.A. Reed, H.N. Flippo, and G.J. Barton. 1995. *Deposition and simulation of sediment transport in the Lower Susquehanna River reservoir system*. Water-Resources Investigations Report 95-4122. U.S. Geological Survey.

Halka, J.P., P. Bergstrom, C. Buchanan, T.M. Cronin, L. Currey, A. Gregg, J. Herman, L. Hill, S. Kopecky, C. Larsen, A. Luscher, L. Linker, D. Murphy, and S. Stewart. 2005. Sediment in Chesapeake Bay and Management Issues: Tidal Sediment Processes, ed. S.W. Tidal Sediment Taskforce, Chesapeake Bay Program Nutrient Subcommittee, 19: USEPA Chesapeake Bay Program.

Halka. 2000. *The Impact of Susquehanna Sediments on the Chesapeake Bay*. Chesapeake Bay Program Scientific and Technical Advisory Committee. USEPA Chesapeake Bay Program.

Halka, J., W. Panageotou, and L. Sanford. 1991. Consolidation and erosion of deposited cohesive sediments in northern Chesapeake Bay, USA. *Geo-Marine Letters* 11: 174–178. doi:10.1007/BF02431008.

Hannigan, R., E. Dorval, and C. Jones. 2010. The rare earth element chemistry of estuarine surface sediments in the Chesapeake Bay. *Chemical Geology* 272: 20–30. doi:10.1016/j.chemgeo.2010.01.009.

Hardaway, C.S., and R.J. Byrne. 1999. Shoreline management in Chesapeake Bay.

Hargrove, W. L., D. Johnson, D. Snethen, and J. Middendorf. 2010. From dust bowl to mud bowl: Sedimentation, conservation measures, and the future of reservoirs. *Journal of Soil and Water Conservation* 65: 14A–17A. doi:10.2489/jswc.65.1.14A.

Helz, G.R., S.A. Sinex, K.L. Ferri, and M. Nichols. 1985a. Processes controlling Fe, Mn and Zn in sediments of northern Chesapeake Bay. *Estuarine, Coastal and Shelf Science* 21: 1–16. doi:10.1016/0272-7714(85)90002-2.

Helz, G.R., G.H. Setlock, A.Y. Cantillo, and W.S. Moore. 1985b. Processes controlling the regional distribution of $^{210}$Pb, $^{226}$Ra and anthropogenic zinc in estuarine sediments. *Earth and Planetary Science Letters* 76: 23–34. doi:10.1016/0012-821X(85)90145-1.

Hennessee, L., K. Offerman, J. Halka. 2006. *Suspended load contributed by shore erosion, Chesapeake Bay, Maryland*. Department of Natural Resources and Maryland Geological Survey: Coastal and Estuarine Geology File Report No. 06-03.

Hennessee, E.L., and J.P. Halka. 2005. Hurricane Isabel and erosion of Chesapeake Bay shorelines, Maryland. Sellner, K.G., Ed.; In *Hurricane Isabel in perspective*, 81-88. Chesapeake Research Consortium, Edgewater, MD, USA.

Hirsch, R.M. 2012. *Flux of nitrogen, phosphorus, and suspended sediment from the Susquehanna River basin to the Chesapeake Bay during Tropical Storm Lee, September 2011, as an indicator of the effects of reservoir sedimentation on water quality*. US Geological Survey Science Investigations Report 2012-5185. U.S. Geological Survey.

Hirschberg, D.J., and J.R. Schubel. 1979. Recent geochemical history of flood deposits in the northern Chesapeake Bay. *Estuarine and Coastal Marine Science* 9: 771–IN7. doi:10.1016/S0302-3524(79)80010-9.

Hobbs, C.H., J.P. Halka, R.T. Kerhin, and M.J. Carron. 1992. Chesapeake Bay sediment budget. *Journal of Coastal Research* 8: 292–300.

Jaeger, J.M., C.A. Nittrouer, N.D. Scott, and J.D. Milliman. 1998. Sediment accumulation along a glacially impacted mountainous coastline: north-east Gulf of Alaska. *Basin Research* 10: 155–173. doi:10.1046/j.1365-2117.1998.00059.x.

Jalowska, A.M., B.A. McKee, J.P. Laceby, and A.B. Rodriguez. 2017. Tracing the sources, fate, and recycling of fine sediments across a river-delta interface. *CATENA* 154: 95–106. doi:10.1016/j.catena.2017.02.016.

Johnson, R., and R.M. Bustin. 2006. Coal dust dispersal around a marine coal terminal (1977–1999), British Columbia: The fate of coal dust in the marine environment. *International Journal of Coal Geology* 68: 57–69. doi:10.1016/j.coal.2005.10.003.

Jones, C.G, J.H. Lawton, and M. Shachak. 1994. Organisms as ecosystem engineers. In *Ecosystem management*, 130–147. Springer.

Jordan, T.E., J.C. Cornwell, W.R. Boynton, and J.T. Anderson. 2008. Changes in phosphorus biogeochemistry along an estuarine salinity gradient: The iron

conveyer belt. *Limnology and Oceanography* 53: 172–184. doi:10.4319/lo.2008.53.1.0172.

Karlsen, A.W., T.M. Cronin, S.E. Ishman, D.A. Willard, R. Kerhin, C.W. Holmes, and M.Marot. 2000. Historical trends in Chesapeake Bay dissolved Oxygen based on benthic foraminifera from sediment cores. *Estuaries* 23: 488. doi:10.2307/1353141.

Kearney, M.S., A.S. Rogers, J.R.G. Townshend, E. Rizzo, D. Stutzer, J.C. Stevenson, and K. Sundborg. 2002. Landsat imagery shows decline of coastal marshes in Chesapeake and Delaware Bays. *Eos, Transactions American Geophysical Union* 83: 173. doi:10.1029/2002EO000112.

Kearney, M.S., and J.C. Stevenson. 1991. Island land loss and marsh vertical accretion rate evidence for historical sea-level changes in Chesapeake Bay. *Journal of Coastal Research*: 403–415.

Kemp, W.M., W.R. Boynton, J.E. Adolf, D.F. Boesch, W.C. Boicourt, G Brush, J.C. Cornwell, et al. 2005. Eutrophication of Chesapeake Bay: historical trends and ecological interactions. *Marine Ecology Progress Series* 303: 1–29. doi:10.3354/meps303001.

Kerhin, R.T., J.P. Halka, D.V. Wells, E.L. Hennessee, P.J. Blakeslee, N. Zoltan, R.H. Cuthbertson. 1988. The surficial sediments of Chesapeake Bay, Maryland: Physical characteristics and sediment budget. Report of Investigations 48.

Kerwin, J.A., R.E. Munro, and W.W.A. Peterson. 1976. Distribution and abundance of aquatic vegetation in the upper Chesapeake Bay, 1971-1974.

Kirwan, M.L., A.B. Murray, J.P. Donnelly, and D.R. Corbett. 2011. Rapid wetland expansion during European settlement and its implication for marsh survival under modern sediment delivery rates. *Geology* 39: 507–510. doi:10.1130/G31789.1.

Koch, E.W. 2001. Beyond light: Physical, geological, and geochemical parameters as possible submersed aquatic vegetation habitat requirements. *Estuaries* 24: 1. doi:10.2307/1352808.

Koide, M., A. Soutar, and E.D. Goldberg. 1972. Marine geochronology with 210Pb. *Earth and Planetary Science Letters* 14: 442–446. doi:10.1016/0012-821X(72)90146-X.

Kuehl, S.A., C.A. Nittrouer, and D.J. DeMaster. 1986. Distribution of sedimentary structures in the Amazon subaqueous delta. *Continental Shelf Research* 6: 311–336. doi:10.1016/0278-4343(86)90066-X.

Lambert, C. P., and D.E. Walling. 1987. Floodplain sedimentation: A preliminary investigation of contemporary deposition within the lower reaches of the River Culm, Devon, UK. *Geografiska Annaler. Series A, Physical Geography* 69: 393. doi:10.2307/521353.

Lanesky, D. E., B. W. Logan, R. G. Brown, and A. C. Hine. 1979. A new approach to portable vibracoring underwater and on land. *Journal of Sedimentary Research* 49: 654–657. doi:10.1306/212F77F2-2B24-11D7-8648000102C1865D.

Langland, M.J. 2015. *Sediment transport and capacity change in three reservoirs, Lower Susquehanna River Basin, Pennsylvania and Maryland 1900-2012*. US Geological Survey Ope- File Report 2014-1235.

Langland, M.J. 2009. *Bathymetry and sediment-storage capacity change in three reservoirs on the Lower Susquehanna River, 1996-2008*. US Geological Survey Science Investigations Report 2009-5110.

Langland, M.J., and T. Cronin. 2003. *A summary report of sediment processes in Chesapeake Bay and watershed*. US Geological Survey Water-Resources Investigations Report 03-4123.

Larsen, I., and N. Cutshall. 1981. Direct determination of 7Be in sediments. *Earth and Planetary Science Letters* 54: 379–384. doi:10.1016/0012-821X(81)90053-4.

Leonard, L.A., and M.E. Luther. 1995. Flow hydrodynamics in tidal marsh canopies. *Limnology and Oceanography* 40: 1474–1484. doi:10.4319/lo.1995.40.8.1474.

Li, X., O.W.H. Wai, Y.S. Li, B.J. Coles, M.H. Ramsey, and I. Thornton. 2000. Heavy metal distribution in sediment profiles of the Pearl River estuary, South China. *Applied Geochemistry* 15: 567–581. doi:10.1016/S0883-2927(99)00072-4.

Loring, D. H. 1991. Normalization of heavy-metal data from estuarine and coastal sediments. *ICES Journal of Marine Science* 48: 101–115. doi:10.1093/icesjms/48.1.101.

Marani, M., E.B., A. D'Alpaos, A. Defina, S. Lanzoni, and A. Rinaldo. 2003. On the drainage density of tidal networks. *Water Resources Research* 39. doi:10.1029/2001WR001051.

Marcus, W.A., and M.S. Kearney. 1991. Upland and Coastal Sediment Sources in a Chesapeake Bay Estuary. *Annals of the Association of American Geographers* 81: 408–424. doi:10.1111/j.1467-8306.1991.tb01702.x.

Mariotti, G., and S. Fagherazzi. 2010. A numerical model for the coupled long-term evolution of salt marshes and tidal flats. *Journal of Geophysical Research: Earth Surface* 115.

Markewich, H.W., M.J. Pavich, and G.R. Buell. 1990. Contrasting soils and landscapes of the Piedmont and Coastal Plain, eastern United States. *Geomorphology* 3: 417–447. doi:10.1016/0169-555X(90)90015-I.

Meade, R.H. 1969. Landward transport of bottom sediments in estuaries of the Atlantic Coastal Plain. *SEPM Journal of Sedimentary Research* Vol. 39. doi:10.1306/74D71C1C-2B21-11D7-8648000102C1865D.

Morse, J.W., and G.W. Luther. 1999. Chemical influences on trace metal-sulfide interactions in anoxic sediments. *Geochimica et Cosmochimica Acta* 63: 3373–3378. doi:10.1016/S0016-7037(99)00258-6.

Mukundan, R., D.E. Walling, A.C. Gellis, M.C. Slattery, and D.E. Radcliffe. 2012. Sediment Source Fingerprinting: Transforming From a Research Tool to a Management Tool [1]: SEDIMENT SOURCE FINGERPRINTING: TRANSFORMING FROM A RESEARCH TOOL TO A MANAGEMENT TOOL. *JAWRA Journal of the American Water Resources Association* 48: 1241–1257. doi:10.1111/j.1752-1688.2012.00685.x.

Munksgaard, N.C, K. Lim, and D.L. Parry. 2003. Rare earth elements as provenance indicators in North Australian estuarine and coastal marine sediments. *Estuarine, Coastal and Shelf Science* 57: 399–409. doi:10.1016/S0272-7714(02)00368-2.

Najjar, R.G., C.R. Pyke, M.B. Adams, D. Breitburg, C. Hershner, M. Kemp, R. Howarth, M.R. Mulholland, M. Paolisso, and D. Secor. 2010. Potential climate-

change impacts on the Chesapeake Bay. *Estuarine, Coastal and Shelf Science* 86: 1–20.
Neubauer, S.C., I.C. Anderson, J.A. Constantine, and S.A. Kuehl. 2002. Sediment deposition and accretion in a Mid-Atlantic (U.S.A.) tidal freshwater marsh. *Estuarine, Coastal and Shelf Science* 54: 713–727. doi:10.1006/ecss.2001.0854.
Nie, Y., I.B. Suayah, L.K. Benninger, and M.J. Alperin. 2001. Modeling detailed sedimentary $^{210}$Pb and fallout $^{239,240}$Pu profiles to allow episodic events: An application in Chesapeake Bay. *Limnology and Oceanography* 46: 1425–1437. doi:10.4319/lo.2001.46.6.1425.
Nittrouer, C.A., R.W. Sternberg, R. Carpenter, and J.T. Bennett. 1979. The use of Pb-210 geochronology as a sedimentological tool: Application to the Washington continental shelf. *Marine Geology* 31: 297–316. doi:10.1016/0025-3227(79)90039-2.
Nixon, S.W. 1995. Coastal marine eutrophication: A definition, social causes, and future concerns. *Ophelia* 41: 199–219. doi:10.1080/00785236.1995.10422044.
Officer, C.B., D.R. Lynch, G.H. Setlock, and G.R. Helz. 1984a. Recent sedimentation rates in Chesapeake Bay. Kennedy, V.S, Ed.; In *The Estuary As a Filter*, 131–157. Academic Press.
Officer, C. B., R. B. Biggs, J. L. Taft, L. E. Cronin, M. A. Tyler, and W. R. Boynton. 1984b. Chesapeake Bay anoxia: Origin, development, and significance. *Science* 223: 22–27. doi:10.1126/science.223.4631.22.
Olsen, C. R., I. L. Larsen, P. D. Lowry, N. H. Cutshall, and M. M. Nichols. 1986. Geochemistry and deposition of $^{7}$ Be in river-estuarine and coastal waters. *Journal of Geophysical Research* 91: 896. doi:10.1029/JC091iC01p00896.
Orth, R.J., and K.A. Moore. 1984. Distribution and abundance of submerged aquatic vegetation in Chesapeake Bay: An historical perspective. *Estuaries* 7: 531. doi:10.2307/1352058.
Orth, R.J., D.J. Wilcox, J.R. Whiting, A.K. Kenne, L. Nagey, E.R. Smith. 2016. 2015 distribution of submerged aquatic vegetation in Chesapeake Bay and Coastal Bays. VIMS Special Scientific Report Number 159. Final Report to EPA, Chesapeake Bay Program, Annapolis MD, Grant No CB96321901-0, http://web.vims.edu/bio/sav/sav15/index.html
Owens, M., and J.C. Cornwell. 1995. Sedimentary evidence for decreased heavy-metal inputs to the Chesapeake Bay. *Ambio* 24: 24–27.
Paerl, H.W. 2006. Assessing and managing nutrient-enhanced eutrophication in estuarine and coastal waters: Interactive effects of human and climatic perturbations. *Ecological Engineering* 26: 40–54. doi:10.1016/j.ecoleng.2005.09.006.
Palinkas, C.M., J.M. Testa, J.C. Cornwell, M. Li, and L.P. Sanford. Submitted. Influences of Conowingo Dam on delivery and fate of sediments and particulate nutrients to Chesapeake Bay.
Palinkas, C.M., L.P. Sanford, and E.W. Koch. 2018. Influence of shoreline stabilization structures on the nearshore sedimentary environment in mesohaline Chesapeake Bay. *Estuaries and Coasts* 41: 952–965. doi:10.1007/s12237-017-0339-6.

Palinkas, C. 2017. The impacts of Conowingo particulates on the Chesapeake Bay. Final report to Maryland Department of Natural Resources.

Palinkas, C.M., N. Barth, E.W. Koch, and D.J. Shafer. 2016. The influence of breakwaters on nearshore sedimentation patterns in Chesapeake Bay, USA. *Journal of Coastal Research* 320: 788–799. doi:10.2112/JCOASTRES-D-14-00138.1.

Palinkas, C.M., and K.A.M. Engelhardt. 2016. Spatial and temporal patterns of modern (~100 yr) sedimentation in a tidal freshwater marsh: Implications for future sustainability: Tidal freshwater marsh sedimentation. *Limnology and Oceanography* 61: 132–148. doi:10.1002/lno.10202.

Palinkas, C.M., J.P. Halka, M. Li, L.P. Sanford, and P. Cheng. 2014. Sediment deposition from tropical storms in the upper Chesapeake Bay: Field observations and model simulations. *Continental Shelf Research* 86: 6–16. doi:10.1016/j.csr.2013.09.012.

Palinkas, C.M., K.A.M. Engelhardt, and D. Cadol. 2013. Evaluating physical and biological influences on sedimentation in a tidal freshwater marsh with 7Be. *Estuarine, Coastal and Shelf Science* 129: 152–161. doi:10.1016/j.ecss.2013.05.022.

Palinkas, C.M., and J.C. Cornwell. 2012. A preliminary sediment budget for the Corsica River (MD): Improved estimates of Nitrogen burial and implications for restoration. *Estuaries and Coasts* 35: 546–558. Doi:10.1007/s12237-011-9450-2.

Palinkas, C.M., and E.W. Koch. 2012. Sediment accumulation rates and submersed aquatic vegetation (SAV) distributions in the mesohaline Chesapeake Bay, USA. *Estuaries and Coasts* 35: 1416–1431. doi:10.1007/s12237-012-9542-7.

Palinkas, C.M., and C.A. Nittrouer. 2007. Modern sediment accumulation on the Po shelf, Adriatic Sea. *Continental Shelf Research* 27: 489–505. doi:10.1016/j.csr.2006.11.006.

Palinkas, C.M., C.A. Nittrouer, R.A. Wheatcroft, and L. Langone. 2005. The use of 7Be to identify event and seasonal sedimentation near the Po River delta, Adriatic Sea. *Marine Geology* 222-223: 95–112. doi:10.1016/j.margeo.2005.06.011.

Prajith, A., V. P. Rao, and P. Chakraborty. 2016. Distribution, provenance and early diagenesis of major and trace metals in sediment cores from the Mandovi estuary, western India. *Estuarine, Coastal and Shelf Science* 170: 173–185. doi:10.1016/j.ecss.2016.01.014.

Rabalais, N.N., R. J. Díaz, L. A. Levin, R. E. Turner, D. Gilbert, and J. Zhang. 2010. Dynamics and distribution of natural and human-caused hypoxia. *Biogeosciences* 7: 585–619. doi:10.5194/bg-7-585-2010.

Reid, M.K., and K.L. Spencer. 2009. Use of principal components analysis (PCA) on estuarine sediment datasets: The effect of data pre-treatment. *Environmental Pollution* 157: 2275–2281. doi:10.1016/j.envpol.2009.03.033.

Restrepo, J., P. Zapata, J. Diaz, J. Garzonferreira, and C. Garcia. 2006. Fluvial fluxes into the Caribbean Sea and their impact on coastal ecosystems: The Magdalena River, Colombia. *Global and Planetary Change* 50: 33–49. doi:10.1016/j.gloplacha.2005.09.002.

Rosati, J.D. 2005. Concepts in sediment budgets. *Journal of Coastal Research* 212: 307–322. Doi:10.2112/02-475A.1.
Rothschild, B.J., J.S. Ault, P. Goulletquer, and M. Héral. 1994. Decline of the Chesapeake Bay oyster population: a century of habitat destruction and overfishing. *Marine Ecology Progress Series* 111: 29–39. doi:10.3354/meps111029.
Russ, E.R., and C.M. Palinkas. 2018. Seasonal-scale and decadal-scale sediment-vegetation interactions on the subaqueous Susquehanna River delta, upper Chesapeake Bay. *Estuaries and Coasts* 41: 2092–2104. Doi:10.1007/s12237-018-0413-8.
Sand-Jensen, K. 1998. Influence of submerged macrophytes on sediment composition and near‐bed flow in lowland streams. *Freshwater Biology* 39: 663–679. doi:10.1046/j.1365-2427.1998.00316.x.
Sanders, J.G. 1985. Arsenic geochemistry in Chesapeake Bay: Dependence upon anthropogenic inputs and phytoplankton species composition. *Marine Chemistry* 17: 329–340. doi:10.1016/0304-4203(85)90006-4.
Sanford, L. P. 1994. Wave-forced resuspension of upper Chesapeake Bay muds. *Estuaries* 17: 148. doi:10.2307/1352564.
Sanford, L.P., and J. Gao. 2018. Influences of wave climate and sea level on shoreline erosion rates in the Maryland Chesapeake Bay. *Estuaries and Coasts* 41: 19–37. Doi:10.1007/s12237-017-0257-7.
Sanford, L.P., S.E. Suttles, and J.P. Halka. 2001. Reconsidering the physics of the Chesapeake Bay estuarine turbidity maximum. *Estuaries* 24: 655. doi:10.2307/1352874.
Schropp, S. J., F.G. Lewis, H.L. Windom, J.D. Ryan, F.D. Calder, and L.C. Burney. 1990. Interpretation of metal concentrations in estuarine sediments of Florida using Aluminum as a reference element. *Estuaries* 13: 227. doi:10.2307/1351913.
Schubel, J.R., and H.H. Carter. 1977. Suspended sediment budget for Chesapeake Bay. In *Estuarine Processes*, 48–62. Elsevier.
Schubel, J.R., and D.W. Pritchard. 1986. Responses of Upper Chesapeake Bay to variations in discharge of the Susquehanna River. *Estuaries* 9: 236. doi:10.2307/1352096.
Schubel, J.R. 1968. *Suspended sediment of the northern Chesapeake Bay*. Technical Report 35. The Johns Hopkins University: Chesapeake Bay Institute.
Shiller, A.M., and L. Mao. 1999. Dissolved vanadium on the Louisiana Shelf: effect of oxygen depletion. *Continental Shelf Research* 19: 1007–1020. doi:10.1016/S0278-4343(99)00005-9.
Sholkovitz, E. R., and H. Elderfield. 1988. Cycling of dissolved rare earth elements in Chesapeake Bay. *Global Biogeochemical Cycles* 2: 157–176. doi:10.1029/GB002i002p00157.
Sholkovitz, E., and R. Szymczak. 2000. The estuarine chemistry of rare earth elements: comparison of the Amazon, Fly, Sepik and the Gulf of Papua systems. *Earth and Planetary Science Letters* 179: 299–309. doi:10.1016/S0012-821X(00)00112-6.

Sinex, S. A., and G. R. Helz. 1981. Regional geochemistry of trace elements in Chesapeake Bay sediments. *Environmental Geology* 3: 315–323. doi:10.1007/BF02473521.

Sommerfield, C.K., C.A. Nittrouer, and C.R. Alexander. 1999. 7Be as a tracer of flood sedimentation on the northern California continental margin. *Continental Shelf Research* 19: 335–361. doi:10.1016/S0278-4343(98)00090-9.

Spencer, K.L., A.B. Cundy, and I.W. Croudace. 2003. Heavy metal distribution and early-diagenesis in salt marsh sediments from the Medway Estuary, Kent, UK. *Estuarine, Coastal and Shelf Science* 57: 43–54. doi:10.1016/S0272-7714(02)00324-4.

Stevenson, J.C., and N.M. Confer. 1978. Summary of available information on Chesapeake Bay submerged vegetation. United States Fish and Wildlife Service Biological Services Program FWS/OBS-78/66, Washington, D.C., USA.

Subramanian, B., J. Martinez, A.E Luscher, and D. Wilson. 2008. Living shorelines projects in Maryland in the past 20 years. *Management, Policy, Science, and Engineering of Nonstructural Erosion Control in the Chesapeake Bay*: 49.

Sun, X., D. Fan, M. Liu, Y. Tian, Y. Pang, and H. Liao. 2018. Source identification, geochemical normalization and influence factors of heavy metals in Yangtze River Estuary sediment. *Environmental Pollution* 241: 938–949. doi:10.1016/j.envpol.2018.05.050.

Sutton-Grier, A.E, K. Wowk, and H. Bamford. 2015. Future of our coasts: The potential for natural and hybrid infrastructure to enhance the resilience of our coastal communities, economies and ecosystems. *Environmental Science & Policy* 51: 137–148.

Syvitski, J.P.M., and A. Kettner. 2011. Sediment flux and the Anthropocene. *Philosophical Transactions of the Royal Society A: Mathematical, Physical and Engineering Sciences* 369: 957–975. doi:10.1098/rsta.2010.0329.

Syvitski, J.P.M., C.J. Vorosmarty, A.J. Kettner, and P. Green. 2005. Impact of humans on the flux of terrestrial sediment to the global coastal ocean. *Science* 308: 376–380. doi:10.1126/science.1109454.

Ta, T., V. Nguyen, M. Tateishi, I. Kobayashi, S. Tanabe, and Y. Saito. 2002. Holocene delta evolution and sediment discharge of the Mekong River, southern Vietnam. *Quaternary Science Reviews* 21: 1807–1819. doi:10.1016/S0277-3791(02)00007-0.

Temmerman, S., T.J. Bouma, J. Van de Koppel, D. Van der Wal, M.B. De Vries, and P.M.J. Herman. 2007. Vegetation causes channel erosion in a tidal landscape. *Geology* 35: 631. doi:10.1130/G23502A.1.

Temmerman, S., T. J. Bouma, G. Govers, and D. Lauwaet. 2005. Flow paths of water and sediment in a tidal marsh: Relations with marsh developmental stage and tidal inundation height. *Estuaries* 28: 338–352. doi:10.1007/BF02693917.

Templet, P.H., and K.J. Meyer-Arendt. 1988. Louisiana wetland loss: A regional water management approach to the problem. *Environmental Management* 12: 181–192. doi:10.1007/bf01873387.

Thieler, E.R., E.A. Himmelstoss, J.L. Zichichi, and A. Ergul. 2009. *The Digital Shoreline Analysis System (DSAS) Version 4.0 – An ArcGIS extension for*

*calculating shoreline change*. Report 2008-1278. Open-File Report. Reston. USGS Publications Warehouse.
Thrush, S.F., J.E. Hewitt, V.J. Cummings, J.I. Ellis, C. Hatton, A. Lohrer, and A. Norkko. 2004. Muddy waters: elevating sediment input to coastal and estuarine habitats. *Frontiers in Ecology and the Environment* 2: 299–306. doi:10.1890/1540-9295(2004)002[0299:MWESIT]2.0.CO;2.
Titus, J.G. 1998. Rising seas, coastal erosion, and the takings clause: how to save wetlands and beaches without hurting property owners. *Md. L. Rev.* 57: 1279.
Totland, M.M., I. Jarvis, and K.E Jarvis. 1995. Microwave digestion and alkali fusion procedures for the determination of the platinum-group elements and gold in geological materials by ICP-MS. *Chemical Geology* 124: 21–36. doi:10.1016/0009-2541(95)00021-D.
US Army Corps of Engineers. 2017. *Baltimore Harbor and channels dredged material management plan update*.
US Army Corps of Engineers. 2015. *Lower Susquehanna River watershed assessment, Maryland and Pennsylvania*.
U.S. Environmental Protection Agency. 2010. Chesapeake Bay Total Maximum Daily Load for Nitrogen, Phosphorus, and Sediment. Retrieved from website: https://www.epa.gov/chesapeake-bay-tmdl/chesapeake-bay-tmdl-document
United States Geological Survey. 2017. Landsat-8. Earth Resources Observation and Science Center. https://earthexplorer.usgs.gov/. Accessed 18 November 2017.
Vandenbruwaene, W., S. Temmerman, T. J. Bouma, P. C. Klaassen, M. B. de Vries, D. P. Callaghan, P. van Steeg, et al. 2011. Flow interaction with dynamic vegetation patches: Implications for biogeomorphic evolution of a tidal landscape. *Journal of Geophysical Research: Earth Surface* 116: n/a–n/a. doi:10.1029/2010JF001788.
van Katwijk, M.M., A.R. Bos, D.C.R. Hermus, and W. Suykerbuyk. 2010. Sediment modification by seagrass beds: Muddification and sandification induced by plant cover and environmental conditions. *Estuarine, Coastal and Shelf Science* 89: 175–181. doi:10.1016/j.ecss.2010.06.008.
van Maren, D.S., T. van Kessel, K. Cronin, and L. Sittoni. 2015. The impact of channel deepening and dredging on estuarine sediment concentration. *Continental Shelf Research* 95: 1–14. doi:10.1016/j.csr.2014.12.010.
van Wesenbeeck, B., J. Koppel, P.M.J. Herman, and T.J. Bouma. 2008. Does scale-dependent feedback explain spatial complexity in salt-marsh ecosystems? *Oikos* 117: 152–159. doi:10.1111/j.2007.0030-1299.16245.x.
Velleux, M., and J. Hallden. 2017. *Hydrodynamic and sediment transport analyses for Conowingo Pond*. Mahwah, New Jersey: HDR.
Voli, M,T., K,W. Wegmann, D.R. Bohnenstiehl, E. Leithold, C.L. Osburn, and V. Polyakov. 2013. Fingerprinting the sources of suspended sediment delivery to a large municipal drinking water reservoir: Falls Lake, Neuse River, North Carolina, USA. *Journal of Soils and Sediments* 13: 1692–1707. doi:10.1007/s11368-013-0758-3.
Walling, D.E. 2006. Human impact on land–ocean sediment transfer by the world's rivers. *Geomorphology* 79: 192–216. doi:10.1016/j.geomorph.2006.06.019.

Walling, D.E. 2005. Tracing suspended sediment sources in catchments and river systems. *Science of The Total Environment* 344: 159–184. doi:10.1016/j.scitotenv.2005.02.011.

Walling, D.E., and Q. He. 1997. Use of fallout 137Cs in investigations of overbank sediment deposition on river floodplains. *CATENA* 29: 263–282. doi:10.1016/S0341-8162(96)00072-0.

Wang, H., Y. Saito, Y. Zhang, N. Bi, X. Sun, and Z. Yang. 2011. Recent changes of sediment flux to the western Pacific Ocean from major rivers in East and Southeast Asia. *Earth-Science Reviews* 108: 80–100. doi:10.1016/j.earscirev.2011.06.003.

Wang, H., Z. Yang, Y. Saito, J.P. Liu, X. Sun, and Y. Wang. 2007. Stepwise decreases of the Huanghe (Yellow River) sediment load (1950–2005): Impacts of climate change and human activities. *Global and Planetary Change* 57: 331–354. doi:10.1016/j.gloplacha.2007.01.003.

Ward, L.G, W.M. Kemp, and W.R. Boynton. 1984. The influence of waves and seagrass communities on suspended particulates in an estuarine embayment. *Marine Geology* 59: 85–103. doi:10.1016/0025-3227(84)90089-6.

Windom, H.L., S.J. Schropp, F.D. Calder, J.D. Ryan, R.G. Smith, L.C. Burney, F.G. Lewis, and C.H. Rawlinson. 1989. Natural trace metal concentrations in estuarine and coastal marine sediments of the southeastern United States. *Environmental Science & Technology* 23: 314–320. doi:10.1021/es00180a008.

Wolanski, E., and S. Spagnol. 2000. Environmental degradation by mud in tropical estuaries. *Regional Environmental Change* 1: 152–162. doi:10.1007/s101130000014.

Wright, L. D. 1977. Sediment transport and deposition at river mouths: A synthesis. *Geological Society of America Bulletin* 88: 857. doi:10.1130/0016-7606(1977)88<857:STADAR>2.0.CO;2.

Yang, S. L., M. Li, S. B. Dai, Z. Liu, J. Zhang, and P. X. Ding. 2006. Drastic decrease in sediment supply from the Yangtze River and its challenge to coastal wetland management. *Geophysical Research Letters* 33. doi:10.1029/2005GL025507.

Yarbro, L.A., P.R. Carlson, T.R. Fisher, J.P. Chanton, and W.M. Kemp. 1983. A sediment budget for the Choptank River estuary in Maryland, U.S.A. *Estuarine, Coastal and Shelf Science* 17: 555–570. Doi:10.1016/0272-7714(83)90007-0.

Zabawa, C. F., and J. R. Schubel. 1974. Geologic effects of Tropical Storm Agnes on upper Chesapeake Bay. *Atlantic Geology* 10. doi:10.4138/1456.

Zeileis, A., C. Kleiber, W. Krämer, and K. Hornik. 2003. Testing and dating of structural changes in practice. *Computational Statistics & Data Analysis* 44: 109–123. doi:10.1016/S0167-9473(03)00030-6.

Zhang, Q., D.C. Brady, and W.P. Ball. 2013. Long-term seasonal trends of nitrogen, phosphorus, and suspended sediment load from the non-tidal Susquehanna River Basin to Chesapeake Bay. *Science of The Total Environment* 452-453: 208–221. doi:10.1016/j.scitotenv.2013.02.012.

Zhang, Q, W.P. Ball, and D.L. Moyer. 2016a. Decadal-scale export of nitrogen, phosphorus, and sediment from the Susquehanna River basin, USA: Analysis

and synthesis of temporal and spatial patterns. *Science of The Total Environment* 563-564: 1016–1029. doi:10.1016/j.scitotenv.2016.03.104.

Zhang, Q, C.J. Harman, and W.P. Ball. 2016b. An improved method for interpretation of riverine concentration-discharge relationships indicates long-term shifts in reservoir sediment trapping: An Improved Method on *C-Q* Relationships. *Geophysical Research Letters* 43: 10,215–10,224. doi:10.1002/2016GL069945.

Zhong, L., and M. Li. 2006. Tidal energy fluxes and dissipation in the Chesapeake Bay. *Continental Shelf Research* 26: 752–770. doi:10.1016/j.csr.2006.02.006.

Zimmerman, A.R, and E.A Canuel. 2000. A geochemical record of eutrophication and anoxia in Chesapeake Bay sediments: anthropogenic influence on organic matter composition. *Marine Chemistry* 69: 117–137. doi:10.1016/S0304-4203(99)00100-0.